

1

NMR Spectroscopy and Homogeneous Catalysis

Eloísa Martínez Viviente, Paul S. Pregosin, and Daniele Schott

1.1

Introduction

NMR spectroscopy continues to develop and refine new techniques and, consequently, has become an indispensable tool in connection with solution studies in the area of homogeneous catalysis. Since the soluble catalyst precursors in transition metal catalyzed reactions often contain a variety of atoms from differing parts of the Periodic Table, it is not surprising that a multinuclear NMR approach plays an important role. Although ^1H NMR is still prevalent, ^{13}C (for metal carbonyls, metal carbenes, metal acyls...etc.), ^{31}P (for phosphine-based catalysts), ^{19}F (for fluororous catalysts), and occasionally even the metal center itself, are all routinely measured. Admittedly, the NMR approach to obtaining these data no longer relies solely on 1-D measurements. A variety of two-dimensional methods, using either one, two or three-bond coupling constants allow the data to be accessed in a much more efficient manner. As examples, Figure 1.1 shows: (a) part of the $^{13}\text{C}, ^1\text{H}$ correlation for the Ru(II) dialkyl, π -arene compound, **1** [1], showing the relatively low frequency positions of the three-coordinated biaryl CH-resonances; (b) a section of the long-range carbon-proton correlation for the zirconium polymerization catalyst precursor, **2**, using $^3J(^{13}\text{C}, ^1\text{H})$ [2]. The observed δ values suggest some π -interaction from the five-membered ring; (c) the use of $^3J(^{31}\text{P}, ^1\text{H})$ in the chiral Pd(II) Duphos complex, **3** [3]; and (d) the ^{103}Rh resonance, for the Biphemp-based hydrogenation catalyst precursor, **4**, via $^3J(^{103}\text{Rh}, ^1\text{H})$ [4].

In addition to chemical shifts, δ , and coupling constants, J , relaxation time data, e. g., T_1 , and, increasingly, diffusion constants, D , are being used to help solve selected structural problems. Although line widths in connection with variable temperature studies are still used to calculate rate constants for processes involving catalysts or intermediates which are dynamic on the NMR time scale, magnetization transfer and, especially, phase sensitive nuclear Overhauser effect (NOE) methods are often the method(s) of choice. These NMR techniques are somewhat more demanding; nevertheless, they are finding increasing acceptance. Further, additional

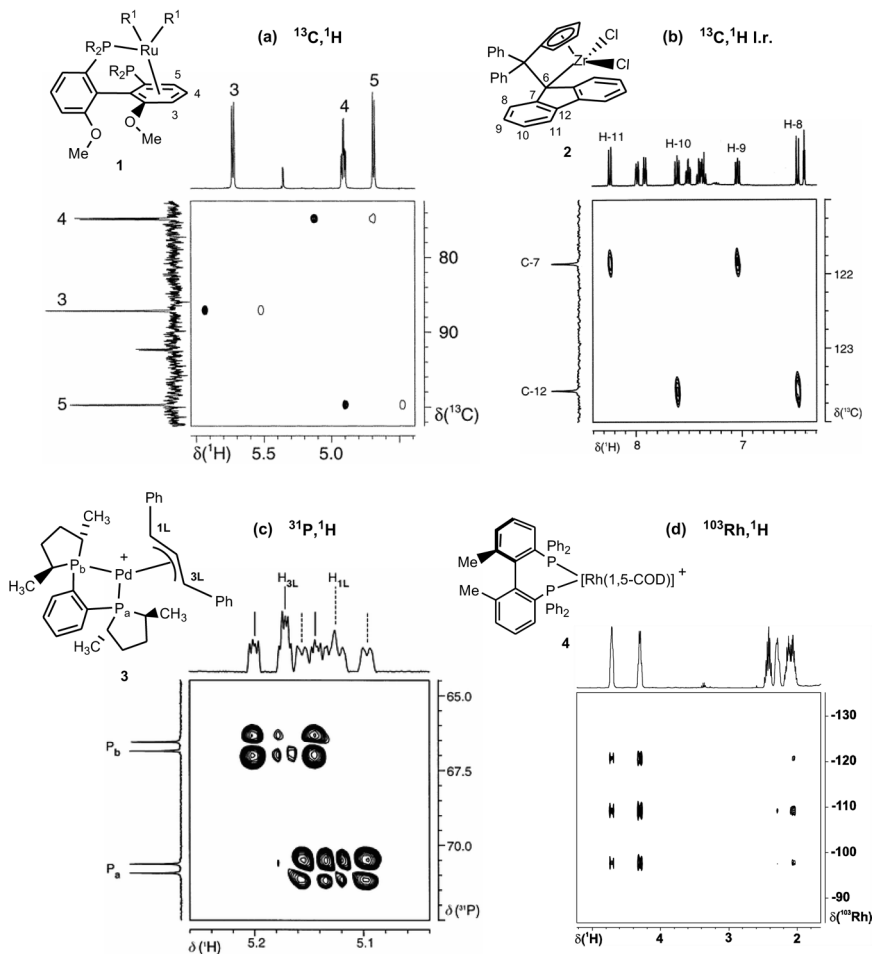


Figure 1.1 (a) Section of the phase-sensitive $^{13}\text{C}, ^1\text{H}$ correlation for **1**, $\text{R}^1 = \text{CH}_3$, $\text{R} = 3,5\text{-di-tert-butylphenyl}$, showing the relatively low frequency positions of the three coordinated biaryl CH-resonances. The open and closed cross-peaks reflect the phases. (b) Section of the $^{13}\text{C}, ^1\text{H}$ long-range correlation for Zr ansa-fluorenyl-complex, **2**, showing the assignment of the fluorenyl carbons, C-7 and C-12. Each of these carbons shows two correlations stemming from the values $^3J(^{13}\text{C}, ^1\text{H})$. (c) $^{31}\text{P}, ^1\text{H}$ correlation showing the cross-peaks which help to identify the two terminal allyl protons of $[\text{Pd}(\eta^3\text{-PhCHCHCHPh})(\text{Me-Duphos})](\text{OTf})$, **3**. These terminal allyl protons, which correlate to their respective pseudo-trans P-atoms, appear as triplets (similar $^3J(^{31}\text{P}, ^1\text{H})$ and $^3J(^1\text{H}, ^1\text{H})$ values) further split by long-range proton–proton and proton–phosphorus interactions. (d) The $^{103}\text{Rh}, ^1\text{H}$ correlation for **4**, showing selective contacts to the two olefinic protons at δ 4.31, and δ 4.72 (one stronger than the other) and an aliphatic proton of the 1,5-COD (there is also a very weak aliphatic second contact). The multiplicity in the rhodium dimension arises due to the two equivalent ^{31}P atoms coordinated to the rhodium.

tools such as: (a) parahydrogen-induced polarisation (PHIP), which may allow one to detect species present in solution at relatively low concentration, (b) high pressure measurements, which simulate catalytic conditions, and (c) NOESY measurements, which allow the determination of 3-D solution structures, are all slowly moving from the hands of the NMR specialist to the practising catalyst chemist. In the following pages we will try to illustrate and summarise some of the more relevant applications of all of these methods.

1.2

Reaction Mechanisms via Reaction Monitoring

Following the course of a reaction by NMR remains one of the most popular applications of this technique in homogeneous catalysis. The resulting kinetic information and/or the detection and identification of intermediates are important sources of mechanistic information. Often, isotopic labeling with ^2H [5–12] or ^{13}C [13–15] facilitates the acquisition and interpretation of the resulting NMR spectra.

1.2.1

Detecting Intermediates

A number of compounds can be recognized in the hydrogenation of ^{13}C labeled MAC (methyl-(Z)- α -acetamidocinnamate, 50% ^{13}C in the α -olefin carbon) using the model Rh catalyst, $[\text{Rh}(\text{diphos})(\text{MeOH})_2]^+$, **5** [16, 17]. Figure 1.2 shows the proposed catalytic cycle and the most relevant sections of the various NMR spectra of **6** and **7**. The ^{31}P spectrum of **6** was measured at 233 K and shows the ^{13}C satellites for P_A (the larger ^{31}P – ^{13}C coupling is associated with the trans-geometry). The ^{13}C NMR spectrum of the α -carbon of **7** (intercepted at -78°C) clearly reveals that H transfer during the migratory insertion step occurs at the β -carbon atom of the $\text{C}=\text{C}$ bond, leaving the α -carbon atom bonded to the Rh ($^1J(^{103}\text{Rh}, ^{13}\text{C}(\alpha)) = 21\text{ Hz}$). The increased ^{13}C S/N and additional spin–spin interactions provided by the ^{13}C labeling are important for the assignment. Monitoring studies on the last step of the cycle via ^{31}P and ^1H NMR allowed the determination of a first-order rate law and the activation parameters.

In a related study using the chelating phosphine chiraphos, several species, **8**–**10**, were recognized by ^{31}P NMR (see Figure 1.3) [18]. Only a single diastereomer, **10**, forms, indicating that the binding is stereospecific.

The catalytic cycle for the Rh-catalyzed 1,4-addition of phenylboronic acid to an α,β -unsaturated ketone could be nicely described by in situ ^{31}P NMR (see Figure 1.4) [19]. The three {S}-Binap species $\text{RhPh}(\text{PPh}_3)(\text{Binap})$, **11**, $\text{Rh}(\text{oxaallyl})(\text{Binap})$, **12** and $[\text{Rh}(\text{OH})(\text{Binap})]_2$, **13**, have all been detected. Complex **11** affords a modestly complicated spectrum (see spectrum A), due to the ABMX spin system. The oxa-allyl complex, **12**, in spectrum B exists in two diastereomeric forms (with overlapping signals between 48 and 49 ppm). The resonances for the bridging hydro-

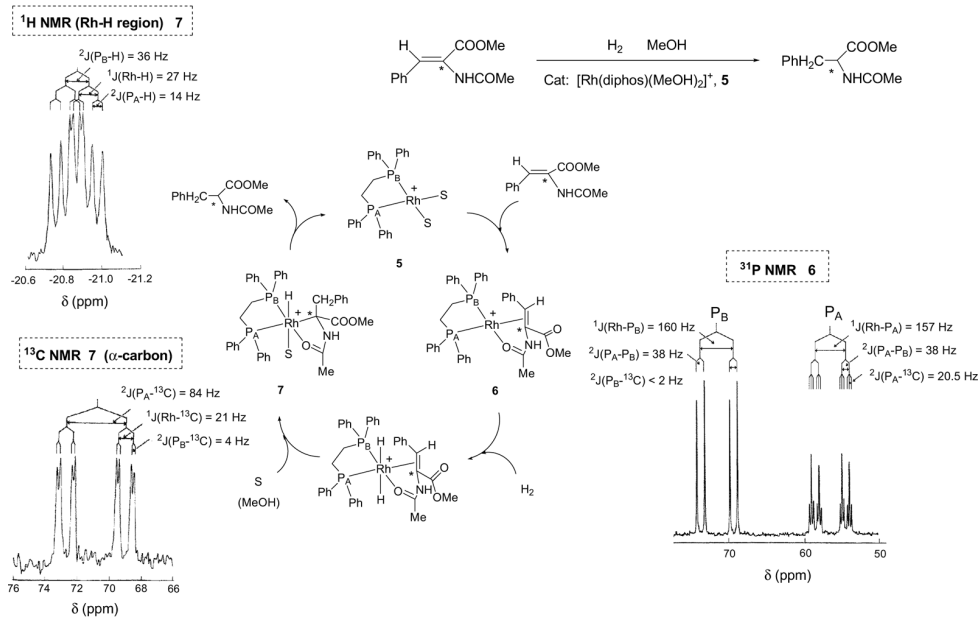


Figure 1.2 Catalytic cycle for the Rh-catalyzed hydrogenation of methyl-(Z)- α -acetamidocinnamate, (50% ^{13}C in the α -C, denoted by *) in MeOH.

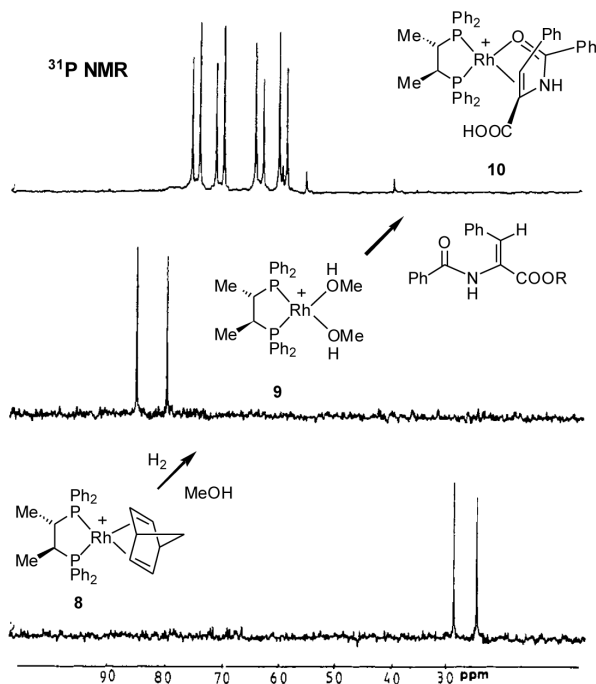


Figure 1.3 Stable intermediates in the enamide hydrogenation by (*S,S*)-trans-bis(2,3-diphenylphosphino-butane)rhodium, detected by ^{31}P NMR. The various multiplicities arise from $^1J(^{103}\text{Rh}, ^{31}\text{P})$ and $^3J(^{31}\text{P}, ^{31}\text{P})$.

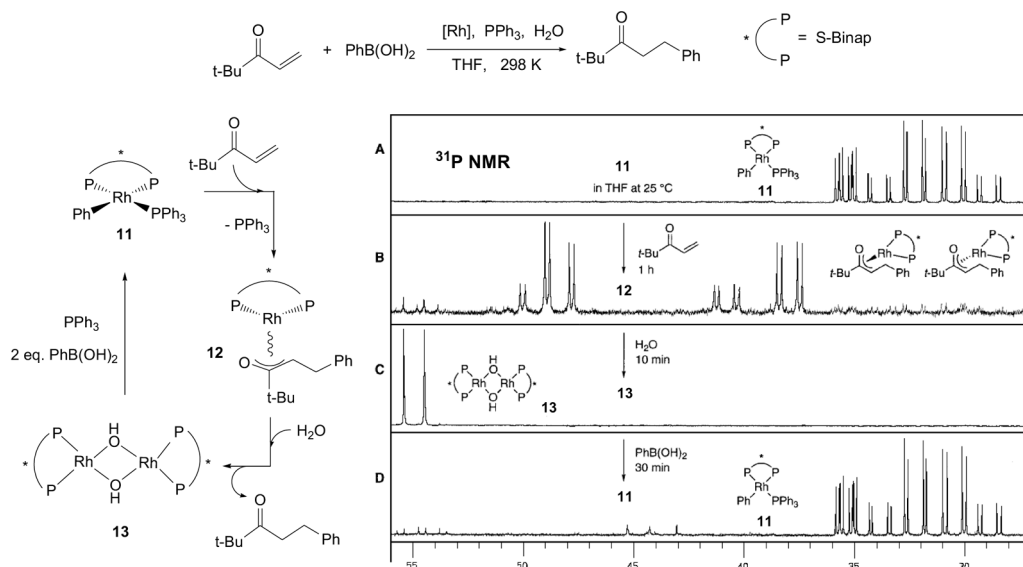


Figure 1.4 Mechanistic aspects of the Rh-catalyzed 1,4-addition of phenylboronic acid to an α,β -unsaturated ketone, monitored by ^{31}P NMR.

xide **13**, with equivalent P-atoms, are observed, in spectrum C, at ca. 55 ppm. The starting PPh_3 complex, **11**, is regenerated in spectrum D.

In the zirconocene-catalyzed polymerization of alkenes, Landis and coworkers [20] have reported in situ observation of a Zr-polymeryl species, **15**, at 233 K (Figure 1.5). Complex **15** is formed by partial reaction of **14** with excess 1-hexene. Derivatives **16** and **17** are generated quantitatively from **15** by addition of ca. 10 equiv. of propene and ethene, respectively. No other intermediates, such as alkene complexes, secondary alkyls, diastereomers of **15** or **16**, or termination products, accumulate to detectable levels. These NMR studies permit direct monitoring of the initiation, propagation and termination processes, and provide a definitive distinction between intermittent and continuous propagation behavior.

Espinet and coworkers [21] have captured an NMR “snapshot” of a catalytic cycle for the Stille reaction, involving compounds **18–22** (see Figure 1.6). The vinylic region of the ^1H and $^1\text{H}\{^{31}\text{P}\}$ NMR spectra of **19–22** is shown. Both $\text{Pd(II)} \text{Pd(vinyl)R(PP)}$, **20** and $\text{Pd(0)} \text{Pd(RCH=CH}_2\text{)(PP)}$, **21** species were identified.

Brown and coworkers [22] have studied the Pd-catalyzed Heck arylation of methyl acrylate via ^{31}P and ^{13}C NMR (see Figure 1.7). Reaction of the aryl iodide complex **23** with AgOTf (THF, 195 K) gives the THF and aquo-complexes **24** and **25**, respectively, which were detected via ^{31}P NMR below 203 K. Addition of H_2O to the sample shifts the equilibrium towards **25**, pointing to an existing fast exchange between solvates **24** and **25**. Reaction of **24/25** with 3- $\{^{13}\text{C}\}$ labeled methyl acrylate (20-fold excess, 213 K) affords the insertion product **26**. Warming to 233 K leads to the formation of **27**, which is in turn converted into **29**, stable to

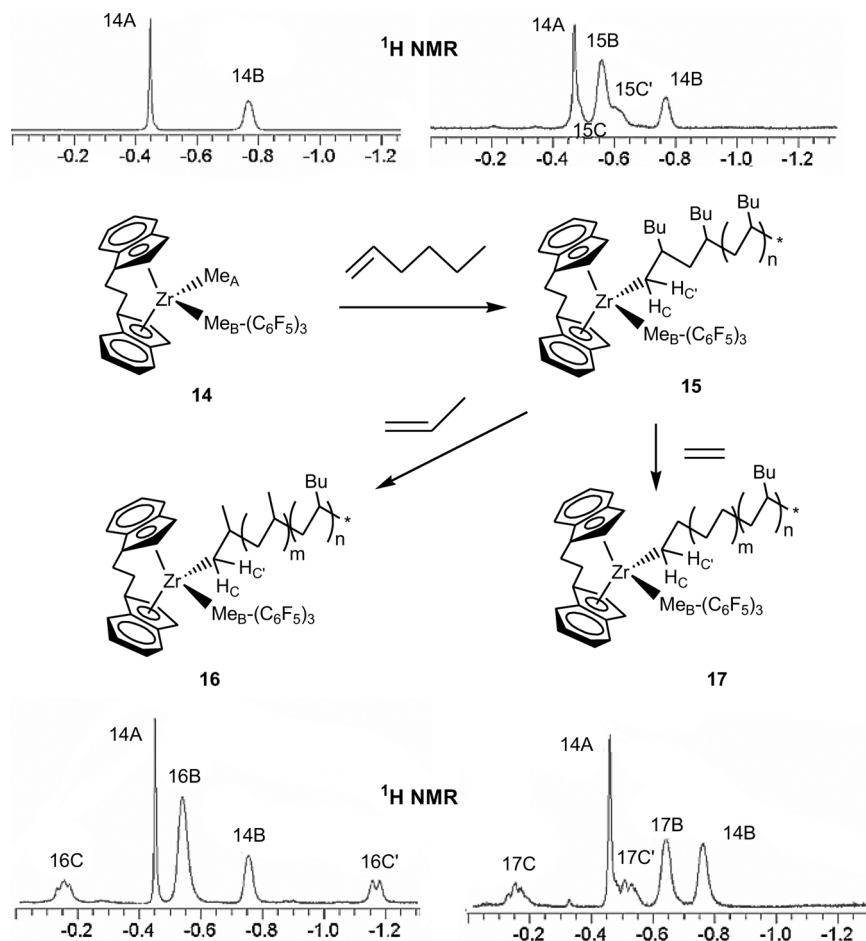
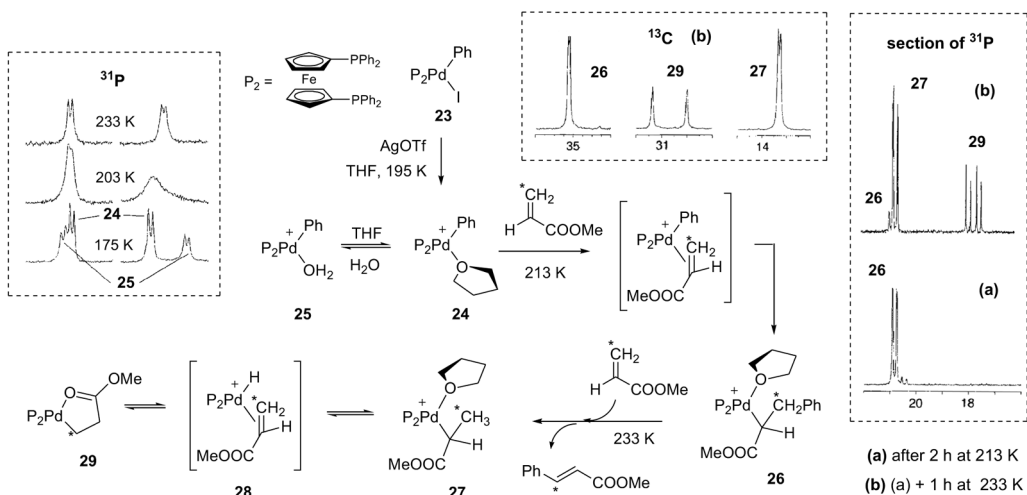
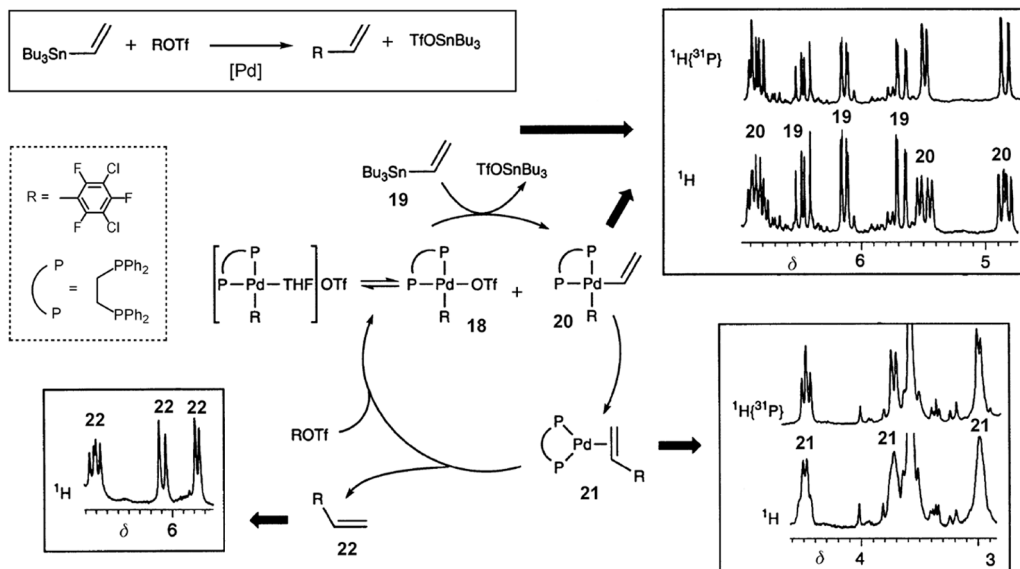


Figure 1.5 *In situ* Detection of Zr-polymer species by ^1H NMR (233 K, d^8 -toluene). Only the region between 0 and -1.3 ppm is shown, in which resolved resonances for the diastereotopic Zr-CH₂-POL protons and the Zr-Me-B groups are detected.

273 K. The rearrangement from 27 to the more stable, primary alkyl regioisomer 29 was shown to be intermolecular. This is thought to occur via the unobserved hydride 28, since addition of unlabeled methyl acrylate leads to the equilibrium distribution of ^{13}C label in 29 (28 exchanges acrylate ligands with the acrylate pool).

Using ^{31}P NMR the same authors have identified several intermediates in the asymmetric Heck arylation of dihydrofuran [23, 24]. Reaction of the Binap salt, 30, with 2,3-dihydrofuran below 233 K gave salt 31 as the single species (see Figure 1.8). A parallel reaction between 30 and $[2\text{-}^2\text{H}]$ 2,3-dihydrofuran confirmed the structure. At 243 K, 31 slowly decomposed to form 32 and 32' with concomitant release of the coupling product 33 (91 % ee).



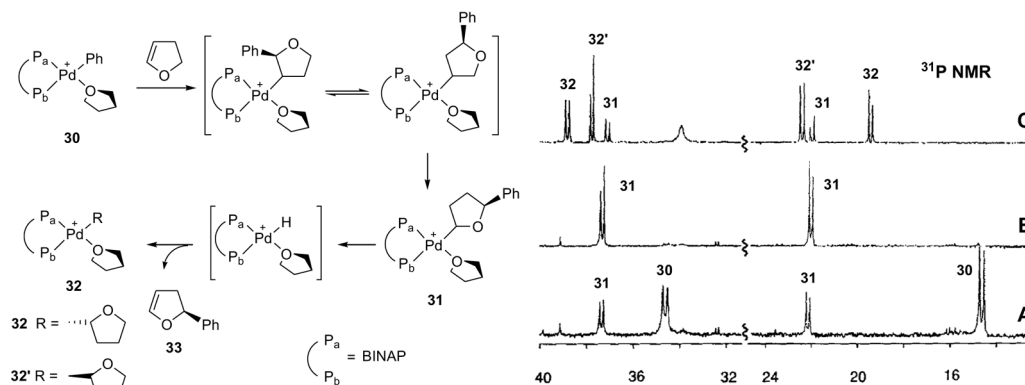
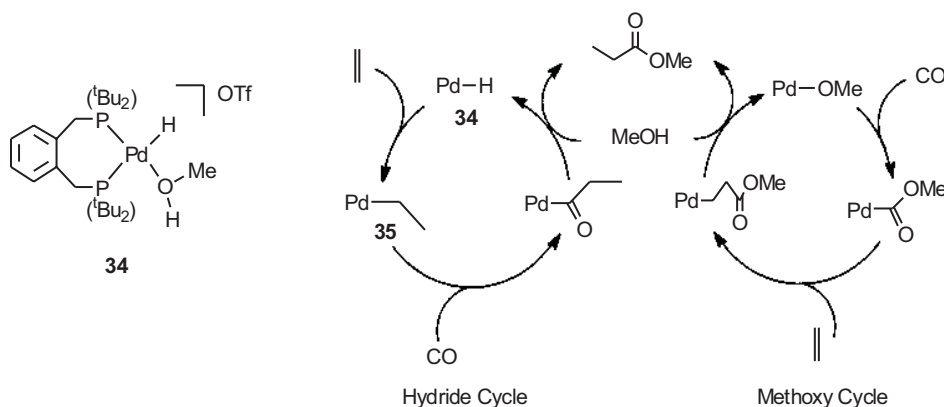


Figure 1.8 ^{31}P NMR spectra of the reaction sequence between **30** and 2,3-dihydrofuran. Spectrum A: partial conversion of **30** to **31** at 223 K. Spectrum B: After complete formation of **31** at 223 K. Spectrum C: nearly complete decomposition of **31** at 243 K to form **32** and **32'**. The signals at higher frequency correspond to P_a .

For the industrially important Pd-catalyzed methoxycarbonylation of ethene to methyl propanoate, all the intermediates of the cycle have been identified. Starting from **34**, $^{13}\text{CH}_2=\text{CH}_2$ and ^{13}CO , the process has been shown to proceed via a hydride rather than a methoxycarbonyl cycle (Scheme 1.1) [25][26]. Figure 1.9 shows the ^{31}P NMR spectrum at 193 K of a 1:1 mixture of the two isotopomers **35a** and **35b**, formed in the reaction of **34** with $^{13}\text{CH}_2=^{12}\text{CH}_2$. The presence of an agostic interaction is supported by the ^{13}C chemical shifts ($\delta(\text{CH}_2)$ 31, and $\delta(\text{CH}_3)$ 8), which are reversed with respect to classical Pd-ethyl complexes.



Scheme 1.1 The two possible mechanisms for the Pd-catalysed methoxycarbonylation of ethene.

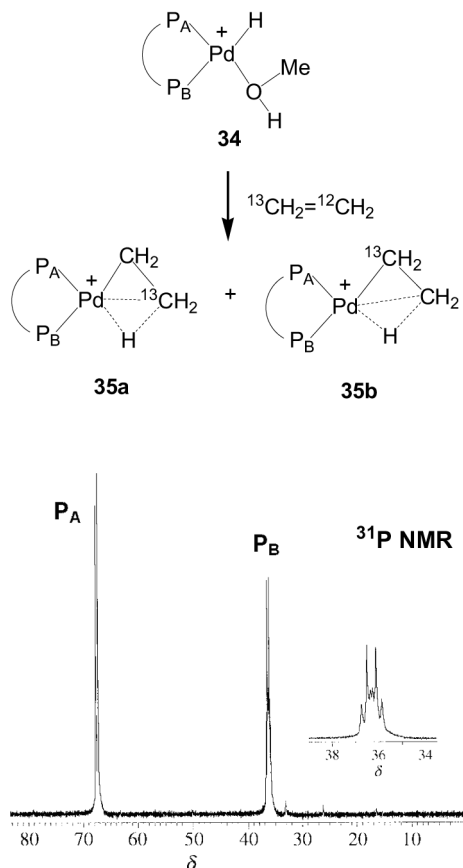


Figure 1.9 ^{31}P NMR spectrum at 193 K of a 1:1 mixture of the two isotopomers $[\text{Pd}(\text{L}-\text{L})(\text{CH}_2^{13}\text{CH}_3)]^+$, **35a**, and $[\text{Pd}(\text{L}-\text{L})(^{13}\text{CH}_2\text{CH}_3)]^+$, **35b**, formed in the reaction of **34** with $^{13}\text{CH}_2=^{12}\text{CH}_2$. For **35a**, the phosphorus trans to the ethyl group (P_B δ 36.1) couples with the cis-phosphorus P_A [δ 68, $^2J(^{31}\text{P}_\text{A}, ^{31}\text{P}_\text{B})$ 31 Hz], while the $^2J(^{31}\text{P}_\text{B}, ^{13}\text{C})$ is not observed due to the low natural abundance of ^{13}C . In **35b**, however, the coupling of P_B with both P_A and the labelled trans carbon atom [$^2J(^{31}\text{P}_\text{B}, ^{13}\text{C})$ 38 Hz] can be observed, resulting in a doublet of doublets, which is superimposed with the doublet originating from **35a**.

In situ NMR studies on analogous Pt catalysts for the methoxycarbonylation reaction reveal CO trapping at *every* step in the catalytic cycle of the active intermediates (Figure 1.10) [27]. This explains the observed slow kinetics. Thus, **36** reacts with ^{13}CO in CH_2Cl_2 at 193 K to form only $[\text{Pt}(\text{L}-\text{L})(\text{C}_2\text{H}_5)(^{13}\text{CO})]^+$, **37**, which upon warming to ambient temperature in the presence of excess CO affords $[\text{Pt}(\text{L}-\text{L})(^{13}\text{C}(\text{O})\text{Et})(^{13}\text{CO})]^+$, **38**. This transformation is *reversible*, and both compounds have been detected by in situ $^{13}\text{C}\{^1\text{H}\}$ NMR spectroscopy.

1.2.2

Reaction Kinetics via NMR

The previous section focused on the detection of intermediates in a catalytic reaction, thereby affording an “NMR picture” of the several steps involved in the mechanism. Occasionally, NMR can be a convenient tool for monitoring reaction rates provided that the reaction is slow enough for a series of 1D spectra to be acquired during its course.

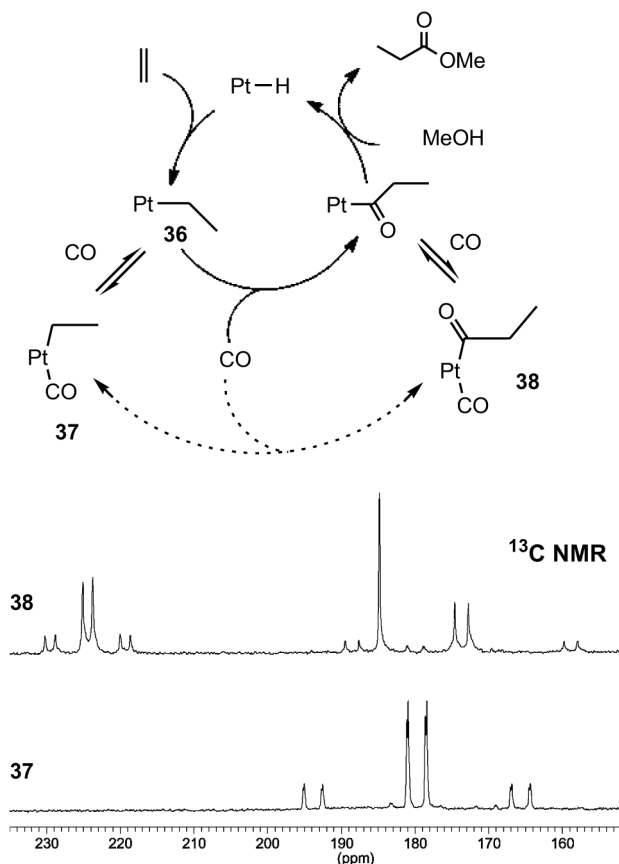


Figure 1.10 Pt-catalysed methoxycarbonylation of ethene, studied by ¹³C NMR.

Figure 1.11 provides an example of ¹H NMR monitoring in the Pd-catalyzed cycloisomerization of dimethyl diallyl malonate, **39** [28]. The kinetic profile reveals a pronounced induction period after which the exocyclic alkene **40a** is formed predominantly as the kinetic product. A hydropalladation mechanism was proposed on the basis of NMR experiments, and the transient species **41**, formed by allylpalladation of the coordinated diene, could be detected and identified with the help of ²H and ¹³C labeling. The hydride Pd catalyst, **42**, would be generated from **41** by water-promoted β-hydride elimination. The observed induction period is associated with the formation of the Pd-hydride **42**.

In the oxidative addition of a fluorinated aryl iodide, **43**, to “Pd(PPh₃)₂” (Figure 1.12) [29], ¹⁹F NMR has been used to follow the cis-to-trans isomerization of the cis-bis-phosphine product, **44**, to the trans-isomer, **45**. The ¹⁹F NMR kinetic study reveals a first order dependence for the rate of isomerization on the concentration of **44**. An application of a ¹⁹F NMR kinetic study to the evaluation of the

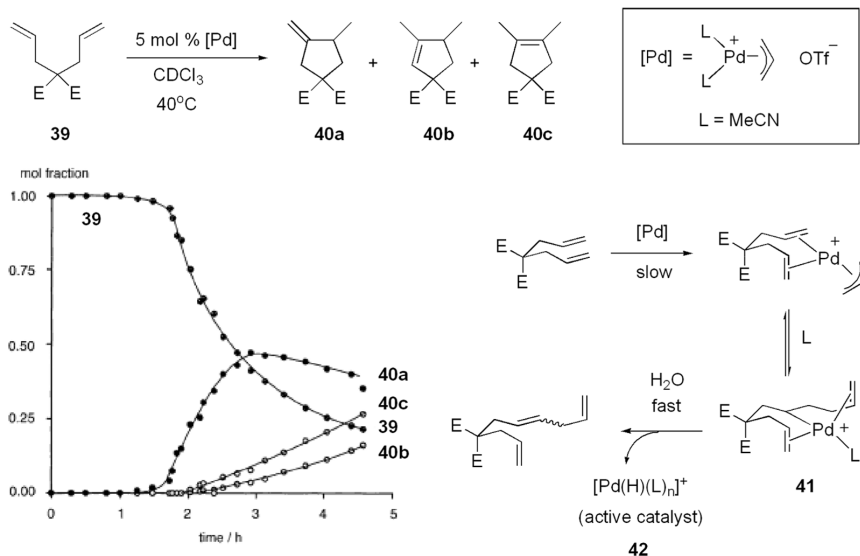


Figure 1.11 Pd-catalysed cycloisomerisation of dimethyl diallyl malonate. Kinetic profile based on ^1H NMR, and proposed reaction mechanism.

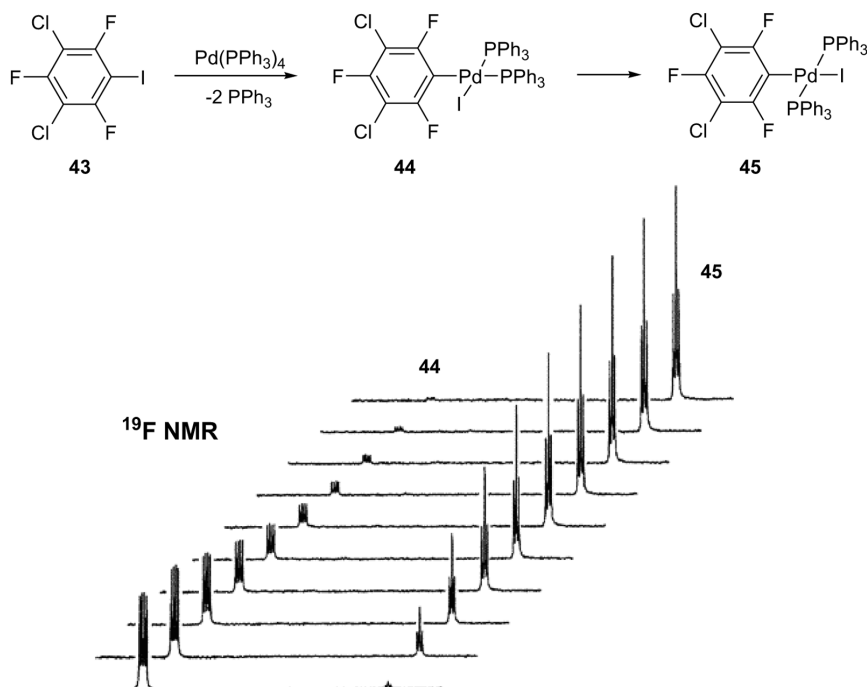
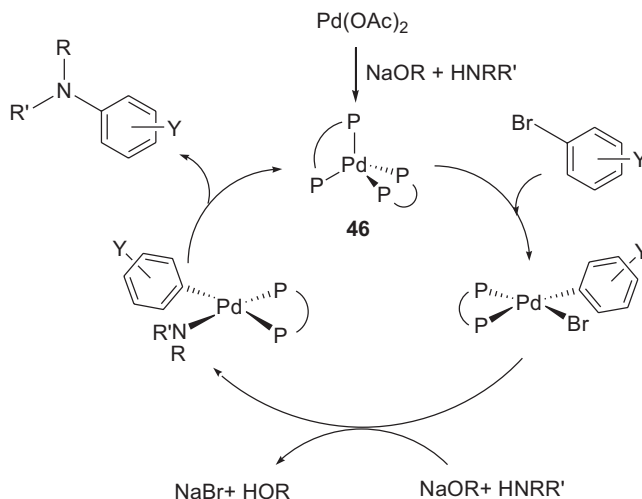


Figure 1.12 ^{19}F NMR study of the cis-to-trans isomerization of **44** to **45**. Only the ortho ^{19}F resonances are shown. In **44**, the coupling with two inequivalent ^{31}P atoms affords a doublet of doublets. For **45**, the spectrum consists of a triplet.



Scheme 1.2 Pd-catalysed amination of aryl halides using the chiral ligand Binap.

factors contributing to the “copper effect” in the Stille reaction has also been reported [30].

In the Pd-catalyzed amination of aryl halides using Binap, the $\text{Pd}(0)$ complex $\text{Pd}(\text{Binap})_2$, **46**, has been identified by ^{31}P NMR as the resting state in the catalytic cycle (Scheme 1.2) [31]. The zero-order dependence of the reaction rate on the amine concentration has been confirmed via a ^1H NMR study with primary amines (Figure 1.13, left). For secondary amines, however, a first-order dependence on amine was apparent (Figure 1.13, right), suggesting a change in the resting state of the catalyst to one that would react with the amine. ^{31}P monitoring of the catalyst concentration (Figure 1.13, center) showed a gradual consumption of **46** in the reaction with the secondary amine, but not with the primary, explaining the different kinetic behavior.

We note that there are NMR-based kinetic studies on zirconocene-catalyzed propene polymerization [32], Rh-catalyzed asymmetric hydrogenation of olefins [33], titanocene-catalyzed hydroboration of alkenes and alkynes [34], Pd-catalyzed olefin polymerizations [35], ethylene and CO copolymerization [36] and phosphine dissociation from a Ru-carbene metathesis catalyst [37], just to mention a few.

Finally, an example of reaction monitoring with a “rare” nucleus: Figure 1.14 reproduces three sequences of ^{11}B NMR spectra of the Zr-catalysts **47–49**/MAO (MAO = methylaluminoxane) during the polymerization of ethylene [38]. No changes are detected in the systems **47**/MAO (a) and **49**/MAO (c) during the course of reaction; however, for **48**/MAO in (b), a new ^{11}B signal appears. This is attributed to an exchange of the boron benzyloxy substituent of **48** with the methyl from the MAO, effectively transforming **48** into **49**. This transformation of the catalyst is thought to explain why the selectivity of the **48**/MAO system

for α -olefin production is intermediate between that of the similar **47**/MAO (more than 99% α -olefins) and **49**/MAO (which reacts with the 1-alkenes and converts them to other isomers).

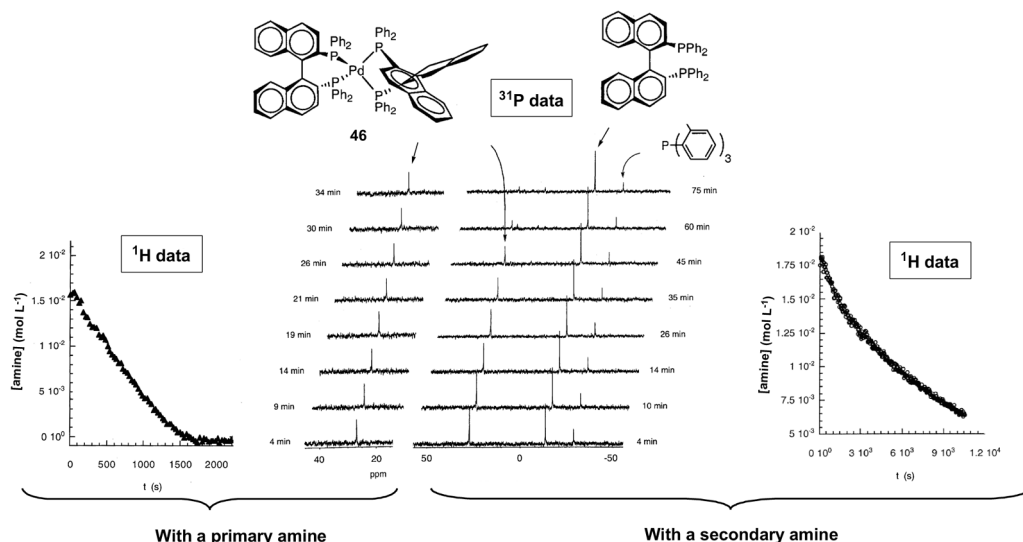


Figure 1.13 Decay of the concentration of a primary amine (hexylamine, left) and a secondary amine (*N*-methylaniline, right) during the reaction with BrC_6H_5 catalyzed by **46**, followed by ^1H NMR. The reaction is zero-order in the primary amine (linear concentration decay) and first-order in the secondary amine (nonlinear concentration decay). Center: ^{31}P NMR spectra acquired during the reaction of aniline (left) and *N*-methylaniline (right) with BrPh catalyzed by **46**. $\text{P}(\text{o-Tol})_3$ is used as internal standard.

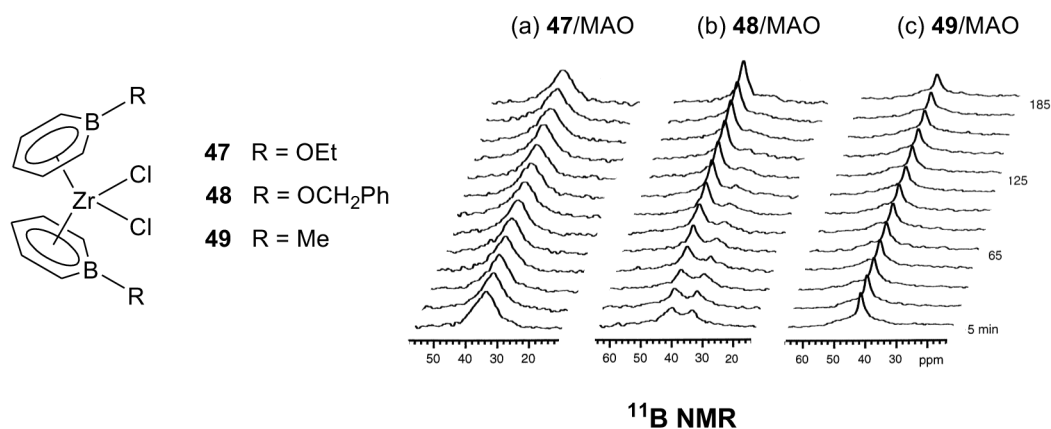


Figure 1.14 A ^{11}B NMR study on the Zr-catalyzed polymerization of ethylene.

1.3

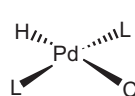
Structural Tools

In the studies on detecting intermediates many of the structural conclusions drawn were based on our (often empirical) understanding of chemical shifts and spin–spin interactions. In the following two sections we show a selection of these in connection with (mostly) catalytically relevant organometallic molecules.

1.3.1

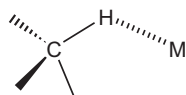
Chemical Shifts

The ^1H signals for transition metal hydrides, $\text{MH}(\text{L})_n$, $\text{M} = \text{Ru}, \text{Rh}, \text{Ir}, \text{Pt}$ etc., afford very low frequency ^1H resonance positions, usually in the range δ ca. -5 to -30 . Several values for palladium hydrides, **50**, (often postulated in catalysis, but rarely observed) are shown below [39].

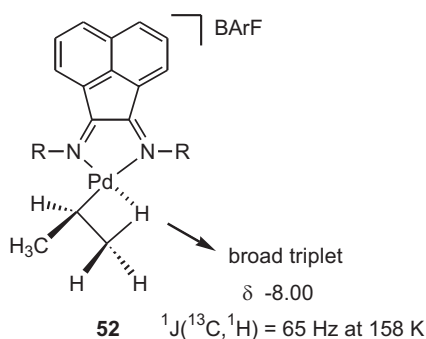
	L	δ
	PEt_3	-13.6
	PCy_3	-14.4
	PPh_3	-13.2
50		

$[\text{RhH}(\text{Cp}^*)(\text{Binap})](\text{SbF}_6)$, a presumed intermediate in the hydrosilylation of phenyl acetylene [40], shows the hydride resonance at $\delta -10.39$. Hydride resonances in $\text{Ru}(\text{II})$ phosphine complexes are often found in the same region [41–43].

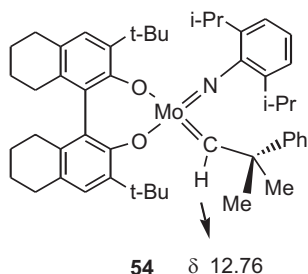
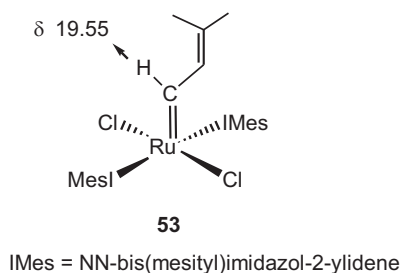
Agostic interactions, i. e., the three-center bonds related to structure **51** [26, 44–49], were noted earlier by Green and Brookhart and have been cited above in the methoxycarbonylation chemistry (Figure 1.9). These bonds are often characterized by low frequency (hydride-like) proton chemical shifts, and/or substantially reduced $^1J(^{13}\text{C}, ^1\text{H})$ values. Often, it is necessary to cool the NMR sample in order to “freeze” the equilibrium. Complex **52** represents a nice example of an agostic C–H bond, with relevance to polymerization chemistry [47].

**51**

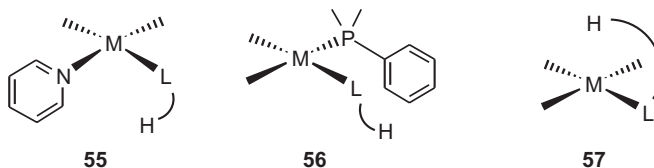
M = transition metal



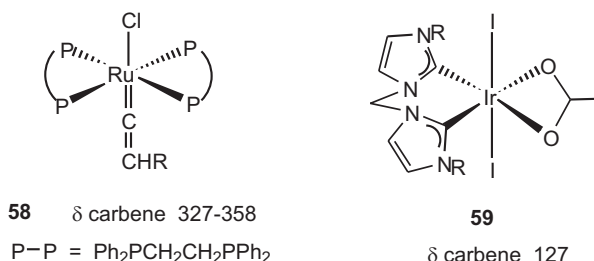
The ^1H signals of carbene-based metathesis catalysts can be found at relatively high frequency, e.g., δ 19.55 in **53** [50], or δ 12.76 in one isomer of **54** [51].



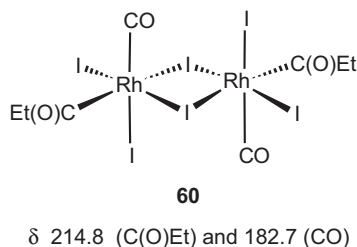
With respect to ^1H chemical shifts, two additional general points are worth noting: (a) due to local anisotropic effects, protons in cis-position to pyridine or phenyl phosphine ligands afford low frequency ^1H signals (Structures **55** and **56**), and (b) not so well recognized, but still useful, is the fact that square planar metal complexes have very anisotropic regions above and below the coordination plane, e.g., in **57**, the proton moves to higher frequency. This positioning can result in a weak bond to the metal [52, 53].



For the heavier nuclei, such as ^{13}C and ^{31}P , where both the nature of the bonding and the corresponding energy level considerations determine the chemical shifts [54–56], the chemical shift range (and variation with structure) is much larger than for protons. The ^{13}C resonances for the Ru(II) carbene atoms in **58** [57] appear at very high frequency. Interestingly, for the Ir(III) bis-carbene complex **59** [58], thought to be involved in transfer hydrogenation chemistry, the observed ^{13}C position for the carbene atom is only ca. 127 ppm.

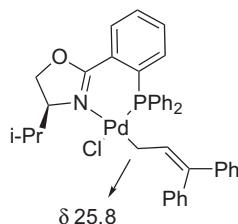


The carbon of complexed CO, i. e., M–CO, can appear at either a lower or higher frequency than CO itself, depending on the metal. A useful list of ^{13}C chemical shifts can be found in a study describing mechanistic aspects of the Rh- and Ir-catalyzed carbonylation of methanol [59]. Additional ^{13}C NMR data on Rh-acyl intermediates, derived from the Rh-catalyzed carbonylation of ethene, e. g., **60**, have been reported [60].



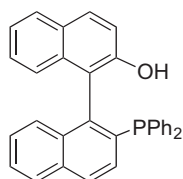
An aliphatic metal–carbon sigma bond, e. g., $\eta^1 \text{M-CH}_3$, affords a fairly small ^{13}C chemical shift, sometimes at negative δ values. The relatively rare η^1 allyl derivative, $\text{PdCl}(\eta^1 \text{allyl})(\text{PHOX})$, **61** [61], which is related to allylic alkylation chemistry, shows

a normal low frequency sigma bound methylene carbon resonance, thereby clearly indicating that the bonding is not of the usual η^3 type.

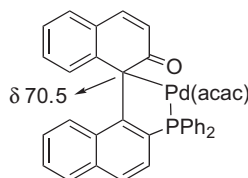


61

The rather novel hydroxy MOP-derived Pd(II) complex **63** [62], derived from the MOP chiral auxiliary **62**, reveals an unexpected σ -bond with the fully substituted coordinated carbon at δ 70.5, thus indicating that this carbon is no longer aromatic.

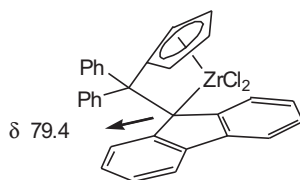


62 OH-MOP



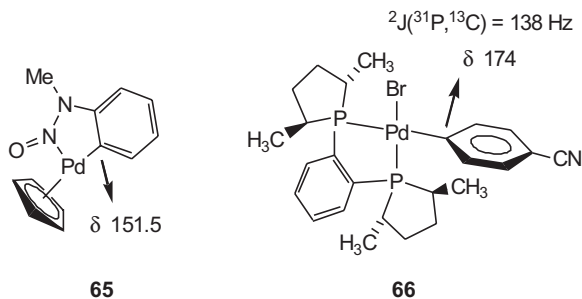
63

In a related fashion, the ^{13}C resonance at δ 79.4 from the Zr(ansa-Fluorenyl) polymerization catalyst precursor **64**, is consistent with substantial sp^3 character at this carbon [2].

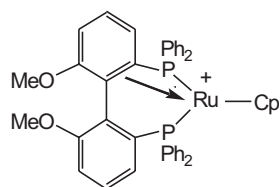


64

However, the ^{13}C chemical shift for a σ -bound M-aryl bond appears at high frequency, often between 130 and 180 ppm. Both the cyclometallated nitrosoamine compound **65** [63–65] and the Pd(II)(Duphos) complex **66** (an intermediate in the enantioselective hydroarylation of norbornene) [66] represent typical examples.

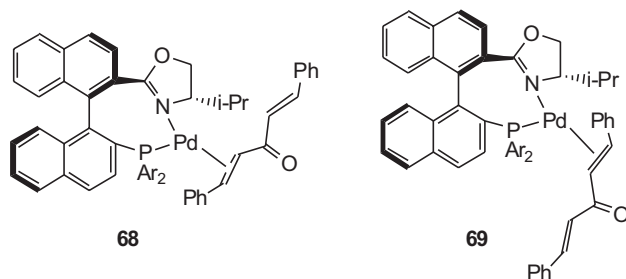


The ^{13}C signals for coordinated olefin ligands are often (but not always) markedly shifted to low frequency. The position of these formerly sp^2 carbons depends strongly on the π -back-bonding characteristics of the metal, together with the donor characteristics of the remaining ligands in the coordination sphere. The Ru(II) compound **67**, in which the MeO-Biphep is acting as a 6e donor, shows the complexed olefinic ^{13}C signals at δ 66.4 and δ 86.5, in the region expected for a coordinated double bond (despite the relatively long Ru–C distances found in the solid state) [67].



67 $\delta(\text{C}=\text{C})$ 66.4 and 86.5

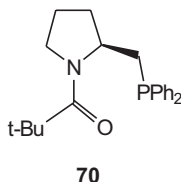
The two isomeric Pd(0)(dba)(phosphino-oxazoline) Heck catalyst precursors **68** and **69** show the two olefinic resonances at δ 56.0 and δ 69.3, plus δ 56.0 and δ 67.3 [68].



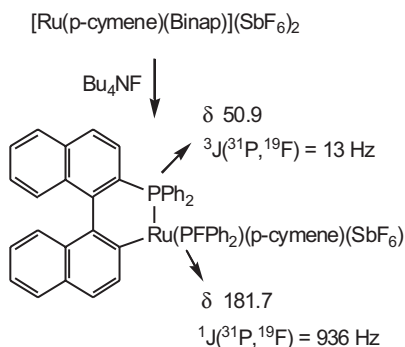
^{13}C resonances for complexed η^6 -arene moieties, e.g. $\text{Ru}(\text{II})(\eta^6\text{-}p\text{-cymene or } \eta^6\text{-benzene})$ are often found between 60 and 100 ppm [69–77].

^{31}P represents a favored NMR nucleus when phosphine precursors are used in catalysis. For tertiary phosphine complexes the normal chemical shift range is several hundred ppm. There are a few useful empiricisms:

1. The coordination chemical shift, $\Delta\delta = \delta(\text{complex}) - \delta(\text{ligand})$, is often fairly large and positive. Via integration of the ^{31}P signal it is possible to determine the number of complexed ligands in a catalyst precursor. In their enantioselective C–C bond-making catalytic studies, Tomioka and coworkers [78] have used this approach to show that $\text{Rh}(\text{acac})(\text{C}_2\text{H}_4)_2$ reacts sequentially with one, two and three equivalents of **70** to form different materials. The first equivalent affords a P,O-chelate complex, the second a bis-phosphine derivative and the third equivalent of phosphine is not complexed to rhodium.



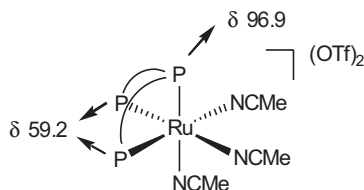
2. Binding strongly electron withdrawing groups to the P-atoms, e.g., several P–F or P–O bonds, usually shifts the ^{31}P signal to higher frequency. Occasionally this can happen when P–C bonds are cleaved, as in Scheme 1.3, where the coordinated PFPh_2 ligand appears at δ 181.7, more than 100 ppm away from the aryl phosphine [79].



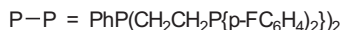
Scheme 1.3 Shift to higher frequency of the ^{31}P chemical shift in a PFPh_2 ligand with respect to an aryl phosphine.

3. Including the P-atom in one or more five-membered rings (chelation or cyclo-metallation) strongly moves the ^{31}P signal to high frequency. The $\text{Ru}(\text{II})$ acetalization catalyst **71** [80] demonstrates the chelation principle in that the central

P-donor appears at much higher frequency, 96.9 ppm, than the two equivalent terminal P-ligand atoms. There are many more useful details and the reader would do well to consult a suitable review [81].

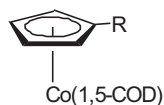


71



Metal chemical shifts have not found extensive use in relation to structural problems in catalysis. This is partially due to the relatively poor sensitivity of many (but not all) spin $I = 1/2$ metals. The most interesting exception concerns ^{195}Pt , which is 33.7% abundant and possesses a relatively large magnetic moment. Platinum chemistry often serves as a model for the catalytically more useful palladium. Additionally, ^{195}Pt NMR, has been used in connection with the hydrosilylation and hydroformylation reactions. In the former area, Roy and Taylor [82] have prepared the catalysts $\text{Pt}(\text{SiCl}_2\text{Me})_2(1,5\text{-COD})$ and $[\text{Pt}(\mu\text{-Cl})(\text{SiCl}_2\text{Me})(\eta^2\text{-}1,5\text{-COD})]_2$ and used ^{195}Pt methods (plus ^{29}Si and ^{13}C NMR) to characterize these and related compounds. These represent the first stable alkene platinum silyl complexes and their reactions are thought to support the often-cited Chalk–Harrod hydrosilylation mechanism.

Philipsborn and coworkers [83] have successfully used the ^{59}Co signals in the substituted $\text{Co}(\text{I})\text{Cp}$ complexes **72**, in connection with understanding the mechanism of pyridine/acetylene trimerization reactions. The metal resonance was found to vary strongly with the catalyst structure and a correlation of $\delta^{59}\text{Co}$ with reactivity was observed.



72

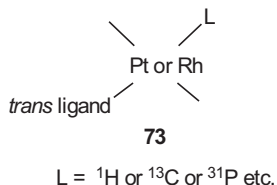
The groups of Philipsborn [84], Heaton [85–88] and Mann [89–91] have used ^{103}Rh NMR extensively to elucidate structural and mechanistic aspects of a wide variety of metal carbonyl and metal cluster complexes. Further, Zamaraev [92] has shown that NMR studies on several quadrupolar nuclei, e.g. ^{95}Mo , help with the characterization of the alkyl peroxo-complexes, which are thought to be inter-

mediates in the course of the homogeneous epoxidation of cyclohexene and oxidation of cyclohexane. Clearly, metal NMR in catalysis remains promising, but relatively undeveloped.

1.3.2

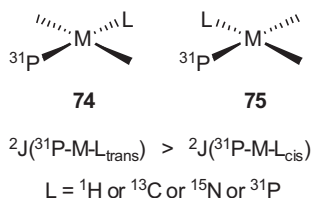
Coupling Constants

All of the many one, two and three-bond interactions in organic molecules, e. g., the various Karplus relations involving $^3J(X,Y)$ as a function of dihedral angle, or the $^3J(^{13}\text{C}, ^1\text{H})$ interaction used to find fully substituted ^{13}C signals in Figure 1.1 (b), find wide ranging applications. However, if we center on those spin–spin interactions that directly involve the transition metal, then $^1J(\text{M},\text{L})$ and $^2J(\text{L}^1\text{--M--L}^2)$ (L = a donor atom) have proven, generally, to be the most helpful in terms of defining the local coordination sphere. In square planar and octahedral complexes, **73**, $^1J(\text{M},\text{L})$ depends on the trans-ligand, with stronger donors reducing the $^1J(\text{M},\text{L})$ value.

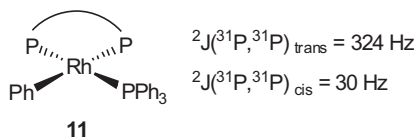


This empiricism (which concerns the concept of trans-influence) [93] is derived from theory and the Fermi contact term. Since the s-component of the M–L bond determines the magnitude of $^1J(\text{M},\text{L})$, bonding considerations which decrease the s-component, e. g., a relatively strong σ -bond in the trans-position, decrease $^1J(\text{M},\text{L})$. In Wilkinson's catalyst, $\text{RhCl}(\text{PPh}_3)_3$, (and the *p*-tolyl analog) the two $^1J(^{103}\text{Rh}, ^{31}\text{P})$ values are quite different: 189 Hz (P trans to Cl) and 142 Hz (P trans to P) [94]. The larger 1J -value arises from the P-atom trans to the weaker donor.

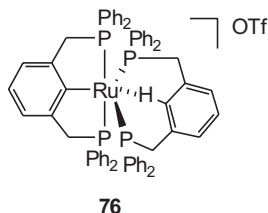
For the second and third transition series, the values $^2J(\text{L}^1\text{--M--L}^2)$ depend strongly on geometry, as indicated in **74** and **75**, with the trans-interactions being normally much larger than those for the corresponding cis-compounds.



A specific example can be found in the Rh-chemistry mentioned in connection with Figure 1.4. The complex $\text{RhPh}(\text{PPh}_3)(\text{Binap})$, **11**, shows very different $^2J(^{31}\text{P}, ^{31}\text{P})$ values with the trans-interaction much larger than the cis. Taken together, the three different ^{31}P chemical shifts and the various $^1J(^{103}\text{Rh}, ^{31}\text{P})$ and $^2J(^{31}\text{P}, ^{31}\text{P})$ values are all important indicators of the correct structure for this complex.



The cationic $\text{Ru}(\text{II})$ phosphine“pincer” complex **76** [95], which contains an agostic $\text{Ru}-\text{H}-\text{C}$ bond, possesses four different P-atoms and thus demonstrates the geometric dependence of $^2J(^{31}\text{P}, ^{31}\text{P})$. The fairly small $^1J(^{13}\text{C}, ^1\text{H})$ value, 112 Hz, helps in the recognition of the agostic bond and is 46 Hz smaller than in the free ligand.



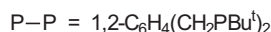
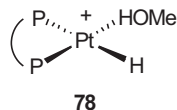
$$^2J(^{31}\text{P}, ^{31}\text{P})_{\text{trans}} = 345.7 \text{ Hz and } 233.3 \text{ Hz}$$

$$^2J(^{31}\text{P}, ^{31}\text{P})_{\text{cis}} = 34.6 \text{ Hz, } 26.7 \text{ Hz and } 27.1 \text{ Hz}$$

We note that in the Palladium salt **35** (Figure 1.9) a large $^2J(^{31}\text{P}, ^{13}\text{C})_{\text{trans}}$ value is reported.

An important consequence of the often relatively large $^2J(^{31}\text{P}, ^{31}\text{P})$ value is that ^{13}C spectra of bis-phosphine complexes are often second order, e. g., the $=\text{CH}$ signals for the two isomers of $[\text{Pd}(\text{NCCH}=\text{CHCN})(\text{Me-Duphos})]$, **77**, see Figure 1.15 [3]. The figure shows that these absorptions appear as complicated multiplets (i. e., the X-part of an ABX spin system).

The cationic $\text{Pt}(\text{II})$ hydride **78** [27], a model for the analogous Pd intermediate which is thought to be involved in the methoxycarbonylation of ethene (see Scheme 1.1 and Figure 1.10), also shows the expected markedly different $^2J(^{31}\text{P}, ^1\text{H})$ values.



$$^2J(^{31}\text{P}, ^1\text{H}) = 176 \text{ Hz (trans) and } 18 \text{ Hz (cis)}$$

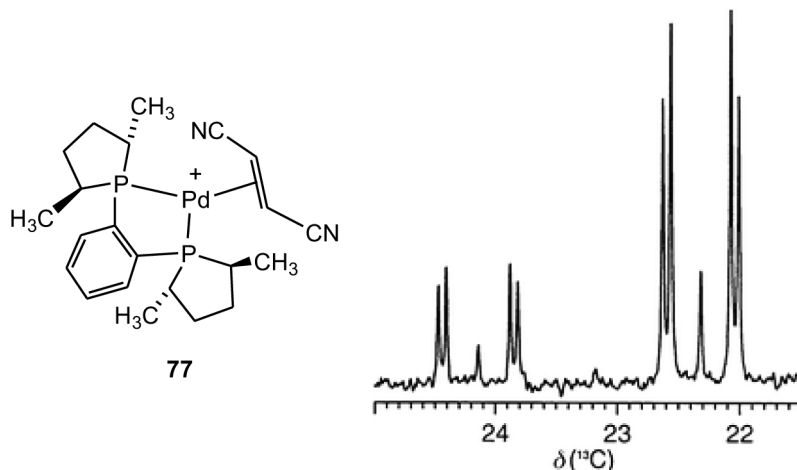
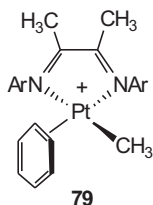


Figure 1.15 Section of the ^{13}C NMR spectrum of **77**, showing the second-order ABX character for the two isomers of the two olefinic $^{13}\text{CH=}$ resonances of the fumaronitrile ligand. The separation of the two most intense lines represents $^2J(^{31}\text{P}, ^{13}\text{C})_{\text{cis}} + ^2J(^{31}\text{P}, ^{13}\text{C})_{\text{trans}}$.

Rounding off this section, the Pt(II) (diimine) complex **79** [96], a possible intermediate in C,H-activation chemistry, shows a 23.5 Hz $^2J(^{195}\text{Pt}, ^1\text{H})$ coupling to the (averaged) $\eta^2\text{-C}_6\text{H}_6$ protons, thus helping to support the η^2 olefin structure.

The examples above comprise only a small fraction of the catalytically relevant NMR literature; however, they are representative.



1.3.3

NOE Spectroscopy and 3-D Structure

The increasing interest in enantioselective homogeneous catalysis has led to questions with respect to how the auxiliaries transfer their chiral information to the coordinated substrate. In solution, the position of the chiral auxiliary relative to the complexed organic ligand is best determined via ^1H - ^1H NOESY studies. Although this methodology enjoys a long history in biochemistry, there are still relatively few applications involving chiral organometallic complexes [22, 61, 97–128].

Early NOE studies on cationic Pd(II) allyl complexes used “reporter ligands” [97, 98], i. e. simple bidentate nitrogen ligands, such as bipy or phenanthroline, whose

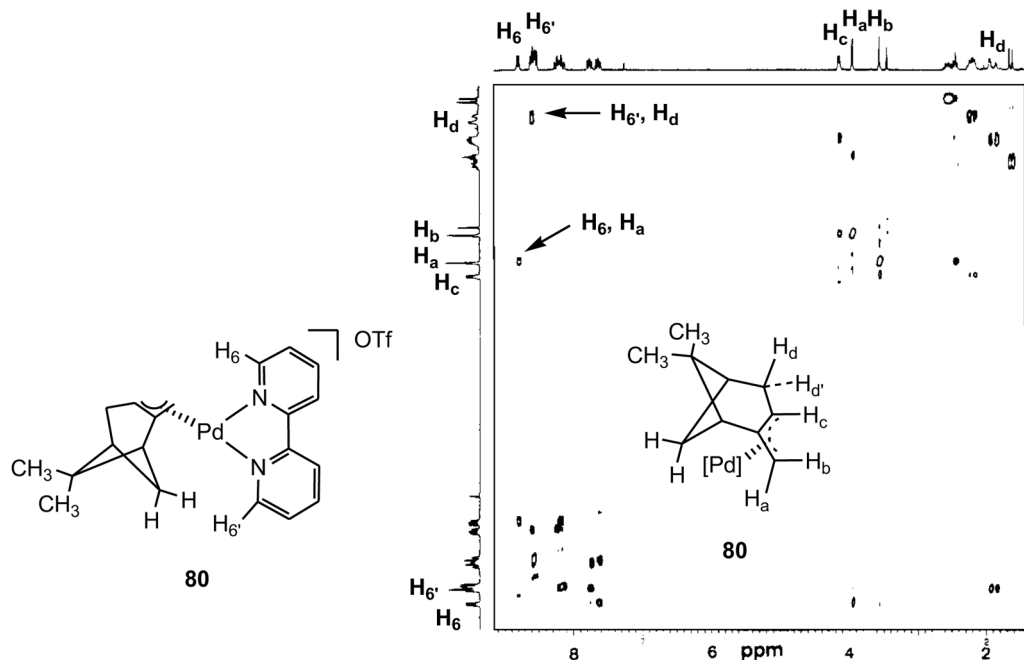


Figure 1.16 $^1\text{H}, ^1\text{H}$ NOESY spectrum of **80**. The cross peaks indicated by the arrows arise from selective interligand NOE effects, i.e., the ortho protons of the bipyridyl recognize the β -pinene protons H_a and H_b , but not H_c or H_c' .

protons, in three-dimensional space, come within 3 Å, or less, of the allyl ligand (see **80**). These chelate ligand protons were then able to “report” on allyl rotations or other molecular distortions via NOEs. Although several allyl ligands were tested, the most useful proved to be that derived from β -pinene. A typical spectrum is given in Figure 1.16 [97].

This NOE idea was then extended to Pd(II) allyl complexes with bidentate phosphine auxiliaries [99–111], with the ortho P-phenyl protons acting as the reporters (see **81**). Figure 1.17 shows a section of the $^1\text{H}, ^1\text{H}$ NOESY for $[\text{Pd}(\beta\text{-pinene allyl})(\text{Chiraphos})](\text{OTf})$ (Chiraphos = $\text{Ph}_2\text{PCH}(\text{CH}_3)\text{CH}(\text{CH}_3)\text{PPh}_2$), **81** [129], and reveals the numerous contacts from the chiral phenyl array to the allyl ligand.

Whereas the simple bidentate nitrogen ligands proved to be rather limited, the frequent occurrence of a set of *four* P-phenyl or alkyl substituents, e.g., in coordinated Binap, MeO-Biphep, Josiphos or Duphos (shown, from left to right in Scheme 1.4), offered many more “reporters”. In this way, one can develop a more detailed NOE picture of how the complexed substrate interacts with the chiral pocket offered by these auxiliaries. From these NOE studies [97, 98] it can be shown that the atropisomeric bidentate ligands Binap and MeO-Biphep tend to have fairly classical axial and equatorial P-phenyl substituents.

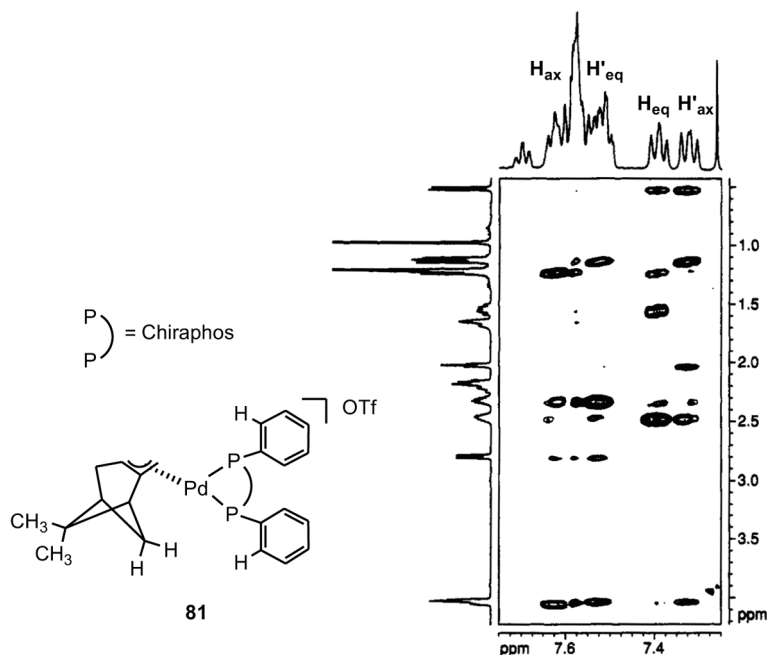
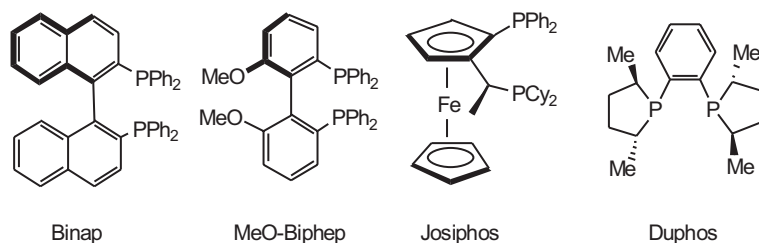
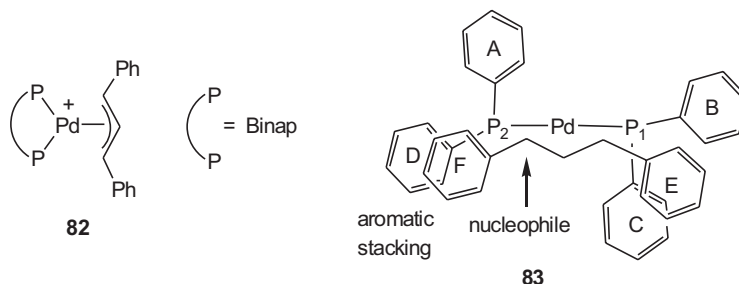


Figure 1.17 Section of the $^1\text{H}, ^1\text{H}$ NOESY showing the contacts from the ortho P-phenyl protons to various β -pinene protons. Chiraphos = $\text{Ph}_2\text{PCH}(\text{CH}_3)\text{CH}(\text{CH}_3)\text{PPh}_2$.

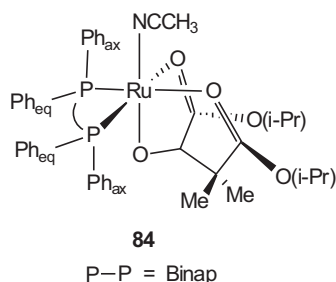


Scheme 1.4 Bidentate chiral phosphorus ligands usually used in catalysis. The four P-phenyl or alkyl substituents are useful NOE reporters.

An NOE study of the intermediate $[\text{Pd}(\eta^3\text{-PhCHCHCHPh})(\text{Binap})]^+$, **82**, thought to be involved in the Pd-catalyzed allylic alkylation of a 1,3-diphenylpropene, revealed that two phenyl rings, one from the auxiliary, D, and one from the substrate, F, are forced to take up parallel positions, i.e., they are π -stacked, as shown in **83** [103]. Since the π -stacking is repulsive, and thus selectively weakens one of the two Pd–C(allyl) bonds, the reaction becomes stereoselective. The D and F rings do not show inter-ligand NOEs.

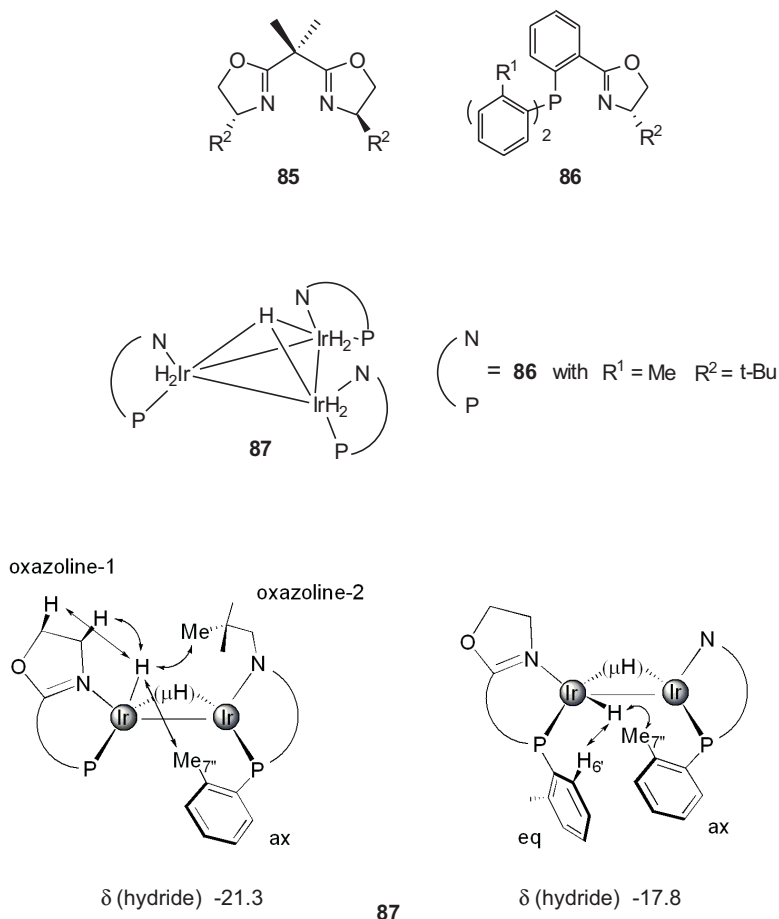


Daley and Bergens [124] have used this approach to characterize the 3-D structure of the intermediate $[\text{Ru}(\text{II})(\text{alkoxide})(\text{CH}_3\text{CN})(\text{Binap})]\text{BF}_4$, **84**, in their study of an enantioselective catalytic hydrogenation of a ketone. The ortho-protons of the equatorial and axial P-phenyl rings provide the reporter protons.



The bidentate oxazoline ligands **85** and **86** (and derivatives thereof) are excellent reporter ligands, and several studies have used NOEs to determine the nature of their chiral pockets [61, 113, 114, 126]. NOESY studies on the cations $[\text{Ir}(\text{1,5-COD})(\textbf{86})]^+$ and several cationic tri-nuclear $\text{Ir}(\text{III})(\text{hydrido})$ compounds [110], e.g. $[\text{Ir}_3(\mu_3\text{-H})(\text{H})_6(\textbf{86})_3]^{2+}$, **87**, in connection with their hydrogenation activity, allowed their 3-D solution structures to be determined. In addition to the ortho P-phenyl protons, the protons of the oxazoline alkyl group R^2 are helpful in assigning the 3-D structure of both the catalyst precursors and the inactive tri-nuclear clusters. Specifically, for one of these tri-nuclear $\text{Ir}(\text{III})$ complexes, **87** [110], with terminal hydride ligands at $\delta -17.84$ and $\delta -21.32$ (and a triply bridging hydride at $\delta -7.07$), the P-phenyl and oxazoline reporters define their relative positions, as shown in Scheme 1.5.

These NOE studies teach us that many successful P (or N...etc) auxiliaries possess a relatively rigid and intrusive chiral pocket [105, 107]. The shape of this pocket is a function of the individual chelate ligand, i.e., there is no one successful shape.



Scheme 1.5 Determination of the 3-D solution structure of **87** via NOEs between the hydride ligands and the P-phenyl and oxazoline reporters.

1.4

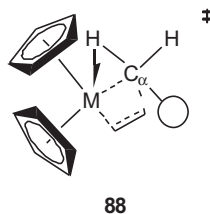
Isotopes in Catalysis

Isotopic labels (and especially enriched materials) have proven crucial in the investigation of the mechanisms of homogeneously catalyzed reactions [130]. Further, isotope effects on the rate or the equilibrium constant of a reaction can be diagnostic, and structural information can be provided by isotope-induced changes in the chemical shifts of neighbouring nuclei, and/or alterations in the coupling pattern of the detected spectra. The isotope- and position-specific information inherent to NMR techniques are ideally suited for the analysis of isotope effects in catalysis [131].

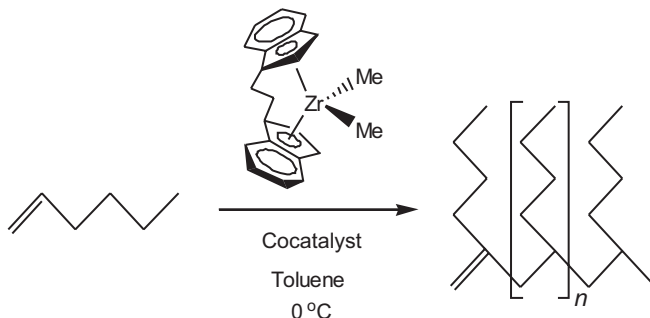
1.4.1

Kinetic Isotope Effect (KIE)

Proton/deuterium isotope effects on reaction rates are useful mechanistic probes. In the zirconocene-catalyzed alkene polymerization, the observed values of $k_{\alpha^1\text{H}}/k_{\alpha^2\text{H}}$ determined by ^1H NMR fall in the range of 1.2–1.3 and support a transition state in which there is an α -agostic interaction (see **88**) [132].

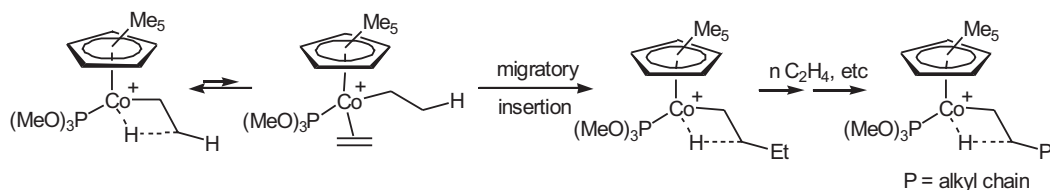


Landis and coworkers [133] have reported the first determination of a $^{12}\text{C}/^{13}\text{C}$ KIE in the $[(rac\text{-C}_2\text{H}_4(1\text{-indenyl})_2)\text{ZrMe}_2]$ -catalyzed polymerization of 1-hexene (Eq. (1)). It is suggested that the transition state, in which the alkene is irreversibly fixed into the growing polymer, does not change significantly as a function of the cocatalyst.

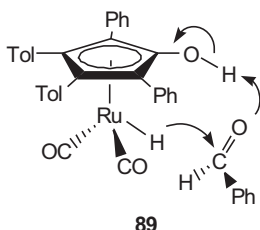


In contrast to the isotope effects observed in d^0 olefin polymerization catalysts, Brookhart and coworkers [134] have detected an inverse $^1\text{H}/^2\text{H}$ isotope effect of 0.59 in the Co(III) -catalyzed polymerization of ethylene. This inverse effect was ascribed to a β -agostic CH bond which is stronger in the ground state than the “free” C–H bond during or just prior to the insertion step (see Scheme 1.6).

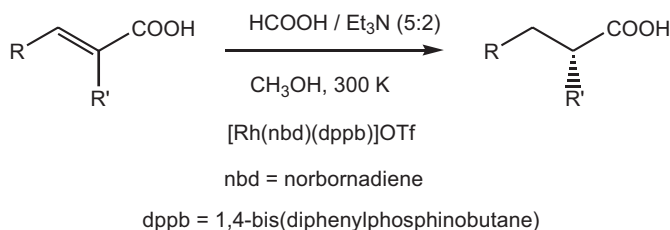
In the hydrogenation of aldehydes catalyzed by the Ru complex **89**, Casey and coworkers [135] have established the individual ($k_{\text{O}^1\text{H}}/k_{\text{O}^2\text{H}} = 2.2$ and $k_{\text{Ru}^1\text{H}}/k_{\text{Ru}^2\text{H}} = 1.5$) and overall ($k_{\text{H}}/k_{\text{D}} = 3.6$) KIEs. As the product of the two individual KIEs ($1.5 \times 2.2 = 3.3$) is in good agreement with the experimentally measured value (3.6 ± 0.3 relative to the RuD-OD analog), a reaction mechanism with concerted delivery of both H^- and H^+ to the carbonyl is proposed.



Scheme 1.6 Proposed β -agostic CH bond in the Co(III)-catalyzed polymerization of ethylene.



A direct kinetic isotope effect of $k_{\text{H}}/k_{\text{D}} = 3.1 \pm 0.1$ is found in the Rh-catalyzed enantioselective transfer hydrogenation of $\alpha\beta$ -unsaturated carboxylic acids using $\text{HCOOH}/\text{Et}_3\text{N}$ vs. $\text{DCOOH}/\text{Et}_3\text{N}$ as the hydrogen source (Eq. (2)) [136]. This observation clearly indicates that the cleavage of the C–H bond of formic acid is the rate-limiting step, and rules out the participation of free molecular hydrogen in the reaction [136].



1.4.2

Structural Effects

The introduction of isotopes into a compound alters the coupling pattern and the chemical shifts of the observed spectrum. As shown in Figure 1.18, deuterium-induced ^{13}C chemical shift variations have allowed the estimation of the ratio of isomers **90a–d** formed in Eq. (2) when $\text{R} = \text{Ph}$, $\text{R}' = \text{CH}_2\text{COOH}$, and $\text{DCOOD}/\text{Et}_3\text{N}$ is used for the hydrogen transfer [136]. The three sp^3 -carbons C1, C2 and C3 each afford a distinct singlet for the four possible isotopomers **90a–d** (replacement of ^1H by ^2H shifts the resonances of the adjacent carbon nuclei to lower frequency) [137].

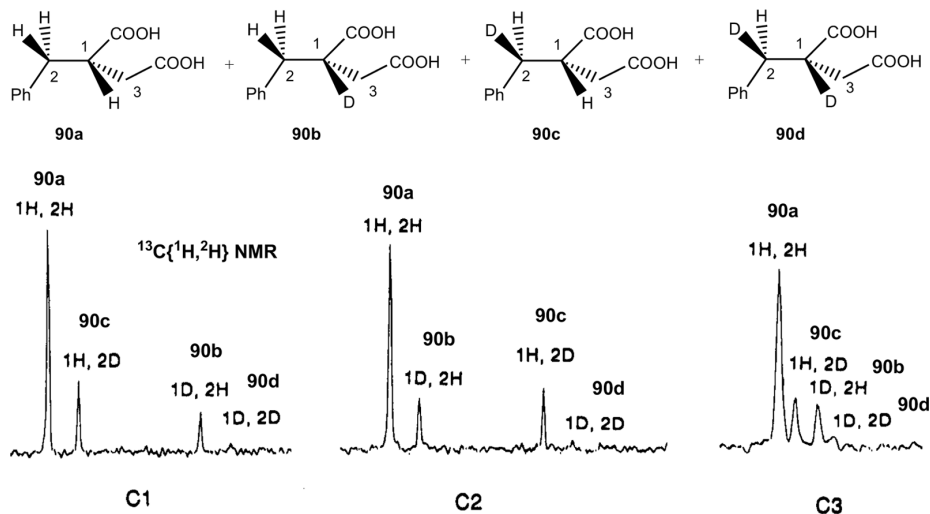


Figure 1.18 The three high-field signals, C1–C3, in the $^{13}\text{C}\{^1\text{H}, ^2\text{H}\}$ NMR spectrum of the product obtained by transfer hydrogenation of $\text{PhCH}=\text{C}(\text{COOH})-\text{CH}_2\text{COOH}$ with $^2\text{HCOOH}/\text{NEt}_3$, at about 25 % conversion. The chemical shifts for the undeuterated isotopomer **90a** are δ C1 44.3, δ C2 38.6 and δ C3 35.9, respectively.

In Figure 1.19, the small difference in δ ^1H between the CH_3 and CH_2D ligands permits the recognition of the exchange between $\text{RhD}(\text{CH}_3)(\text{Tp}')(\text{CNCH}_2\text{Bu}^t)$ and $\text{RhH}(\text{CH}_2\text{D})(\text{Tp}')(\text{CNCH}_2\text{Bu}^t)\text{Tp}'\text{Rh}(\text{L})$, (Tp' = tris-3,5-dimethylpyrazolylborate, L = $\text{CNCH}_2\text{CMe}_3$), as a function of time [138]. The methyl signal of the CH_2D ligand is found at slightly lower frequency.

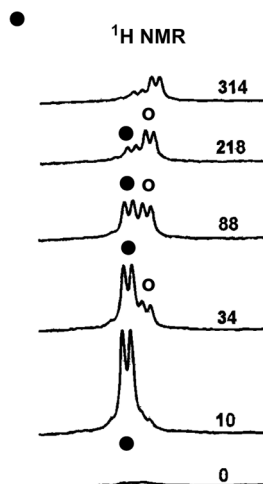
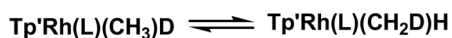


Figure 1.19 Methyl region as a function of time (minutes) of the ^1H NMR spectrum from the rearrangement of $\text{RhD}(\text{CH}_3)(\text{Tp}')(\text{CNCH}_2\text{Bu}^t)$ to $\text{RhH}(\text{CH}_2\text{D})(\text{Tp}')(\text{CNCH}_2\text{Bu}^t)$ in d^6 -benzene at 295 K.

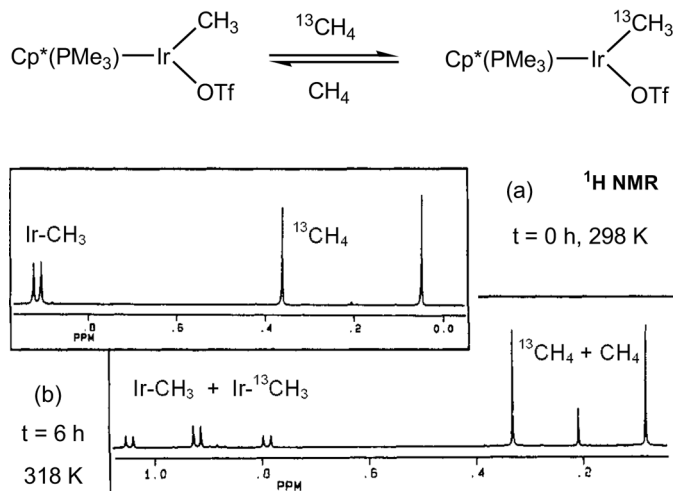


Figure 1.20 Methyl region of the ^1H NMR spectra arising from a solution of $\text{Ir}(\text{OTf})\text{-Me}(\text{Cp}^*)(\text{PMe}_3)_2$: Top: in CD_2Cl_2 under 2 bar of $^{13}\text{CH}_4$ immediately after mixing (298 K). Bottom: after heating at 318 K for 6 h.

And in a last example, facile $\text{Ir}(\text{III})$ C–H activation is proven via Figure 1.20, where $[\text{Ir}(\text{CF}_3\text{SO}_3)(\text{CH}_3)(\text{Cp}^*)(\text{PMe}_3)_2]$ is allowed to react with $^{13}\text{CH}_4$. After warming for 6 h, incorporation of ^{13}C -labelled methane to give $[\text{Ir}(\text{CF}_3\text{SO}_3)(^{13}\text{CH}_3)(\text{Cp}^*)(\text{PMe}_3)_2]$ and CH_4 had occurred to an extent of 50 %, as observed from the new signals deriving from the large $J(^{13}\text{C}, ^1\text{H})$ spin–spin coupling [139].

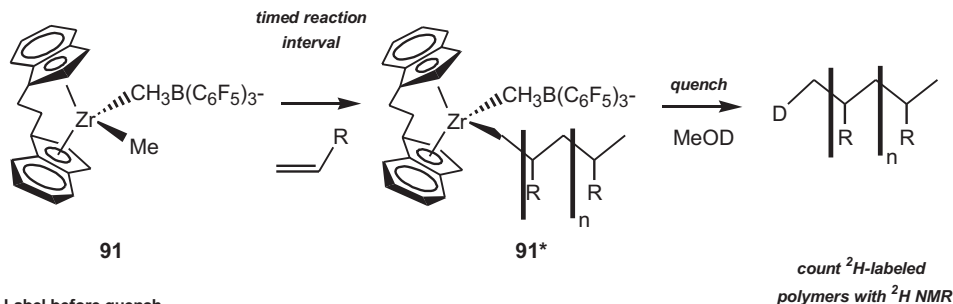
1.4.3

An Active Site Counting Method

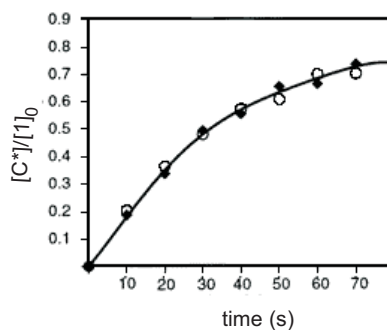
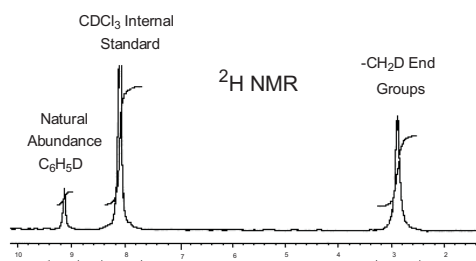
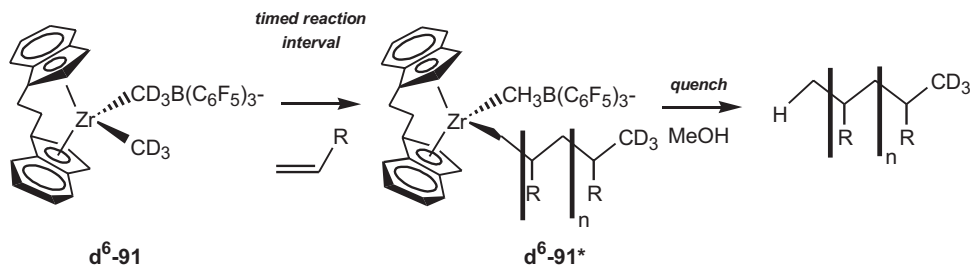
Landis and coworkers [140] have developed an active-site counting method based on ^2H -labelling, for the metallocene-catalyzed alkene polymerization. After quenching the reaction by addition of methanol, the polymer is analyzed by ^2H NMR, which allows the quantification of Zr-alkyl sites. A typical ^2H NMR of quenched polymer is shown in Scheme 1.7 (label is found at terminal positions only). This technique has been applied to the polymerization of 1-hexene catalyzed by $[\text{Zr}(\text{rac-C}_2\text{H}_4(1\text{-indenyl})_2)\text{Me}][\text{MeB}(\text{C}_6\text{F}_5)_3]$, **91**. As shown in Scheme 1.7, there are two possible approaches:

- Quenching with CH_3OD , and analysis of the polymer by ^2H NMR yields the number of active sites *at the time of quench*.
- Carrying out the reaction with the labeled catalyst $\text{d}^6\text{-91}$ $[\text{Zr}(\text{rac-C}_2\text{H}_4(1\text{-indenyl})_2)\text{CD}_3][\text{CD}_3\text{B}(\text{C}_6\text{F}_5)_3]$ and quenching with unlabelled CH_3OH yields the number of sites that were active *at any point before the quench*.

A) Label at quench



B) Label before quench



Scheme 1.7 Active-site counting method based on ^2H -labelling, in the zirconocene-catalyzed polymerization of 1-hexene. Lower left: typical ^2H NMR of the quenched polymer according to method A. The integrals allow the quantification of the Zr-alkyl active sites. All labels are found in the terminal position. Lower right: comparison of fractional active-site counts using Method A (open circles, \circ) or Method B (diamonds \blacklozenge).

The plot shown in Scheme 1.7 shows that both labeling methods yield similar active-site counts. From this observation it can be concluded that the catalyst **91** does not deactivate during the time scale of the experiments.

This active site counting methodology has been applied to the determination of initiation, propagation and termination rate laws and activation parameters for the polymerization of 1-hexene [141] catalyzed by **91** in toluene solution.

1.5

Dynamic NMR Spectroscopy

Since NMR spectroscopy involves the storage of information relating to the precession frequencies of individual nuclei over periods up to and including a few minutes, it provides the opportunity to study equilibrium and chemical exchange effects during this time [107, 142–145]. Suitable chemical exchange processes may be inter- or intramolecular, and correspond to internal rotations, conformational changes and even tautomerism. The time scale of NMR is such that first-order rate constants in the range of $10^{-2} - 10^6 \text{ s}^{-1}$ can be measured. Both irreversible and reversible processes can be affected by temperature changes. The use of NMR spectroscopy in the study of irreversible changes has been illustrated in Section 1.2. Reversible intramolecular and intermolecular exchange processes may be slow, intermediate or fast, according to the frequency difference between the two (or more) exchanging sites [146].

1.5.1

Variable Temperature Studies

Macchioni and coworkers [147] have investigated the effect of the counterion on CO/Styrene copolymerization catalyzed by $[\text{Pd}(\eta^1\text{-}\eta^2\text{-C}_8\text{H}_{12}\text{OMe})\text{bipy}]\text{X}$, (**92**, Figure 1.21) where X is the counterion. The bipyridine ligand shows dynamic behavior and a series of ^1H NMR spectra recorded between 204 and 302 K (Figure 1.21) pro-

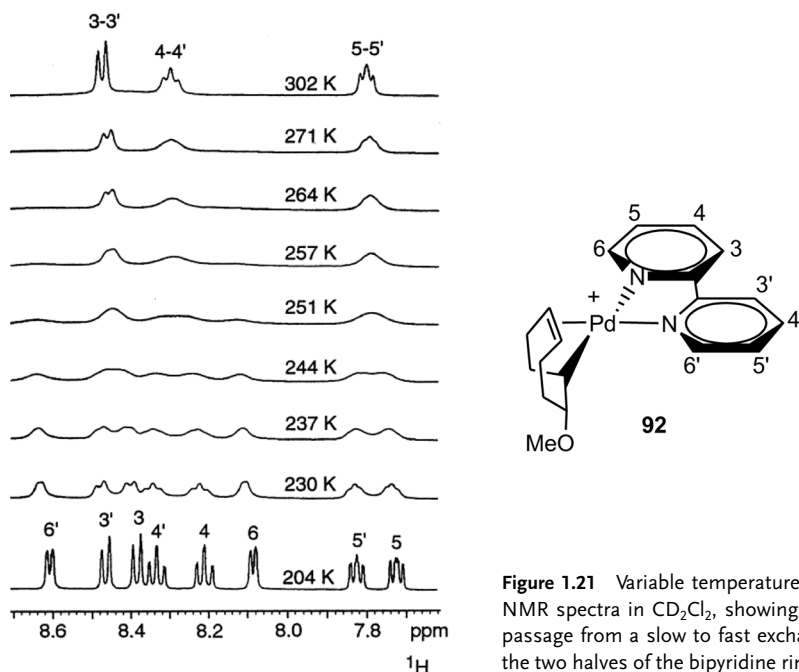
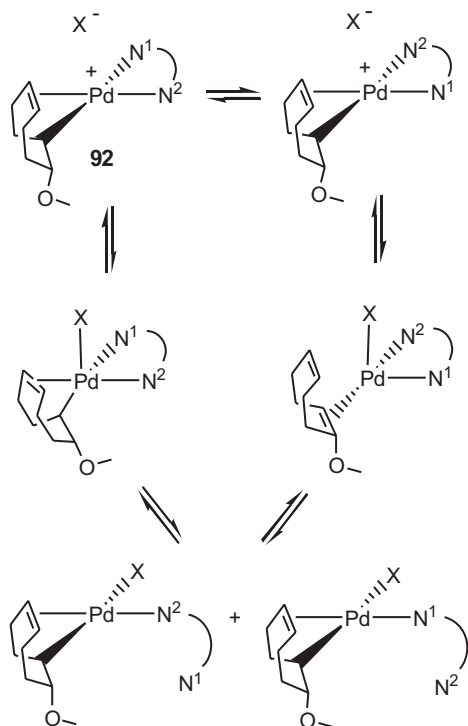


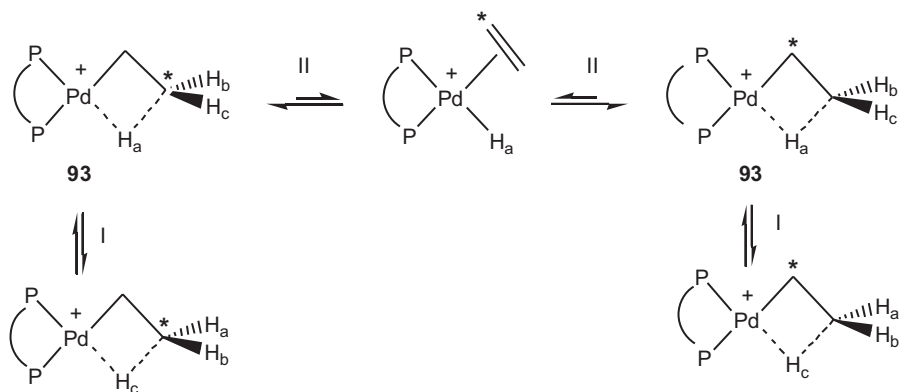
Figure 1.21 Variable temperature ^1H NMR spectra in CD_2Cl_2 , showing the passage from a slow to fast exchange for the two halves of the bipyridine ring in **92**.

vide data for the determination of the activation parameters for the exchange of the two halves of the bipyridine ligand. At 204 K, the NMR spectrum in Figure 1.21 clearly exhibits well separated and well defined signals such as 5 and 5', which coalesce at 251 K, and finally resharpen to provide a broad triplet. The situation is similar for the protons 3 and 3', and 4 and 4'. For 6 and 6' it is difficult to distinguish the averaged peak at high temperature. These four sets of protons resonances, 3, 4, 5, 6 and 3', 4', 5' and 6', belonging to the bipyridine ligand, interchange positions via the mechanism shown in Scheme 1.8.



Scheme 1.8 Mechanism of the reversible exchange of the bipyridine ligand in **92**.

Brookhart et al. [148] have reported a variable temperature NMR study for a Pd CO/olefin copolymerization catalyst. They studied the bite angle effect of the bidendate phosphine ligand in a series of complexes $[\text{Pd}(\text{CH}_3)(\text{OEt}_2)(\text{P-P})(\text{BAr}_4)]$, on the rate of migratory insertion of both ethylene and carbon monoxide, and isolated the resting state for the catalytic cycle involving C_2H_4 . With the ligand (1,3-diisopropylphosphino)propane (dipp), upon insertion of ethylene, the β -agostic ethyl complex $[\text{Pd}(\text{CH}_2\text{CH}_3)(\text{dipp})]^+$, **93**, is the resting state for the catalytic cycle. This complex exhibits two dynamic processes, described as the interchange of C_α and C_β (pathway II in Scheme 1.9) and rotation of the agostic methyl group (pathway I in Scheme 1.9).



Scheme 1.9 Fluxional processes observed for **93**.

In a quest to increase the efficiency of olefin polymerization catalysts and their selectivity in the orientation of the polymerization, the highly effective Group IV metallocene catalysts, $M(\text{Cp})_2(\text{L})_2$, have been studied, since they all display high fluxionality. Following methide abstraction, the metallocene catalysts of general formula $M(\text{Cp-derivatives})_2(\text{CH}_3)_2$ ($M = \text{Ti, Zr, Hf}$), were turned into highly reactive $M^+-\text{CH}_3$ cationic species. The activation parameters for the methide abstraction, derived from variable temperature NMR experiments, establish a correlation between the enthalpies of methide abstraction, the ^{13}C chemical shift in the resulting cation, and the ethylene polymerization activities [149].

At ambient temperature the ^1H NMR spectrum of $\text{Zr}(\text{C}_7\text{H}_9\text{NCH}_3)_2\text{Cl}_2$, **94**, shows a simple pattern, characteristic of a molecule with C_{2v} symmetry (Figure 1.22) [150]. However, upon cooling, the signals for the three allylic and two bridgehead resonances broaden, and at 183 K they separate into 10 different signals. The coalescence temperature for the central allyl ^1H resonance is 225 K.

The alkyne hydrogenation catalyst $[\text{Rh}(\text{7-SPh-8-Ph-7,8-C}_2\text{B}_9\text{H}_{10})(\text{COD})]$, **95**, (and derivatives thereof) shows dynamic behavior at ambient temperature (Figure 1.23) [151]. The carborane is bonded to the rhodium center via a thiolate anion and a bridging B–H–Rh bond. Complex **95** undergoes B–H/B–H–Rh interchange coupled with an apparent rotation of the $\text{Rh}(\text{COD})^+$ fragment. Variable temperature ^1H NMR spectra were recorded between 293 and 179 K. The apparent rotation of 1, 5-COD is found in a rather large number of Rh-complexes [152].

The zwitterionic rhodium complex $\text{Rh}(\eta^6\text{-PhBPh}_3)(\text{COD})$ is an effective catalyst for regioselective hydroformylation, silylformylation and hydrogenation reactions in the presence of dppb (1,2-bis(diphenylphosphino)butane) [153]. Alper and coworkers [153] have studied the interconversion of the zwitterionic $\text{Rh}(\eta^6\text{-PhBPh}_3)(\text{diene})_n(\text{dppb})_{1-n}$ and cationic $[\text{Rh}(\text{diene})_n(\text{dppb})_{2-n}](\text{BPh}_4)$ ($n = 0$ or 1) complexes in solution and showed fluxional behavior for the η^6 -tetraphenylborate-coordinated complexes. The ^{31}P variable temperature NMR spectra in Figure 1.24 show the solution behavior of the zwitterion $\text{Rh}(\eta^6\text{-PhBPh}_3)(\text{dppb})$,

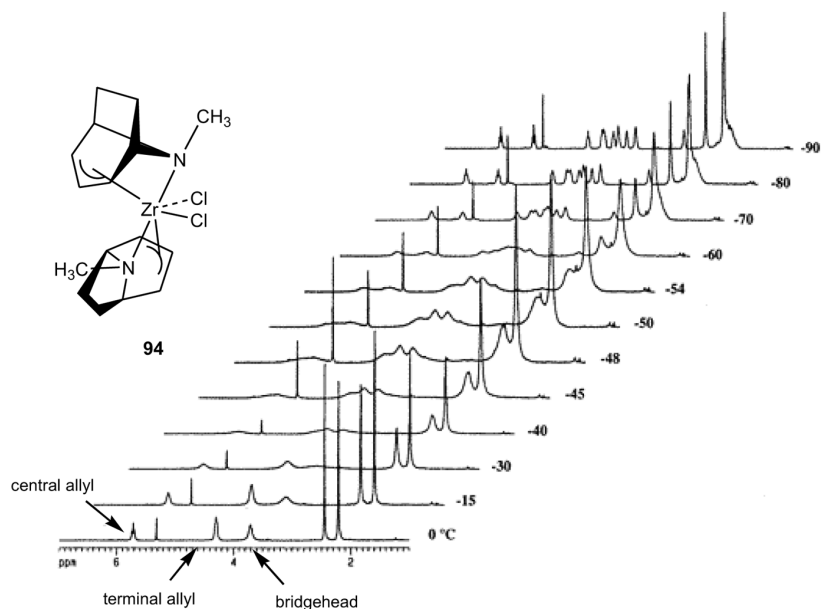


Figure 1.22 Variable temperature ^1H NMR spectra of **94**.

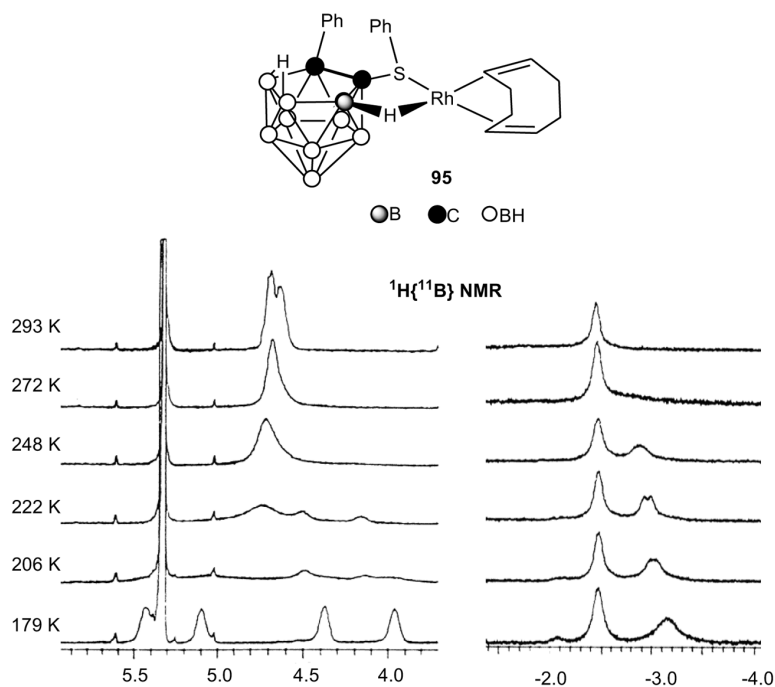


Figure 1.23 Variable temperature spectra in the olefinic and B–H regions of the $^1\text{H}\{^{11}\text{B}\}$ NMR spectra, showing nonequivalent four 1,5-COD protons and the B–H/B–H–Rh interchange in **95**.

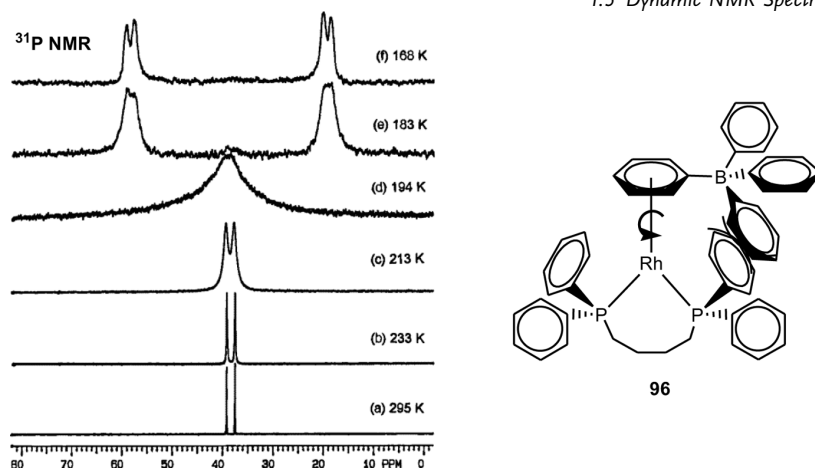
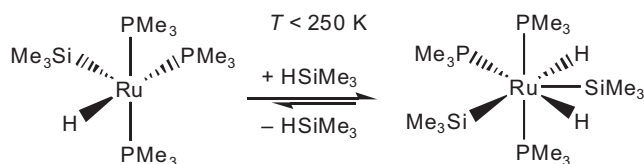


Figure 1.24 Variable temperature ^{31}P NMR spectra of **96** in $\text{CD}_2\text{Cl}_2/d^8\text{-toluene}$, and the proposed dynamic process responsible for the exchange of the ^{31}P nuclei.

96. At ambient temperature, equivalent P atoms are observed ($^1J(^{103}\text{Rh}, ^{31}\text{P}) = 200 \text{ Hz}$), due to a rapid exchange of the two ^{31}P nuclei. As the temperature decreases the signal broadens and decoalesces to provide two rather broad doublets at 168 K (although $^1J(^{103}\text{Rh}, ^{31}\text{P})$ is resolved, $^2J(^{31}\text{P}, ^{31}\text{P})$ is not). This indicates that, although the presumed rotation is slowed significantly, some exchange is still occurring at 168 K (the lowest temperature reachable). Hindered rotation of the η^6 -coordinated phenyl ring is believed to be responsible for the observed dynamics.

The Ru(IV) complex $\text{Ru}(\text{SiMe}_3)_2(\text{H})_2(\text{PMe}_3)_3$ is a model for dehydrogenative C–Si bond formation chemistry. Berry and coworkers have shown that, at low temperature, this complex undergoes fast reversible SiH reductive elimination on the NMR time scale (Eq. (3)), and slow H_2 reductive elimination as a minor process [154].



1.5.2

Line Shape Analysis [142, 146, 155–159]

In solution, rate constants and activation parameters for dynamic processes can be estimated by direct analysis of the change of the NMR signal shape as a function of temperature. This technique is called line shape analysis (LSA) and it is best suited when the rate of exchange ranges from ca. 10 to 10^3 s^{-1} [142, 159].

If the exchange rate, k_{ex} , is much smaller than the frequency difference between the signals for the exchanging sites, then the NMR spectrum will exhibit well separated peaks for these resonances. Based on the Bloch equation [146], it is possible to find relationships connecting the shape of the NMR signal, $\Delta\nu_{1/2}$, the lifetime, τ , for a nucleus in different positions of a molecule and the rate constant, k . The lifetime is related to the rate constant by Eq. (4).

$$\tau = \frac{1}{k}$$

At values where k equals the difference in resonance frequencies, the peaks coalesce. The rate of interchange at coalescence, k_{coal} , can be determined via Eq. (5) [155], for exchange between two equally populated sites that do not exhibit scalar coupling [160].

$$k_{\text{coal}} = \sqrt{2\pi\Delta\nu}$$

Although this equation only applies when the coalescence point is reached, rate constants for the exchange between two or more exchanging sites are accessible by analysis of line widths at half height, $\Delta\nu_{1/2}$, and shift differences, $\Delta\nu$, in Hz. The comparison between the experimental spectrum and the spectrum calculated by use of a simulation package for line shapes provides the mechanism for determining the rate constant of exchange [161, 162].

NCN-pincer ligands show synthetic potential as catalysts [163, 164]. Chung and coworkers [165] have developed an efficient pincer catalyst for the Heck reaction, by a judicious modification of the classical NCN ligands (see **97**). Interestingly, at elevated temperatures the methyl signals of the Pd–NMe of **97** coalesce with those for the noncoordinated N–CH₃ arms, suggesting a ligand exchange reaction (Figure 1.25). The entropy of activation derived from the temperature dependent rate constants supports an associative mechanism.

Casey et al. have studied complex **98** as a model for intermediates in metallocene catalyzed alkene polymerization, by means of LSA [166].

At 195 K, the resonances for the Cp ligands, silyl methyl groups and the methylene fragment in **98** exhibit diastereotopic resonances in CD₂Cl₂. As the temperature is increased, coalescence of the pairs of diastereotopic resonances occurs at different temperatures (Cp rings at 245 K, silyl methyl groups at 240 K). All the tem-

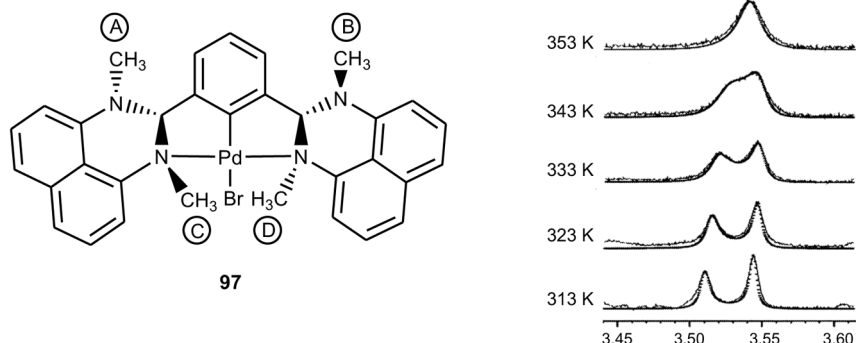
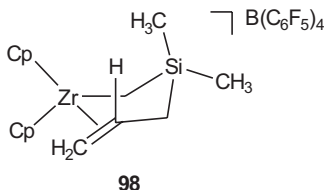
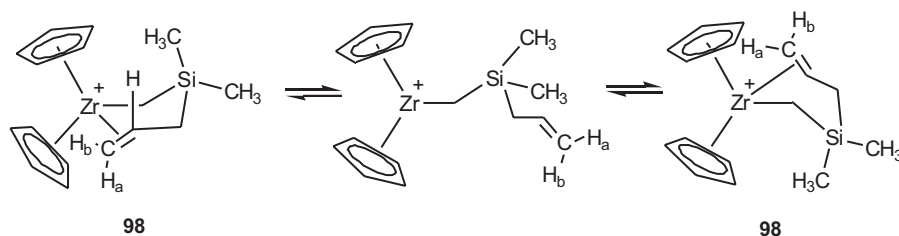


Figure 1.25 Experimental (solid line) and calculated (dotted line) variable temperature ^1H NMR spectrum of the *N*-methyl resonances of **97**, in d^7 -DMF. This series of spectra shows the exchange of the methyl group A with C, and B with D. The resonances for A and B, and for C and D overlap at all temperatures considered.

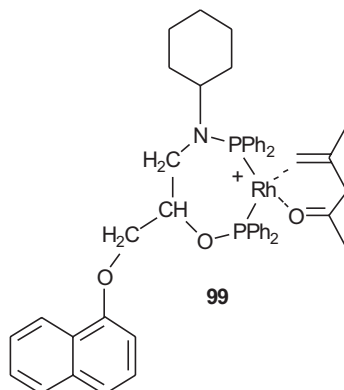


perature-dependent changes observed are reversible up to 248 K, and decomposition begins at 253 K. An LSA study affords an activation barrier of $12.8 \text{ kcal mol}^{-1}$ at 248 K for alkene dissociation. The proposed explanation for the fluxional behavior of the model is shown in Scheme 1.10. Alkene dissociation, followed by rotation around the $\text{Zr}-\text{C}$ bond and subsequent recoordination to the opposite face of the alkene are required. The study also shows that the resonances of the terminal vinyl protons are not affected by temperature, thereby ruling out a mechanism involving intramolecular insertion followed by ring-opening.



Scheme 1.10 Mechanism for the fluxional behaviour of the model Zr complex **98**.

The dynamic behavior of the model intermediate rhodium-phosphine **99**, for the asymmetric hydrogenation of dimethyl itaconate by cationic rhodium complexes, has been studied by variable temperature ^{31}P NMR LSA [167]. The line shape analysis provides rates of exchange and activation parameters in favor of an intermolecular process, in agreement with the mechanism already described for bis(phosphinite) chelates by Brown and coworkers [168]. These authors describe a dynamic behavior where two diastereoisomeric enamide complexes exchange via olefin dissociation, subsequent rotation about the N–C(olefinic) bond and recoordination. These studies provide insight into the electronic and steric factors that affect the activity and stereoselectivity for the asymmetric hydrogenation of amino acid precursors.



Complexes based on seven-membered bis(phosphane) chelate ligands show very high catalytic activity in hydrogenation chemistry. Kadyrov and coworkers [169] have studied the temperature-dependent ^{31}P NMR spectra for $[\text{Rh}(\text{R,R-diop})(\text{COD})](\text{BF}_4)$, **100**. At 240 K (Figure 1.26, top), the ^{31}P NMR spectrum of this complex exhibits a sharp doublet. As the temperature is decreased, the signals broaden and a second component is observed. At 123 K, a complex with two non-equivalent ^{31}P signals is present. The signal for the major isomer is thought to reflect a rigid conformation with C_2 symmetry, due to the sharpening of the signal at low temperature. This major species is believed to contain a seven-membered ring in a twist chair conformation. The minor species was described as a distorted boat. Line shape analysis performed using WIN-DYNAMICS [170] provided activation parameters for the interchange between these conformations. The results are interpreted as arising from a temperature-dependent equilibrium of at least two different seven-membered ring conformers.

In an attempt to evaluate the parameters that influence the production of methyl propanoate versus CO–ethylene copolymer, Doherty and coworkers [171] have probed the dynamic processes connected with the catalyst precursors $[\text{PdCl}(\text{CH}_3)(\text{P-P})]$, **101**, where P–P is a bidentate phosphine bearing a cyclohexane or norbornane group, containing a C_4 -backbone. The variable temperature ^{31}P

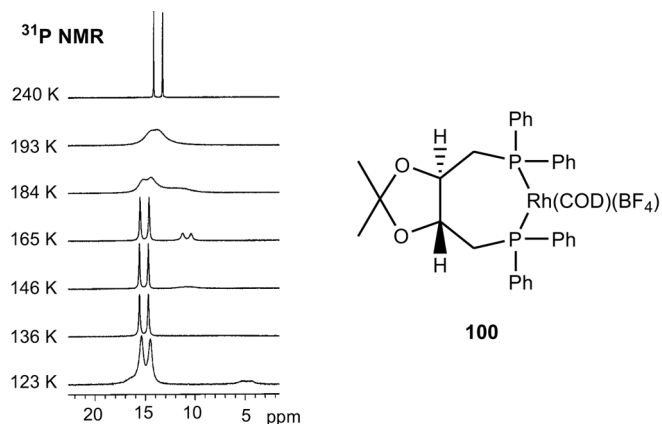


Figure 1.26 Variable temperature ^{31}P NMR study for **100**. The second ^{31}P resonance for the minor component lies under the signal for the major resonance.

NMR spectra (Figure 1.27) revealed an equilibrium. The analysis of the variation of the shape and position of these ^{31}P resonances provided the activation parameters for these processes.

In a similar fashion, the dynamic behavior of $\text{Ni}(\beta\text{-agostic alkyl})(\alpha\text{-diimines})$ cationic complexes, e. g. **102**, which are models for the intermediates involved in Ni catalyzed polymerization of ethylene, has been studied by LSA and provides insight into the mechanism of ethylene polymerization [44]. Eq. (6), shows the exchange between two of these species.

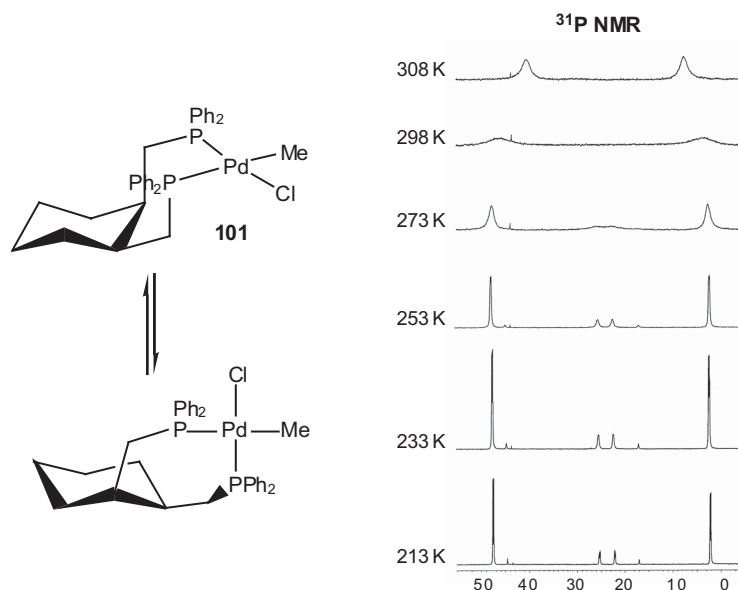
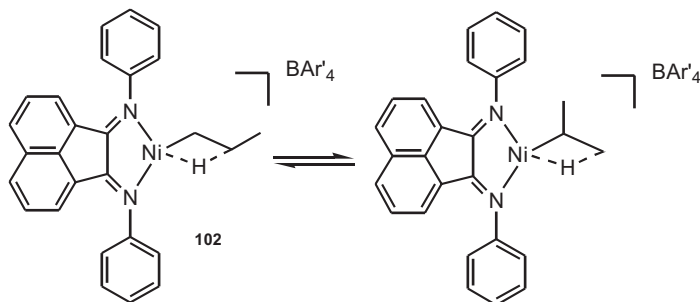


Figure 1.27 Variable temperature ^{31}P NMR spectra of **101**, in THF.



These few examples illustrate how the shape of NMR signals is affected by dynamic phenomena within the molecule. The analysis of these effects provides a useful tool for both a qualitative (localisation of exchanging sites) and quantitative (kinetic data) understanding of fluxionality within metal complexes.

1.5.3

Magnetization Transfer

Magnetization transfer techniques [146, 172] are used to study systems under conditions of slow exchange, where variation of the temperature is either undesirable or not relevant. If the exchange rate is comparable to T_1 (the spin–lattice relaxation time), rate constants can be determined by these double resonance experiments. By selectively irradiating one of the exchanging sites, observable transfer of magnetization occurs from the irradiated site to all sites directly involved in the exchange. The intensity of the signals after transfer of magnetization has a characteristic time dependence, from which the rate constant for the exchange can be derived [173]. In this respect, magnetization transfer techniques can be viewed as a quantitative method.

One can imagine two protons, H_A and H_B , being part of the same molecule and undergoing chemical exchange, at a rate k_{HH} . When H_A is irradiated, it “remembers” the new condition and transfers this information to H_B as a result of the chemical exchange. The newly arrived H_B proton does not contribute to the normal amount of signal intensity in the final NMR spectrum. If the initial intensity of H_B is I_o , and the final intensity for H_B as a result of irradiation of H_A is I_f , then the rate of exchange k_{HH} is defined by Eq. (7), where T_1 refers to the spin–lattice relaxation time.

$$\frac{I_o}{I_f} = \frac{T_1(H_B)^{-1}}{k_{HH} + T_1(H_B)^{-1}}$$

Brown and coworkers [128] have studied the exchange process for the enamide complex **103**, using magnetization transfer techniques (Figure 1.28). Compound **103** represents the catalytic resting state in the asymmetric homogeneous hydroge-

nation of dehydroamino acid derivatives and exists as a mixture of two diastereoisomers, **103a** and **103b**. Figure 1.28 shows the exchange between the saturated ^{31}P nucleus *trans* to amide in the major diastereoisomer, **103a**, and the ^{31}P nucleus *trans* to amide in the minor diastereoisomer, **103b**, (exchanging resonances indicated by arrows). The use of this NMR technique, coupled to other studies, allows extrapolation to the mechanism shown in Figure 1.28. The exchange pathway involves dissociation of the olefin with subsequent rotation about the N–C(olefin) bond and recoordination of the olefin to the metal center. The amide oxygen atom remains coordinated to the rhodium during the entire process. An understanding of the mechanism of this diastereomeric interchange is of importance since the minor diastereoisomer, **103b**, is believed to carry the flux of catalysis.

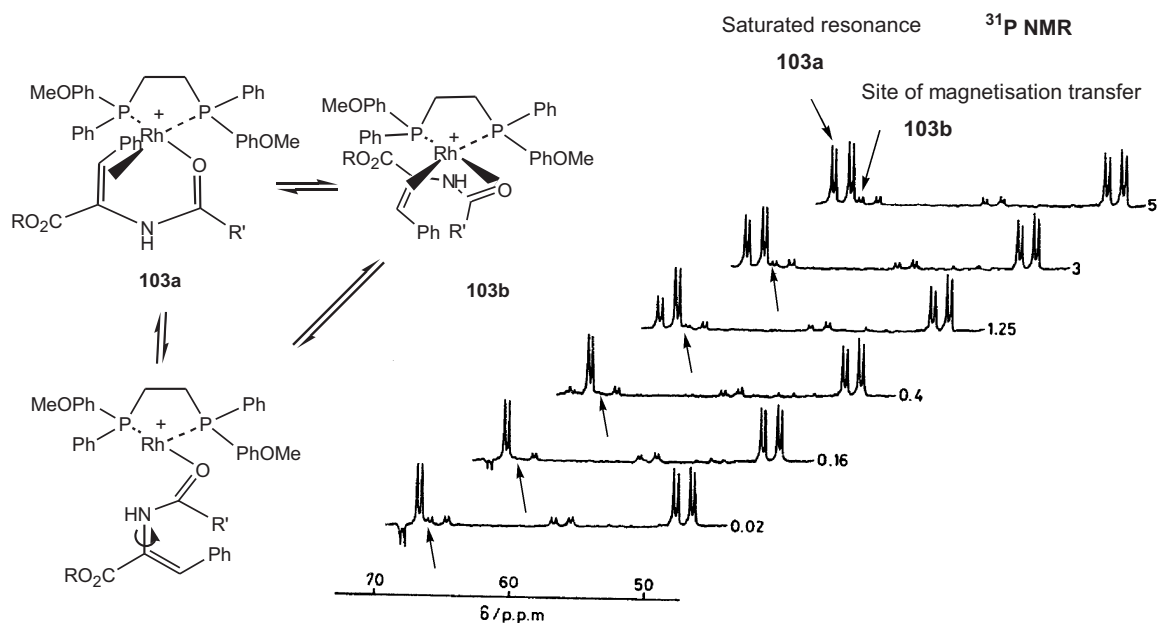


Figure 1.28 ^{31}P NMR spectra obtained after saturation transfer of the ^{31}P nucleus *trans* to amide in the $[\text{Rh}(\text{dipamp})(\text{enamide})]^+$ diastereoisomer **103a**. Direct exchange of magnetisation is observed between the ^{31}P atoms *trans* to amide in the diastereoisomers **103a** and **103b**. The arrows pointing upwards indicate the most affected resonance. The proposed mechanism of intramolecular equilibration of **103a** and **103b** is shown.

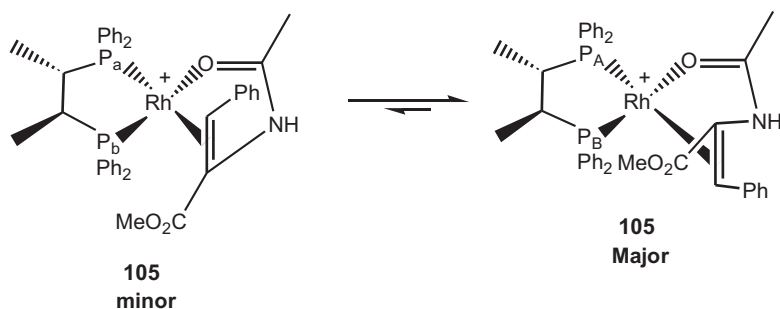
1.5.4

NOESY/EXSY/Hidden Signals [146, 174]

A number of 2D NMR experiments have been developed which allow the study of slow exchange phenomena. The most common (Exchange Spectroscopy, EXSY), is based on the standard pulse sequence $90^\circ_x - t_1 - 90^\circ_x - t_m - 90^\circ_x - \text{FID}(t_2)$, where t_1 is an evolution delay, t_m is the mixing time, and t_2 is the detection period [175, 176].

The first 90°_x pulse produces transverse magnetization, M_y , which develops during the evolution time, t_1 , by precessing around B_0 with the different Larmor frequencies. The second 90°_x pulse rotates the magnetization into the z direction. The longitudinal magnetization, M_z , evolves further under two effects, spin-lattice relaxation (T_1) and chemical exchange. The latter effect induces a transfer of magnetization between the exchanging sites and leads to off-diagonal cross-peaks. This effect is read-out by the third 90°_x pulse, which creates the magnetization in the xy plane that produces the FID during t_2 . The amplitude of the transverse magnetization depends directly on the mixing time, t_m , and the efficiency of the magnetization transfer. Whereas the time t_1 is incremented sequentially to produce the second chemical shift axis, the acquisition time, t_2 , is equal to the acquisition time in a normal 1D NMR experiment. Typically, t_m ranges from 0.03 to 1 s. Double Fourier transformation of the time domains t_1 and t_2 results in a 2D NMR spectrum [145]. From these data, the rate of magnetization transfer during the mixing time, t_m , can be estimated. For the extreme narrowing condition, these cross peaks have the same phase as the diagonal, whereas the NOE cross-peaks possess an opposite phase. EXSY is a very effective method where no insight with respect to the exchange pathway is available, e.g. for systems undergoing multiple site exchange (e.g. three or more nuclei exchanging their positions at the same or at different rates of exchange), and/or where signals are broad or hidden.

Returning to the enantioselective hydrogenation chemistry with rhodium [177, 178], Landis and Halpern [33] have proposed an intermolecular pathway based on their ^{31}P NMR spectra, while Brown and coworkers [128, 168] have proposed an intramolecular pathway, according to the dynamic data obtained from DANTE inversion-recovery NMR experiments. In a later publication, Philipsborn and coworkers have studied the dynamic behavior of the model intermediate $[\text{Rh}(\text{S,S-chiraphos})(\text{MAC})]^+$, **105**, (Eq. (8)) [179]. Their new data supported both the intra- and intermolecular exchange mechanisms, and showed that there is a unique pathway that can possibly account for both suggestions. Figure 1.29(a) shows the ^{31}P EXSY spectrum of **105** in the presence of excess olefin substrate. The phosphorus nuclei of the major and minor diastereoisomers exchange with partial retention of the configuration. For instance, P_A (trans to the olefin in the major diastereoisomer) exchanges with P_a (trans to the olefin in the minor diastereoisomer, exchange cross-peaks circled). Further, P_B exchanges with P_b (both trans



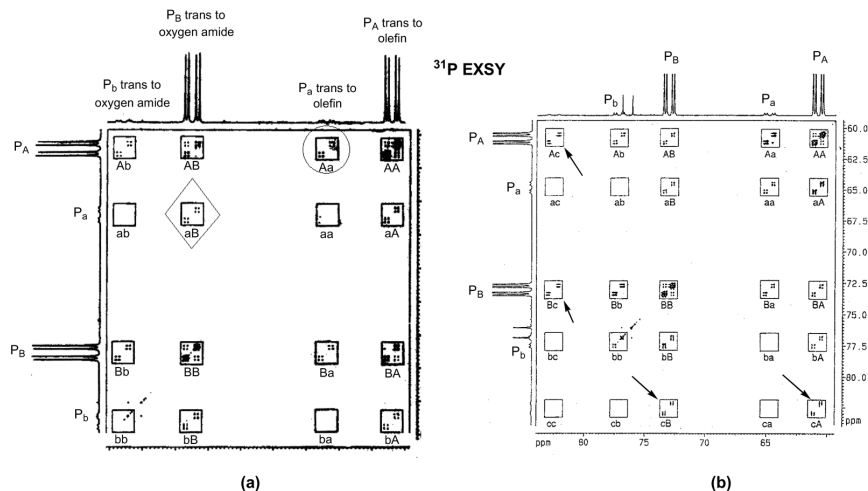
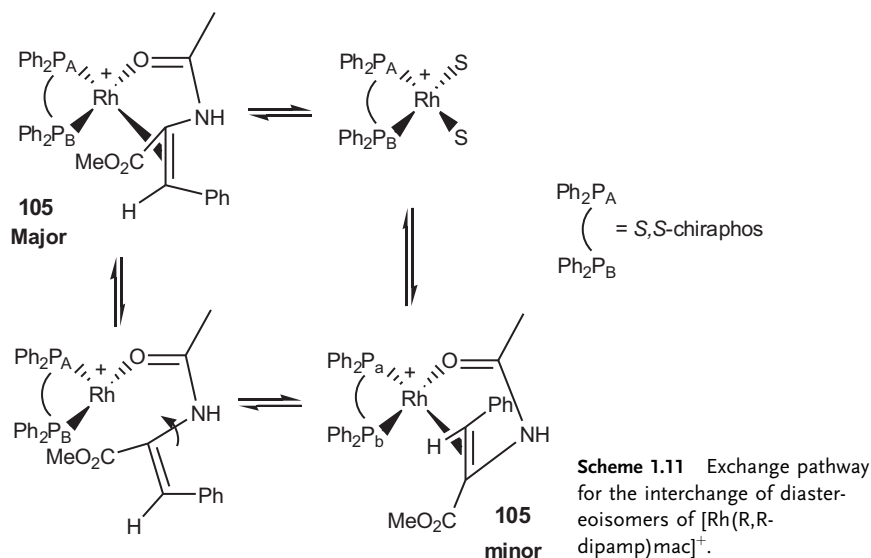


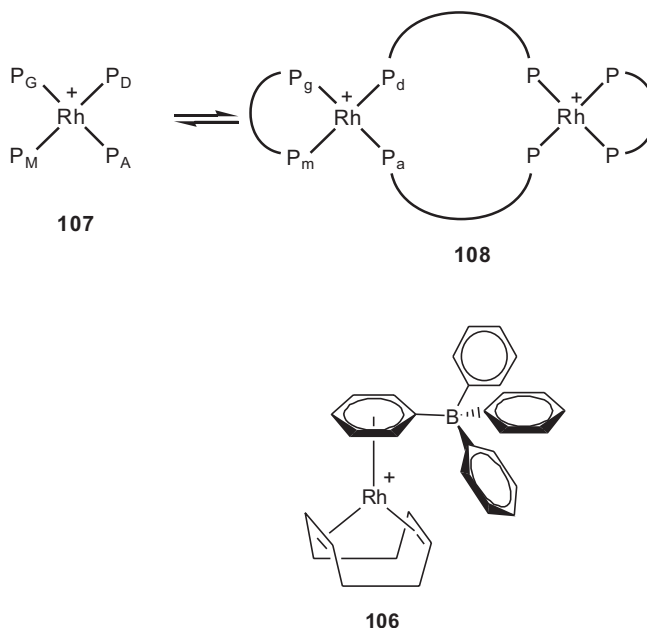
Figure 1.29 ^{31}P EXSY spectrum of $[\text{Rh}(\text{S,S-chiraphos})(\text{mac})]^+$ in CD_3OD with (a) a mixing time of 200 ms in the presence of mac , (b) a mixing time of 40 ms and a deficiency of mac .

to the amide oxygen). These observed exchange processes are consistent with an intramolecular exchange pathway. Nevertheless, an exchange of the ^{31}P nuclei between the two diastereoisomers without retention of configuration was also observed (e.g. P_A interchanges with P_B , as indicated by the diamond) which points to an intermolecular pathway. Moreover, a ^{31}P EXSY spectrum of a sample of **105** with a deficiency in MAC (Figure 1.29(b)) shows a similar exchange pattern, but also exchange with a bis-solvated species, $[\text{Rh}(\text{S,S-chiraphos})(\text{solvent})_2]^+$ (indicated by an arrow). Scheme 1.11 shows the proposed exchange pathway for **105**, involving



the bis-solvent complex. This mechanism accounts for intra- and intermolecular exchange. This study illustrates the substantial advantage of using EXSY NMR when exchange occurs between more than two sites on one or more molecules, since it provides a complete mapping of the dynamics.

A mixture of the zwitterionic rhodium complex $\text{Rh}(\eta^6\text{-PhBPh}_3)(1,5\text{-COD})$, **106**, and dppb affords the mono- and dinuclear complexes **107** and **108** (Eq. (9)) [153]. Alper and coworkers [153] have used 2D EXSY spectroscopy in order to map the exchange pathway between ^{31}P nuclei in these two rhodium complexes (Figure 1.30) [153]. The mixture shows four ^{31}P resonances for each cation, marked ADGM for **107** and adgm for **108**, and the exchange is shown to be both inter- and intramolecular in nature. Each species undergoes slow selective intramolecular exchange of its four ^{31}P nuclei. Within the monomeric species, P_D undergoes intramolecular exchange with P_A (circled) and with P_M (indicated by an arrow). Further, P_C exchanges position with P_m and P_a (squared), indicating an intermolecular exchange. The intensity of these peaks is directly related to the rate constant of the exchange considered.



Perutz and coworkers [180] have used 2D EXSY to study the dynamic behavior of $\text{RhCp}(\text{PMe}_3)(\eta^2\text{-naphthalene})$, **109**, which is thought to be a model intermediate for the oxidative addition of arenes to a metal center. In this complex, there are two processes taking place. The first involves an equilibrium between the η^2 -naphthalene complex, **109**, and the naphthyl hydride complex, **110**. The second process involves an intramolecular [1,3]-shift which moves the coordination site of the naphthalene ring from one side of the ring to the other (Scheme 1.12).

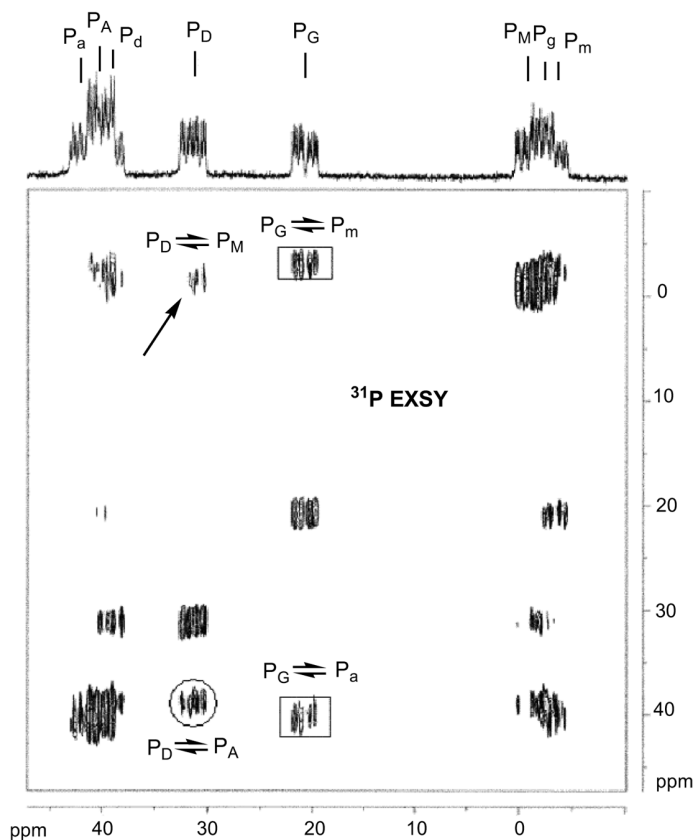
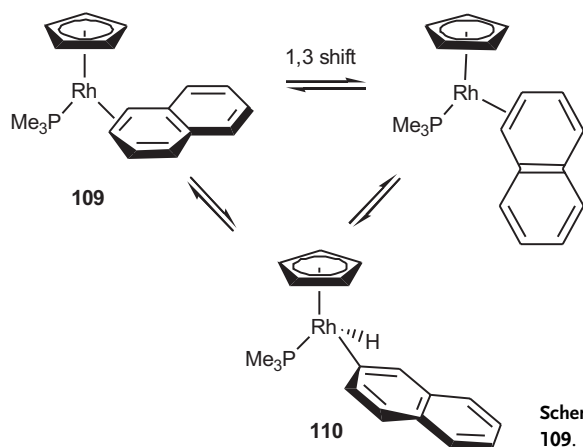


Figure 1.30 ^{31}P EXSY spectrum (CD_2Cl_2 , 176 K) showing cross-peaks for the intra- and inter-molecular exchange between ^{31}P nuclei of the monomeric, **107**, and dimeric, **108**, forms of $[\text{Rh}(\text{dppb})_2](\text{BPh}_4)$.



Scheme 1.12 Dynamic processes in **109**.

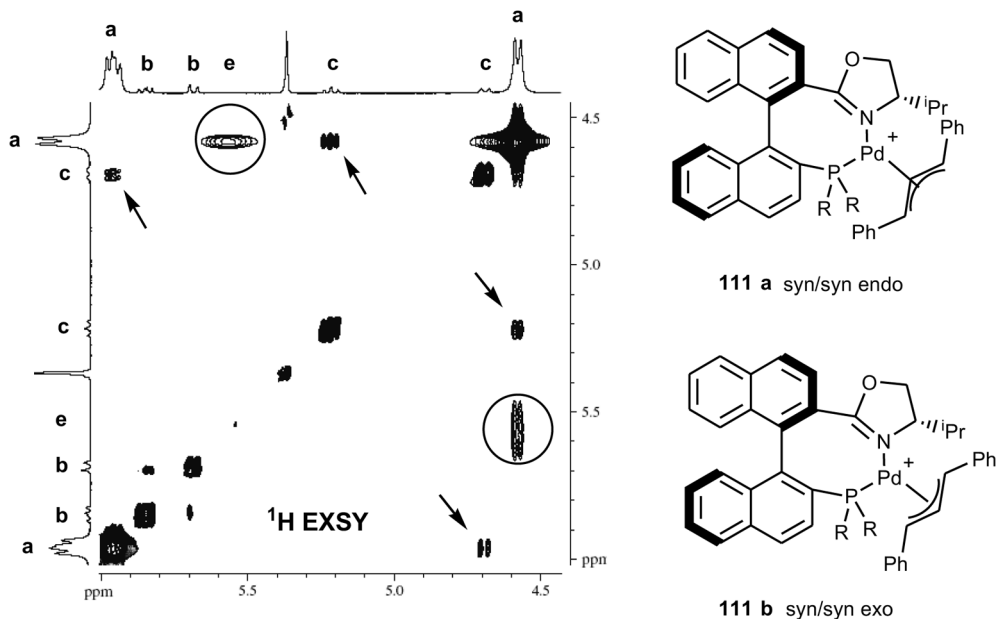


Figure 1.31 Section of the ^1H EXSY NMR spectrum showing selective exchange between the species **a** and **c** (indicated by arrows), and the species **a** and the minor allyl compound **e** (circled), in **111**.

$\text{Pd}(\text{II})$ allyl phosphino-oxazoline complexes can be intermediates in allylic alkylation chemistry [181–184]. $[\text{Pd}(\eta^3\text{-PhCHCHCHPh})(\text{phosphino-oxazoline})]^+$, **111**, reveals a mixture of four species **a**, **b**, **c**, **d** with “**a**” dominating [185]. Figure 1.31 shows a section of the ^1H EXSY spectrum in the region of the terminal allyl protons. The species **a** and **c**, corresponding to the syn/syn endo and syn/syn exo diastereoisomers, are clearly exchanging. However, a major feature of the spectrum is the intense cross-peaks between species **a** and a fifth complex, **e**. Complex “**e**”, present at very low concentration, was not detected by conventional 1D NMR spectroscopy. This species was later identified as a syn/anti allyl compound, using low temperature NMR techniques. This application represents a classic example of the detection of a hidden species using 2D EXSY.

2D EXSY has also proven to be a useful tool for the study of the dynamic behavior of transition metal carbonyl clusters [186]. These complexes have diverse applications in homogenous catalysis, including carbonylation, hydrogenation and hydroformylation reactions [187–189]. The dynamic behavior of such compounds is often viewed in terms of the migration of the CO ligand about the surface of the metallic skeleton [190]. Figure 1.32 shows the ^{13}C EXSY spectrum recorded at 240 K for $\text{Rh}_4(\text{CO})_6(\text{PPh}_2)_4$, **112**. Two pairs of ^{13}C nuclei are undergoing interchange, while a set of ^{31}P EXSY spectra (not shown) also showed that the two ^{31}P nuclei are exchanging their positions. The evaluation of the activation parameters for these processes and the analysis of the possible mechanism led the

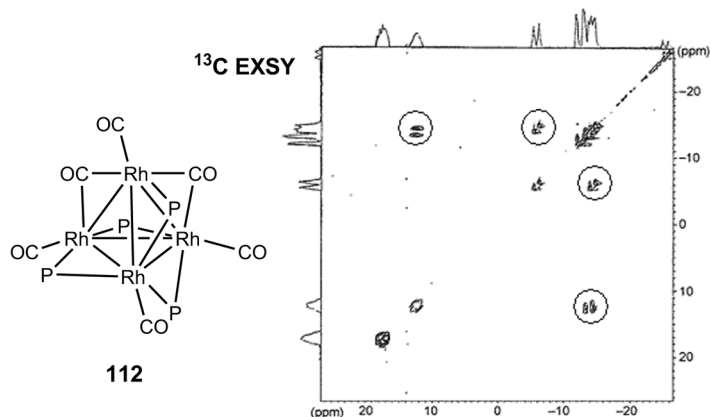


Figure 1.32 ^{13}C EXSY spectrum of **112** in CD_2Cl_2 at 240 K, showing pairwise exchange of ^{13}C nuclei (circled).

authors to propose an exchange pathway where the strongly bridging PPh_2 ligand actually hops between rhodium atoms.

On the more exotic side, we note an example of EXSY using ^{195}Pt and ^{125}Te as probes. Orrell and coworkers [174, 191] have studied the dynamic behavior of a series of trimethylplatinum(IV) iodide complexes with ditelluroether bridging ligands, $\text{Pt}(\text{Me}_3\text{L})_3$ [$(\text{L-L}) = \text{MeTe}(\text{CH}_2)_3\text{TeMe}$ and $\text{PhTe}(\text{CH}_2)_3\text{TePh}$], as shown in Figure 1.33. At ambient temperature, the complexes exist as distinct DL isomers that

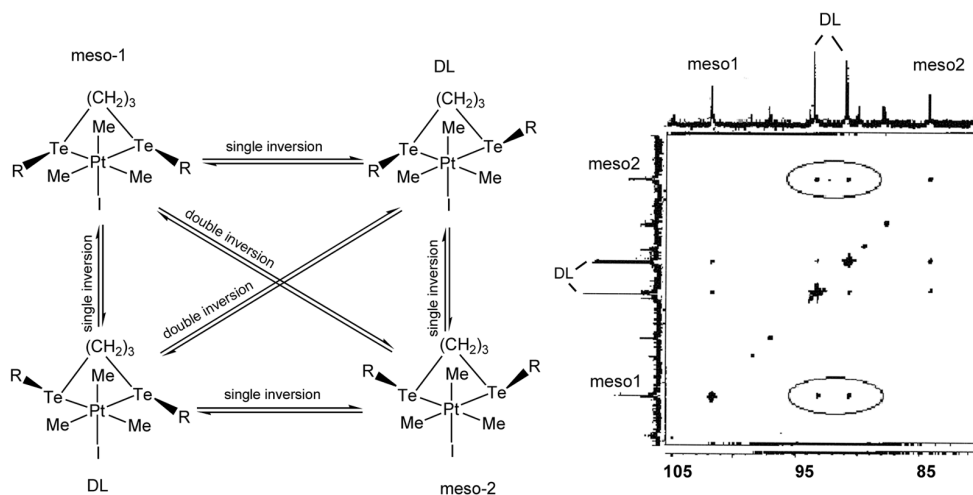


Figure 1.33 Possible exchange pathways for the inversion at Te in complexes of the type $[\text{Pt}(\text{Me}_3\text{L})_3]$, ($\text{L-L} = \text{MeTe}(\text{CH}_2)_3\text{TeMe}$ and $\text{PhTe}(\text{CH}_2)_3\text{TePh}$). ^{125}Te EXSY spectrum of $[\text{Pt}(\text{Me}_3\{\text{MeTe}(\text{CH}_2)_3\text{TeMe}\})_3]$ in CDCl_3 at 313 K. The circles indicate the position of the exchange cross peaks between the DL and the meso isomers. No exchange between the two meso isomers is observed in this compound.

undergo slow pyramidal inversion at tellurium on the NMR time scale. ^{195}Pt (not shown) and ^{125}Te EXSY spectra (Figure 1.33) afforded both qualitative and quantitative information with respect to the exchange observed between the DL and the meso species. Note that the ^{195}Pt satellites *do not exhibit cross-peaks* between the various species. This absence of ^{195}Pt to ^{195}Pt exchange processes supports an intramolecular process.

1.6

Special Topics

1.6.1

T_1 and Molecular H_2 Complexes

The longitudinal relaxation time (often called the spin–lattice relaxation time), T_1 , is concerned with the rate at which nuclei in a molecule exchange energy with their surroundings (the lattice). This time constant can vary from 10^{-3} to 10^2 s and is directly related to the efficiency of the coupling between the nuclear spin and the lattice [142, 143, 192].

The measurement of spin–lattice relaxation times, T_1 , has been proposed as a method of distinguishing between hydride and dihydrogen complexes [193]. Dihydrogen complexes [194] are recognized as intermediates in the oxidative addition of dihydrogen to a metal center. Crabtree has proposed that T_1 values are much shorter for $\eta^2\text{-H}_2$ complexes (a few milliseconds) than for hydride complexes (several hundred milliseconds) [193]. The short H–H distances in η^2 -dihydrogen ligands, typically between 0.82 and 1 Å, lead to efficient dipole–dipole relaxation. The corresponding H–H separations in hydride complexes are larger than 1.6 Å. Other authors have urged caution in using this approach, arguing that the ranges of relaxation rates for the two types of complex actually overlap [195]. However, recent calculations have shown that the method is valid, and that it can be rationalised considering that both slow (static) and fast (rotation) motions for the dihydrogen ligand are of importance in solution [196–198]. Protonation of a hydride can readily lead to an, e.g., $\text{Ru}(\text{H}_2)$ complex [199].

Since a correlation between $^1J(^2\text{H}, ^1\text{H})$ and $d(\text{H}–\text{D})$ has been suggested (Eq. (10)), the three parameters, T_1 values, coupling constants $^1J(^2\text{H}, ^1\text{H})$, and $d(\text{H}–\text{H})$ in hydrogen complexes are related.

$$d(\text{H}–\text{D}) \approx -0.0167 \, ^1J(^2\text{D}, ^1\text{H}) + 1.42$$

Morris and coworkers have studied $\text{trans}[\text{OsH}(\text{H}_2)(\text{depe})_2]^+$ (depe = diethylphosphinoethane) using several spectroscopic methods, and in particular by $T_1(\text{H}_2)$ inversion–recovery methods in solution between 190 and 300 K [200]. They conclude that if the motion of the H_2 ligand is much faster than the tumbling frequency, Eq. (11) applies. If the motion of the H_2 ligand is slower than the tumbling frequency,

$$d(\text{H-H}) = 4.611(T_1(\text{min})/\nu)^{1/6}$$

then Eq. (12) is applicable (ν is the frequency of the spectrometer and the H–H distance is given in Å).

$$d(\text{H-H}) = 5.815(T_1(\text{min})/\nu)^{1/6}$$

In a later publication, Morris and Wittebort re-examined the $^1J(^2\text{H}, ^1\text{H})$, T_1 and $d(\text{H-H})$ correlation for 73 complexes already reported in the literature [196]. For most complexes the calculated H–H distances, based on T_1 , lie between those found for the slow and fast motion conditions for the $\eta^2\text{-H}_2$, relative to the motion of the molecule. Dihydrogen fast rotation was proposed for 32 complexes, whereas six complexes appeared to have a H_2 ligand with slow internal motion. Further, torsional oscillation of the H_2 ligand, or fast 90° hopping, may still play a significant role in the T_1 relaxation value of the remaining 35 complexes. It would seem that employing T_1 values as a measure for distances in complexed H_2 is still not straightforward.

1.6.2

Parahydrogen Induced Polarization (PHIP) [201, 202]

The study of detailed chemical reaction mechanisms in homogeneous catalysis requires the identification and characterization of reaction intermediates. However, limitations arise due to both the short life time (transient type) and the low concentration of such species [203].

In 1986, Bowers and Weitekamp demonstrated the existence of hydrogen in its para spin state, which opened yet another possibility for intermediate detection [204]. Molecular hydrogen exists in two isomeric forms, with its two spins aligned either parallel, orthohydrogen, with the possible spin state combinations $\alpha\alpha$, $\alpha\beta + \beta\alpha$ and $\beta\beta$ (nuclear triplet state), or antiparallel, parahydrogen, bearing the $\alpha\beta\text{-}\beta\alpha$ spin state (nuclear singlet state). Interconversion between these two isomers is spin-forbidden. Under equilibrium conditions at ambient temperature, dihydrogen contains 25 % parahydrogen and 75 % orthohydrogen. At low temperature, parahydrogen is preferred, and the mixture can be enriched in this isomer by use of a paramagnetic catalyst (e. g. 50 % para-enriched hydrogen is obtained at 77 K) [201, 205]. Since ortho–para interconversion is slow, it is possible to separate and store the para-enriched hydrogen for subsequent hydrogenation reactions.

Parahydrogen is not directly detectable by NMR, as it has no magnetic moment. To achieve an NMR signal, the two hydrogen atoms of the para-enriched hydrogen molecule must (a) be delivered to the substrate in pairs (so that the original nuclear spin state is retained), and (b) form a product with two magnetically distinct protons (so that the spin symmetry is broken during the transfer) [204]. The product will experience non-Boltzman spin populations and, hence, yield substantially en-

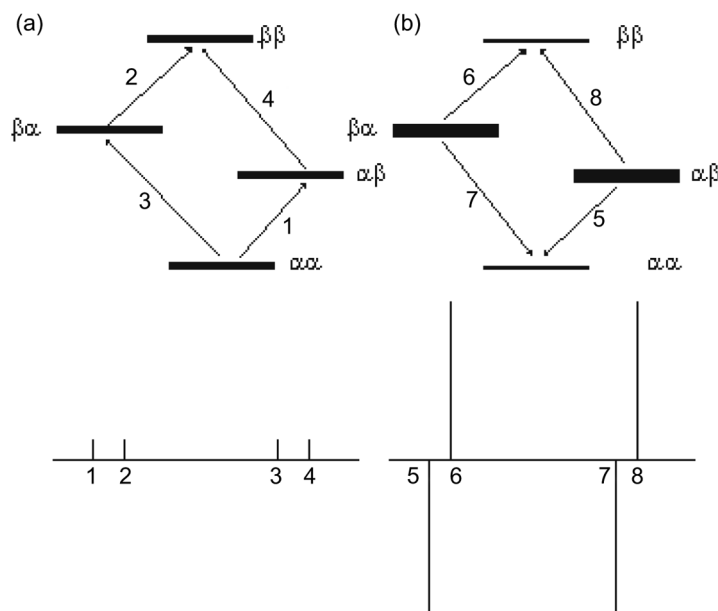


Figure 1.34 Energy level diagram for a two spin AX system, where A and X are inequivalent. Their corresponding NMR patterns are shown. (a) regular distribution (b) parahydrogen-derived distributions.

hanced and phase distorted NMR signals. Thus, this technique permits the detection of minor reaction products and intermediates, while simultaneously providing a signature for the transfer of hydrogen atoms from the same hydrogen molecule to a specific substrate. Figure 1.34 illustrates this effect by reference to the formation of a $M(H)_2$ complex where the two hydride ligands are inequivalent [206]. The thicker lines associated with the $\alpha\beta$ and $\beta\alpha$ levels on Figure 1.34(b) correspond to parahydrogen-derived population changes, while those on the left correspond to the normal (Boltzmann) distribution. For a successful observation of PHIP signals, the overall process must be faster than thermal spin relaxation.

1.6.2.1 Hydrogenation Mechanism Studies [201–203, 207]

One of the first molecules studied using parahydrogen techniques involved Vaska's complex, *trans*- $IrCl(CO)(PPh_3)_2$. Oxidative addition of H_2 was thought to proceed solely over the $CO-Ir-Cl$ axis, yielding *cis-cis-trans*- $IrCl(CO)(H)_2(PPh_3)_2$ [208, 209]. However, calculations showed that H_2 addition over the $P-Ir-P$ axis, forming the all-*cis*- $IrCl(CO)(H)_2(PPh_3)_2$, should be energetically accessible [210]. When para-enriched hydrogen was added to Vaska's complex at 295 K (Figure 1.35), the expected PHIP resonances were observed for *cis-cis-trans*- $IrCl(CO)(H)_2(PPh_3)_2$, but a minor species could also be detected. This minor product was identified as the all-*cis*-

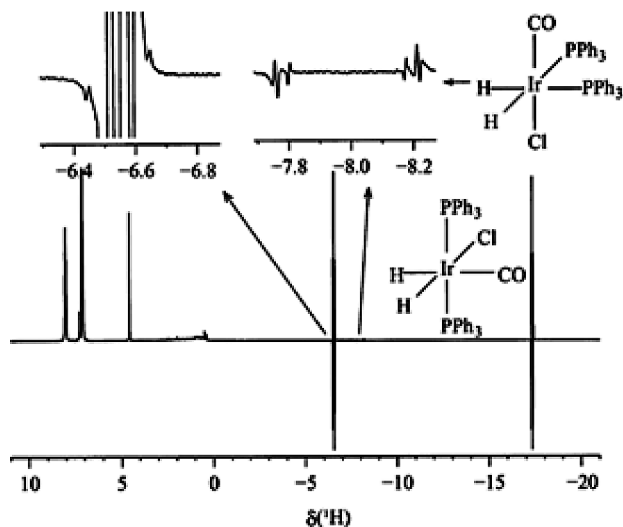


Figure 1.35 ^1H NMR spectrum obtained upon addition of parahydrogen to Vaska's complex $\text{trans-IrCl(CO)(PPh}_3)_2$ in C_6D_6 at 295 K, showing the extra species resulting from addition of H_2 over the P–Ir–P axis.

$\text{IrCl(CO)(H)}_2(\text{PPh}_3)_2$, with two chemically equivalent but magnetically inequivalent hydrides [203, 211, 212].

Catalytic hydrogenation of alkynes by a monomeric transition metal complex was thought to yield exclusively the *Z*-alkene. However, Bargon and coworkers [213, 214], who have been active in PHIP research, observed the formation of *E*-alkenes using $[\text{RuCp}^*(\text{alkene})]^+$ as catalyst. Figure 1.36 shows the ^1H NMR spectrum after

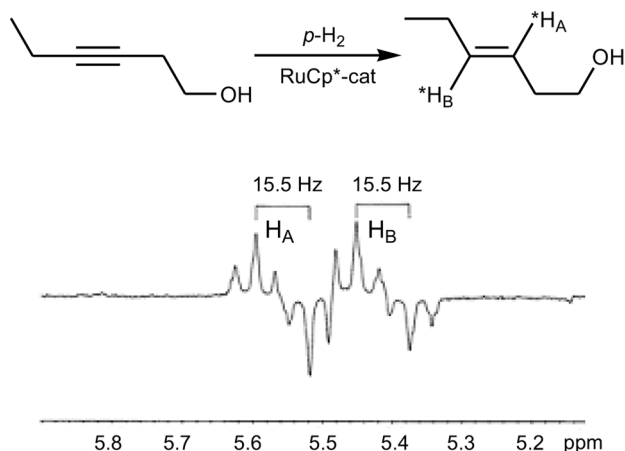
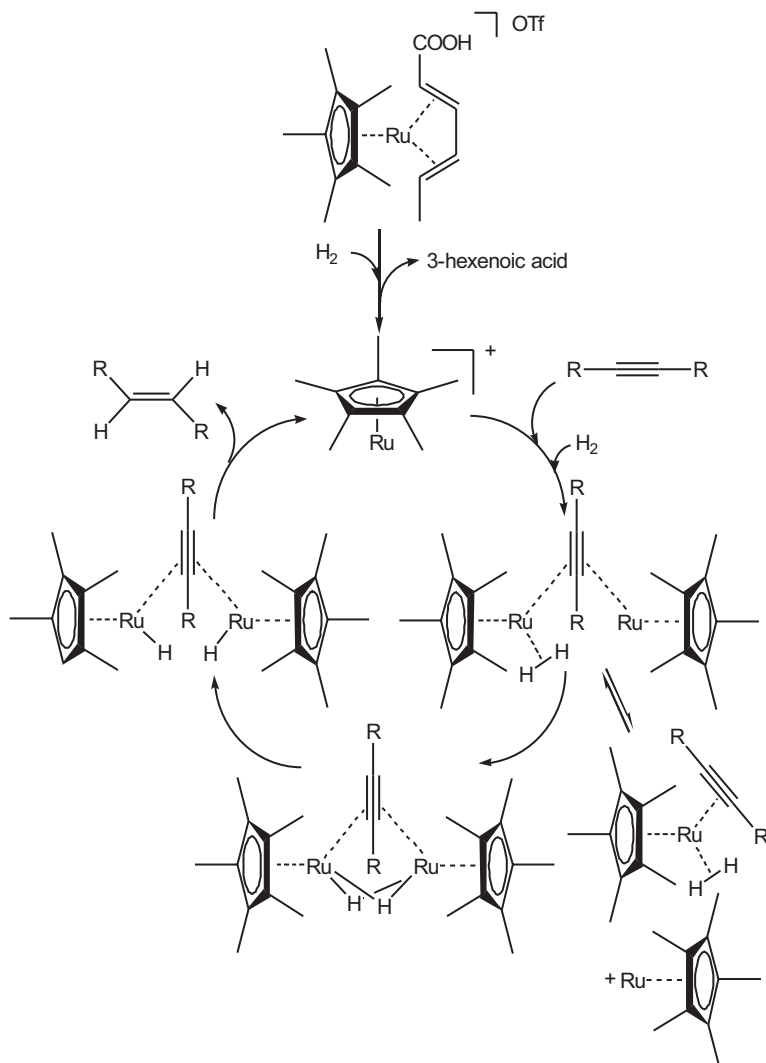
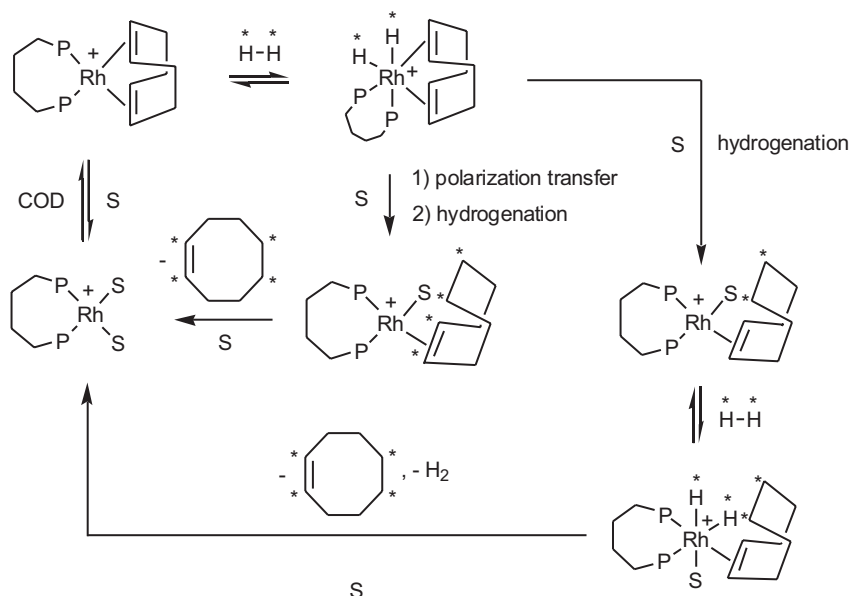


Figure 1.36 Olefinic region of the ^1H NMR spectrum for the product of the hydrogenation reaction of 3-hexyne-1-ol in presence of $[\text{RuCp}^*(\text{alkene})]^+$ (alkene = 3-hexenoic acid) and para-enriched hydrogen, under mild reaction conditions (300 K, 1 bar of H_2) and low conversion rate.

the hydrogenation of 3-hexyne-1-ol using para-enriched hydrogen and in the presence of $[\text{RuCp}^*(\text{alkene})]^+$ (alkene = 3-hexenoic acid). This spectrum is the result of a pairwise transfer of para- H_2 to the substrate, and shows a $^3J(^1\text{H}, ^1\text{H})$ of 15 Hz, typical of a trans coupling. The formation of *E*-alkene by trans hydrogenation of the substrate is undisputable, and unlikely with a single metal center catalyst. Initial formation of a *Z*-alkene was not detected, even at low temperature. Moreover, the *Z*-alkene was found not to isomerise in the presence of $[\text{RuCp}^*(\text{alkene})]^+$. A mechanism involving two ruthenium centers, as shown in Scheme 1.13, was therefore proposed.



Scheme 1.13 Proposed mechanism for the hydrogenation of alkynes in the presence of $[\text{RuCp}^*(\text{alkene})]^+$ (alkene = 3-hexenoic acid), involving two ruthenium centers.



Scheme 1.14 Possible mechanisms for the transfer of polarisation from parahydrogen onto cyclooctene via $[\text{Rh}(\text{COD})(\text{dppb})]^+$: (a) and (b) are the possible intermediate dihydride species responsible for the polarisation transfer at cyclooctene.

In the previous example, the addition of para-hydrogen at a transition metal has led to the observation of PHIP at the substrate [213, 214]. In a similar manner, Aime and coworkers [215] have studied the hydrogenation of cyclooctadiene from $[\text{Rh}(\text{COD})(\text{dppb})]^+$ in the presence of parahydrogen, and observed strongly polarized hydrogen resonances at both the hydrogenated sites *and* the olefinic region of the ^1H spectrum of the free cyclooctene formed. In view of these data, they suggested two possible mechanisms (Scheme 1.14), and showed that the enhanced absorption for the olefinic protons of cyclooctene is due to NOE transfer both within the para-hydrogenated substrate and the transition metal hydride complex formed during hydrogenation.

1.6.2.2 Parahydrogen as a Magnetic Probe

The electronic spin state requirement for observation of PHIP at a transition metal center makes it a very good magnetic probe [202, 203, 216]. $\text{Ru}(\text{CO})_2\text{H}_2(\text{dppe})$ ($\text{dppe} = \text{Ph}_2\text{PCH}_2\text{CH}_2\text{PPh}_2$) is highly fluxional and undergoes a pairwise interchange of the two hydrides, the two P-atoms, and the two CO ligands at the same rate. H_2 readily eliminates from the ruthenium center at high temperature ($> 330\text{ K}$) [216]. Para- H_2 was used to investigate this reductive elimination, pointing to a diamagnetic intermediate, $\text{Ru}(\text{CO})_2(\text{dppe})$. Indeed, the ^1H spectrum observed upon addition of parahydrogen to $\text{Ru}(\text{CO})_2(\text{dppe})$ showed strongly polarized

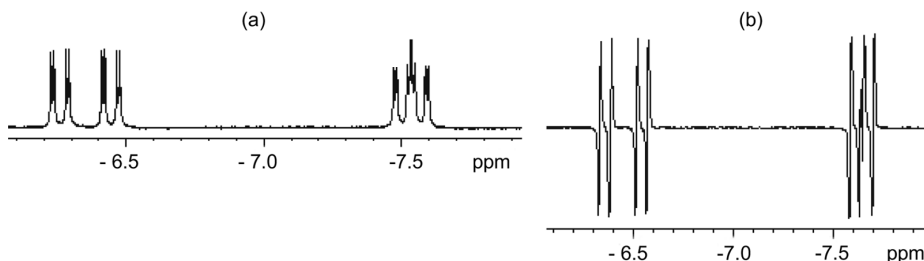


Figure 1.37 ^1H NMR spectrum of the product of oxidative addition of H_2 to $\text{Ru}(\text{CO})_2(\text{dppe})$, (a) with normal hydrogen, (b) with para-enriched hydrogen

signals in the hydride region of the ^1H spectrum, (Figure 1.37(b)). Therefore, $\text{Ru}(\text{CO})_2(\text{dppe})$ exists in a singlet electronic spin state (a paramagnetic intermediate would have quenched the enhancement through magnetic anisotropy-induced relaxation and no polarised resonance would have been observed). Further, this observation is consistent with an exchange mechanism involving a trigonal bipyramidal transition state containing an η^2 -coordinated hydrogen.

1.6.3

High Pressure NMR

1.6.3.1 Introduction

High gas pressures are widely used in many homogeneous catalytic processes, such as hydrogenations, hydroformylations or polymerizations. The use of pressure has a number of advantages: (a) increasing the concentration of the reactant gas (usually CO or H_2) in solution, thereby achieving faster reaction rates; (b) controlling dynamic equilibria; (c) suppressing the boiling of a solvent at high temperature; or (d) avoiding decomposition of the catalyst. Although NMR is slow and insensitive compared to the well-established high pressure infrared spectroscopy [217], NMR under pressure is advantageous in that it is non-invasive and provides detailed structural information. Several reviews on the subject have been published, and the reader is advised to consult Chapter 2 for instrumental details [218–222].

1.6.3.2 Applications

The main applications of high pressure NMR (HP NMR) to homogeneous catalysis include [219–221]:

1. Monitoring reactions under conditions similar to the catalytic reaction.
2. Stabilization and identification of intermediates.
3. Measurement of kinetic and thermodynamic parameters.
4. Investigation of reactions in supercritical fluids.

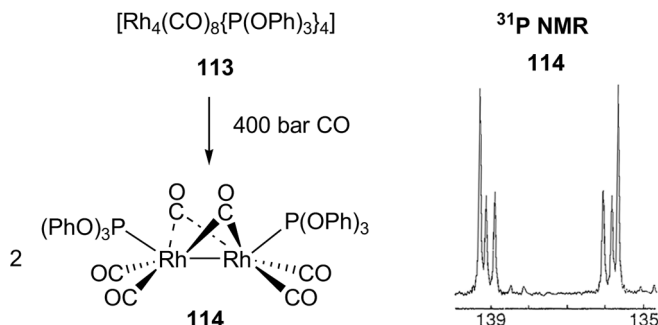


Figure 1.38 ^{31}P HP NMR spectrum of **114**. δ ^{31}P 138. The observed second-order spin system, AA'XX', is consistent with the complete conversion of **113** into **114**.

Some of these applications will be illustrated in the next paragraphs, and many others can be found in the literature [223–225].

The first application of HP NMR to homogeneous catalysis was reported by Heaton, Jonas and coworkers [226, 227], who measured ^{13}C under pressure of the Rh carbonyl clusters $[\text{Rh}_{12}(\text{CO})_{30}]^{2-}$ and $[\text{Rh}_5(\text{CO})_{15}]^-$, involved in the catalytic synthesis of ethylene glycol from CO and H_2 . In a related application, the olefin hydroformylation catalyst precursors $[\text{Rh}_4(\text{CO})_{12-x}\{\text{P}(\text{OPh})_3\}_x]$ ($x = 1-4$) were studied using high pressures of CO and CO/H_2 , while monitoring ^{13}C and ^{31}P [228]. Figure 1.38 shows the ^{31}P HP NMR spectrum for **114**, formed when $[\text{Rh}_4(\text{CO})_8\{\text{P}(\text{OPh})_3\}_4]$, **113**, is submitted to 400 bar CO at 260 K.

The dinuclear Rh complex, $\text{rac-}[\text{Rh}_2\text{H}_2(\mu\text{-CO})_2(\text{CO})_2(\text{et,ph-P4})]^{2+}$, **115**, ($\text{et,ph-P4} = \text{Et}_2\text{PCH}_2\text{CH}_2\text{P}(\text{Ph})\text{CH}_2\text{CH}_2\text{P}(\text{Ph})\text{CH}_2\text{CH}_2\text{PEt}_2$), was identified by ^1H HP NMR as the active catalyst in the regioselective Rh-catalyzed hydroformylation of 1-alkenes [229]. Figure 1.39 shows the hydride region of the ^1H and $^1\text{H}\{^{31}\text{P}\}$ HP NMR spectra of catalyst **115**.

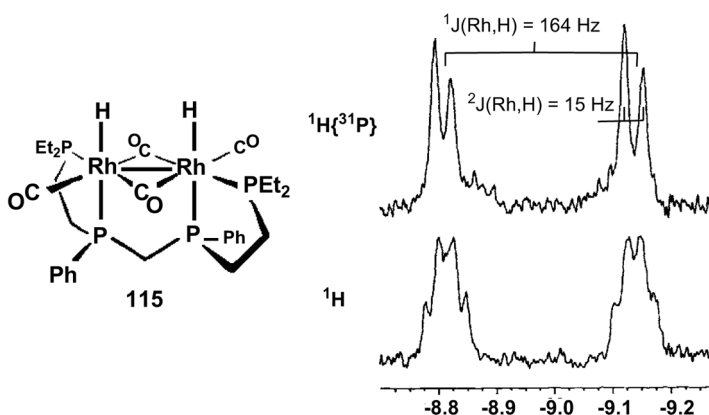


Figure 1.39 Hydride region of the ^1H and $^1\text{H}\{^{31}\text{P}\}$ HP NMR spectra of the hydroformylation catalyst **115**.

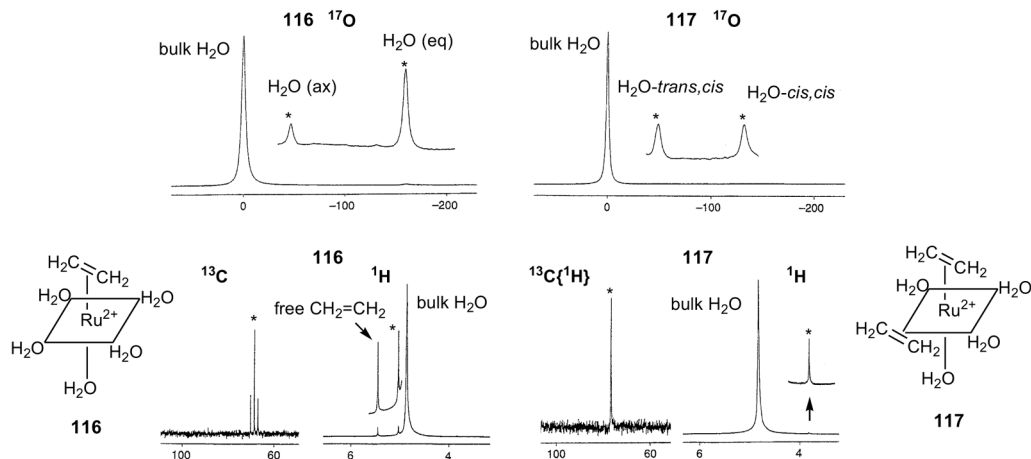


Figure 1.40 ^{17}O , ^{13}C and ^1H HP NMR spectra of aqueous solutions of **116** and **117**, (in 10% [^{17}O]water) under 60 bar ethylene at 298 K. For **116**, the ^{17}O NMR spectrum shows signals at δ -160.1 and δ -46.9, in ratio 4:1, corresponding to the equatorial and axial water oxygens, respectively. For **117** the ^{17}O NMR spectrum shows two signals with 1:1 intensity ratio at δ -49.52 and -132.1, which can be assigned to the cis,trans and cis,cis water oxygens, respectively.

of **115**, acquired under 13.8 bar H_2/CO , at 295 K. An extremely large $^1J(^{109}\text{Rh}, ^1\text{H})$ coupling constant (164 Hz) was reported [229].

Additional applications involving CO [220, 230–238] and CO_2 [239–241], plus an elegant combination of ^{103}Rh NMR [242] together with high pressure have been reported.

In the $[\text{Ru}(\text{H}_2\text{O})_6]^{2+}$ -catalyzed dimerisation of ethylene at 60 bar [243] ^{17}O labeling and a multinuclear NMR approach (^{17}O , ^{13}C and ^1H , see Figure 1.40) have allowed the identification of the reaction intermediates $[\text{Ru}(\text{CH}_2=\text{CH}_2)(\text{H}_2\text{O})_5](\text{tos})_2$, **116**, and $[\text{Ru}(\text{CH}_2=\text{CH}_2)_2(\text{H}_2\text{O})_4](\text{tos})_2$, **117**, (tos = toluene-*p*-sulfonate).

As noted above, molecular hydrogen complexes are important intermediates in homogeneous catalytic hydrogenation reactions. When a solution of $[\text{Cr}(\text{CO})_3(\text{PCy}_3)_2]$, **118**, reacts with 28 bar H_2 at ambient temperature, $[\text{Cr}(\eta^2\text{-H}_2)(\text{CO})_3(\text{PCy}_3)_2]$, **119**, is formed (Eq. (13)) [244]. The rate of $\eta^2\text{-H}_2$ elimination from **119** was determined by ^1H HP NMR inversion recovery experiments in which both the bound and dissolved H_2 were measured (Figure 1.41) [244]. Although this is not a generally applicable method for obtaining rate information, it works in this case due to the large difference in the intrinsic relaxation rates of the two H_2 species. The calculated rate constants are found to be independent of the H_2 pressure, showing that the elimination is a first-order process.



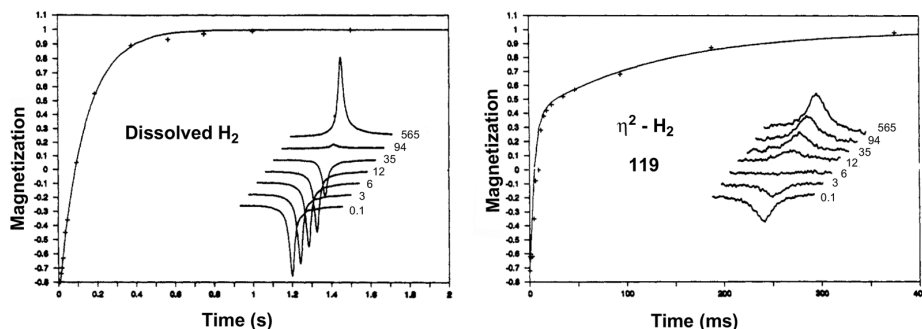


Figure 1.41 ^1H HP NMR inversion-recovery experiments on dissolved and bound H_2 in a d^8 -toluene solution of $[\text{Cr}(\eta^2\text{-H}_2)(\text{CO})_3(\text{PCy}_3)_2]$, **119**.

Iggo and coworkers have recently developed a high pressure NMR flow cell for the study of homogeneous reactions and reported several interesting applications [245, 246]. In the reaction of $[\text{RuCp}(\mu\text{-CO})_2(\mu\text{-dcpm})\text{RhCl}_2]$ ($\text{dcpm} = (\text{C}_6\text{H}_{11})_2\text{PCH}_2\text{P}(\text{C}_6\text{H}_{11})_2$, **120**, with CO, the intermediate bimetallic complex **121** could be detected by in situ ^{31}P HP NMR (Figure 1.42) [247]. Previous attempts to detect **121** by high pressure infrared spectroscopy had proven unsuccessful [248].

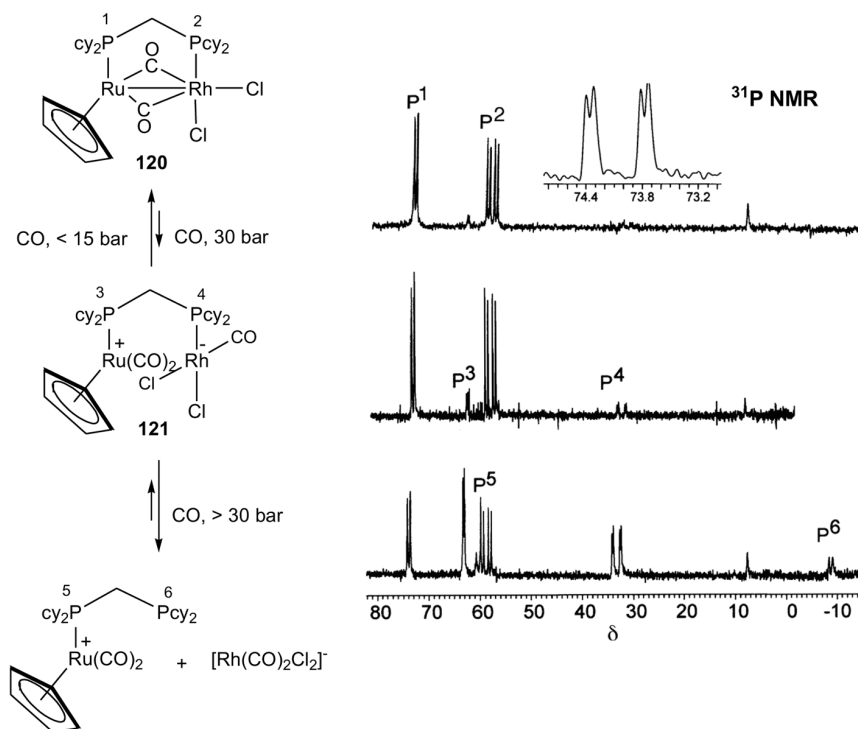


Figure 1.42 ^{31}P HP NMR investigation of the reaction of **120** with CO.

The toroidal pressure probe, introduced in 1989 by Rathke and coworkers [249, 250], has been modified by Woelk and coworkers [249, 251], who have used a toroid cavity NMR autoclave for high pressure PHIP NMR experiments. Figure 1.43 shows the PHIP spectrum of the $[\text{Rh}(\text{norbornadiene})(\text{PPh}_3)_2]\text{PF}_6$ -catalyzed hydrogenation of 1,4-diphenylbutadiyne with 40 bar of 50% enriched para- H_2 [252]. The spectrum from the same reaction at ambient H_2 pressure is shown in the inset [253]. The two absorption/emission PHIP patterns in both spectra indicate that para- H_2 is transferred pairwise during the catalytic cycle.

A special area of HP NMR in catalysis involves supercritical fluids, which have drawn substantial attention in both industrial applications and basic research [249, 254, 255]. Reactions in supercritical fluids involve only one phase, thereby circumventing the usual liquid/gas mixing problems that can occur in conventional solvents. Further advantages of these media concern their higher diffusivities and lower viscosities [219]. The most commonly used supercritical phase for metal-catalyzed processes is supercritical CO_2 (scCO_2), due to its favorable properties [256–260], i.e., nontoxicity, availability, cost, environmental benefits, low critical temperature and moderate critical pressure, as well as facile separation of reactants, catalysts and products after the reaction.

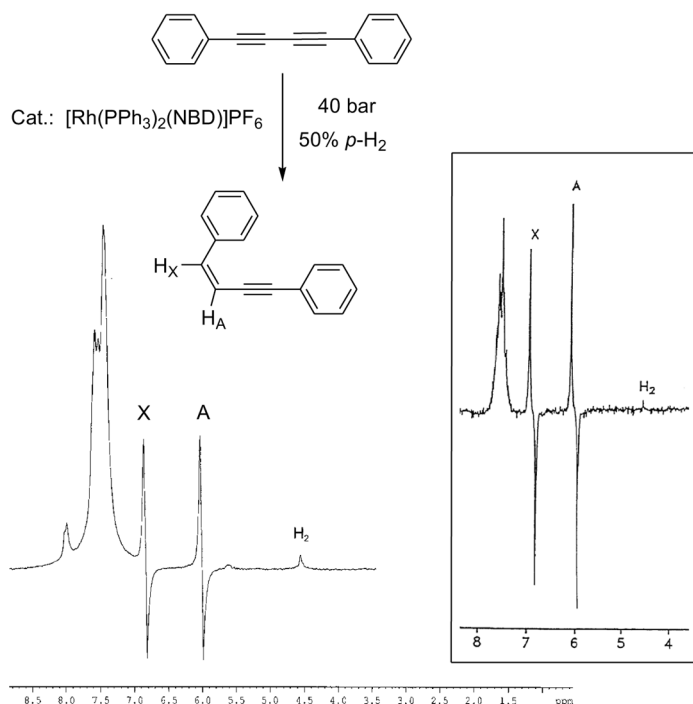


Figure 1.43 HP PHIP NMR spectrum of the $[\text{Rh}(\text{norbornadiene})(\text{PPh}_3)_2](\text{PF}_6)$ -catalyzed hydrogenation of 1,4-diphenylbutadiyne with 40 bar of 50% enriched $p\text{-H}_2$, plus the spectrum from the same reaction at ambient H_2 pressure (in the inset).

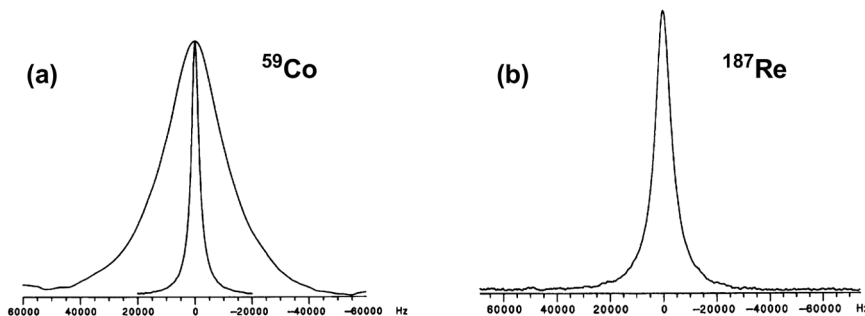
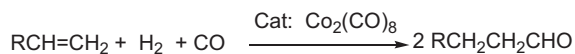


Figure 1.44 (a) ^{59}Co NMR spectra of a 0.04 M solution of $\text{Co}_2(\text{CO})_8$ in scCO_2 (303 K) and liquid C_6D_6 (298 K) solutions (^{59}Co quadrupole moment: $Q = 0.4 \times 10^{-28} \text{ cm}^2$). (b) ^{187}Re NMR spectrum of a solution of $\text{Re}_2(\text{CO})_{10}$ in scCO_2 (473 K, 145 bar) (^{187}Re quadrupole moment: $Q = 2.6 \times 10^{-28} \text{ cm}^2$).

Supercritical fluids possess several advantages from the NMR point of view [249]. The very low viscosity of these solvents produces a beneficial line-narrowing effect on quadrupolar nuclei such as ^{59}Co , ^{14}N , ^{53}Cr , ^{91}Zr , ^{95}Mo , ^{55}Mn and ^{103}Re , due to their increased transverse relaxation times, T_2 [219, 254, 261–264]. The improvement in observed line-widths can be clearly appreciated in Figure 1.44(a), which shows ^{59}Co NMR spectra of the olefin hydroformylation catalyst $\text{Co}_2(\text{CO})_8$ [249, 265]. While in C_6D_6 at 298 K the half-height line-width ($\Delta\nu_{1/2}$) equals 30.0 kHz, in scCO_2 at 305 K $\Delta\nu_{1/2}(^{59}\text{Co})$ is only 5.1 kHz. Hence, the distinction between cobalt complexes with similar ^{59}Co chemical shifts, e. g. $\text{Co}(\text{C}_3\text{H}_7\text{C}(\text{O}))(\text{CO})_4$ and $\text{Co}_2(\text{CO})_8$, is facilitated in the supercritical medium. Figure 1.44(b) reproduces the ^{187}Re NMR spectrum from $\text{Re}_2(\text{CO})_{10}$, which, due to the high quadrupole moment of ^{187}Re , cannot be observed at all under routine conditions in normal solvents [249].

An even more useful property of supercritical fluids involves the near temperature-independence of the solvent viscosity and, consequently, of the line-widths of quadrupolar nuclei. In conventional solvents the line-widths of e. g. ^{59}Co decrease with increasing temperature, due to the strong temperature-dependence of the viscosity of the liquid. These line-width variations often obscure chemical exchange processes. In supercritical fluids, chemical exchange processes are easily identified and measured [249]. As an example, Figure 1.45 shows ^{59}Co line-widths of $\text{Co}_2(\text{CO})_8$ in scCO_2 for different temperatures. Above 160 °C, the line-broadening due to the dissociation of $\text{Co}_2(\text{CO})_8$ to $\text{Co}(\text{CO})_4$ can be easily discerned [249].

There are an increasing number of applications of high pressure NMR in supercritical fluids to homogeneous catalysis [266]. Using their toroidal pressure probe, Rathke and coworkers [249, 267–269] have extensively studied the $\text{Co}_2(\text{CO})_8$ -catalyzed hydroformylation of olefins in scCO_2 (Eq. (14)). The hydrogenation of $\text{Co}_2(\text{CO})_8$ (Eq. (15)) is a key step in this reaction.



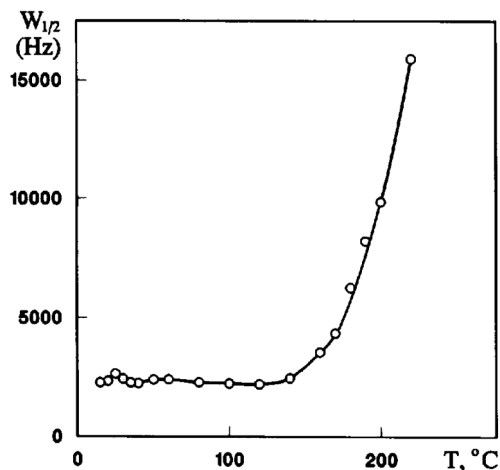


Figure 1.45 Temperature dependence of the ^{59}Co NMR line widths for a 4.8 mM solution of $\text{Co}_2(\text{CO})_8$ in scCO_2 .

^{59}Co variable temperature HP NMR (Figure 1.46(a)) revealed an equilibrium reaction which exchanges the cobalt centers in $\text{Co}_2(\text{CO})_8$ and $\text{CoH}(\text{CO})_4$, in the higher temperature region. This process does not broaden the ^{59}Co signal of $\text{Co}_4(\text{CO})_{12}$, even at 473 K (Figure 1.46(b)), nor the ^1H signals of H_2 or $\text{CoH}(\text{CO})_4$ at 453 K (Figure 1.46(c)). These observations point to a process involving dissociation of $\text{Co}_2(\text{CO})_8$ into two $\text{Co}(\text{CO})_4$ radicals, followed by hydrogen atom transfer

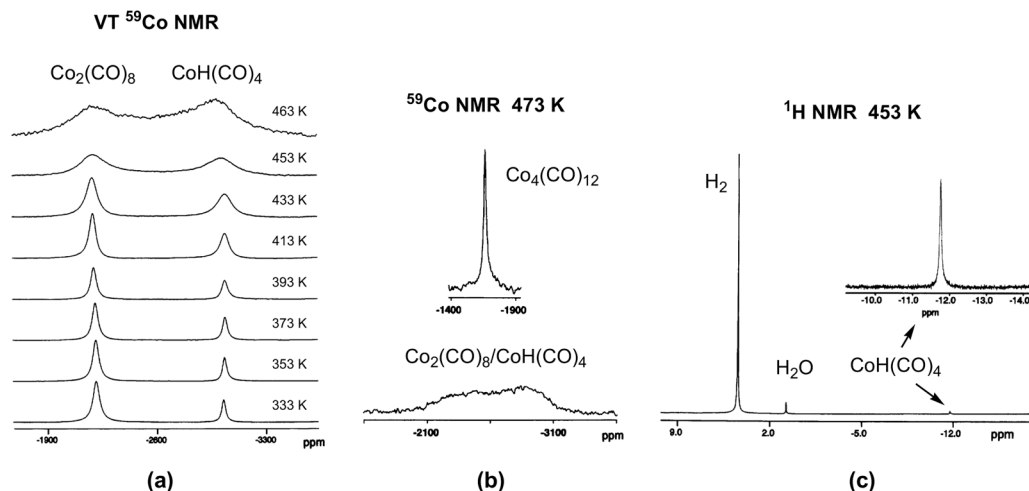


Figure 1.46 (a) ^{59}Co VT-NMR spectra for the reaction of $\text{Co}_2(\text{CO})_8$ with H_2 in scCO_2 . (b) ^{59}Co NMR spectrum of a mixture containing $\text{Co}_4(\text{CO})_{12}$, $\text{Co}_2(\text{CO})_8$ and $\text{CoH}(\text{CO})_4$ at 473 K in scCO_2 . (c) ^1H NMR spectrum at 453 K. Conditions as in (a).

from $\text{CoH}(\text{CO})_4$ to the radical $\text{Co}(\text{CO})_4$ (Eqs. (16) and (17)). Such a mechanism would interconvert the ^{59}Co signals of $\text{Co}_2(\text{CO})_8$ and $\text{HCo}(\text{CO})_4$ without affecting the ^1H signals [249, 267, 268].



In a related study, the hydroformylation of propene to *n*- and iso-butyraldehydes, catalyzed by $\text{Co}_2(\text{CO})_8$, was followed by ^1H (Figure 1.47(a)) and ^{59}Co HP NMR (Figure 1.47(c)) [249, 265]. A typical ^{59}Co spectrum at 353 K and 219 bar is shown in Figure 1.47(b) and reveals $\text{Co}(\text{C}_3\text{H}_7\text{C}(\text{O}))(\text{CO})_4$, $\text{Co}_2(\text{CO})_8$ and $\text{CoH}(\text{CO})_4$. As shown in Figure 1.47(c), the cobalt complexes reach a nearly steady-state condition early in the hydroformylation, which persists during the 15 h period that the olefin is still present at significant levels.

Woelk and coworkers [252, 270] have provided a detailed view into the activation and transfer of the dihydrogen molecule during hydrogenations in scCO_2 , using PHIP and their toroid cavity NMR autoclave. For the asymmetric hydrogenation

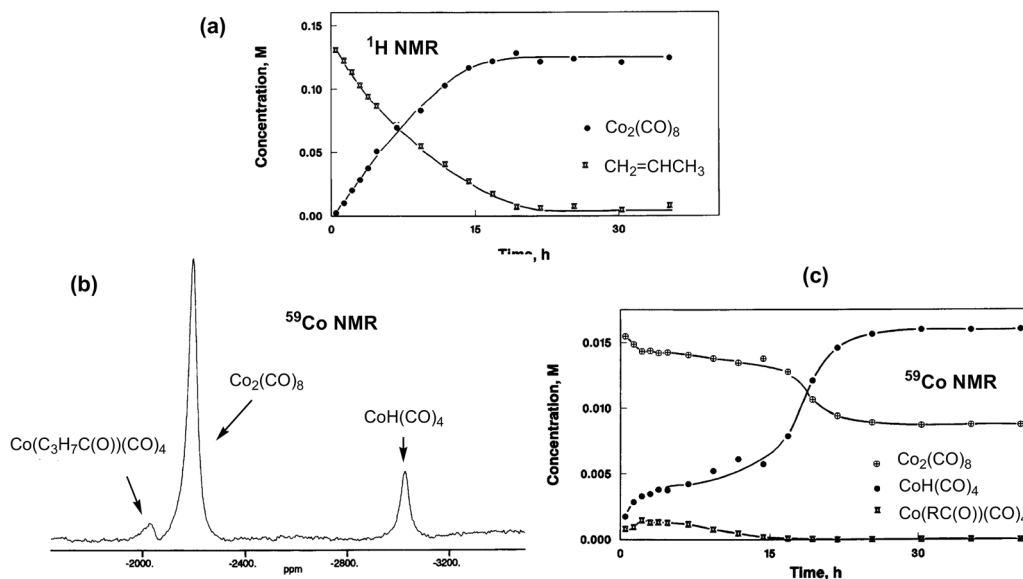


Figure 1.47 (a) Conversion of propylene (0.14 M) to *n*- and iso-butyraldehydes in scCO_2 in the presence of $\text{Co}_2(\text{CO})_8$ (0.017 M) at 353 K, using H_2 and CO pressures of 42 bar each, followed by ^1H NMR. (b) In situ ^{59}Co NMR spectrum showing the catalytic intermediates, near the steady state, during hydroformylation of propylene in scCO_2 at 353 K. (c) Concentrations of catalytic intermediates during propylene hydroformylation in scCO_2 at 353 K, followed by ^{59}Co NMR

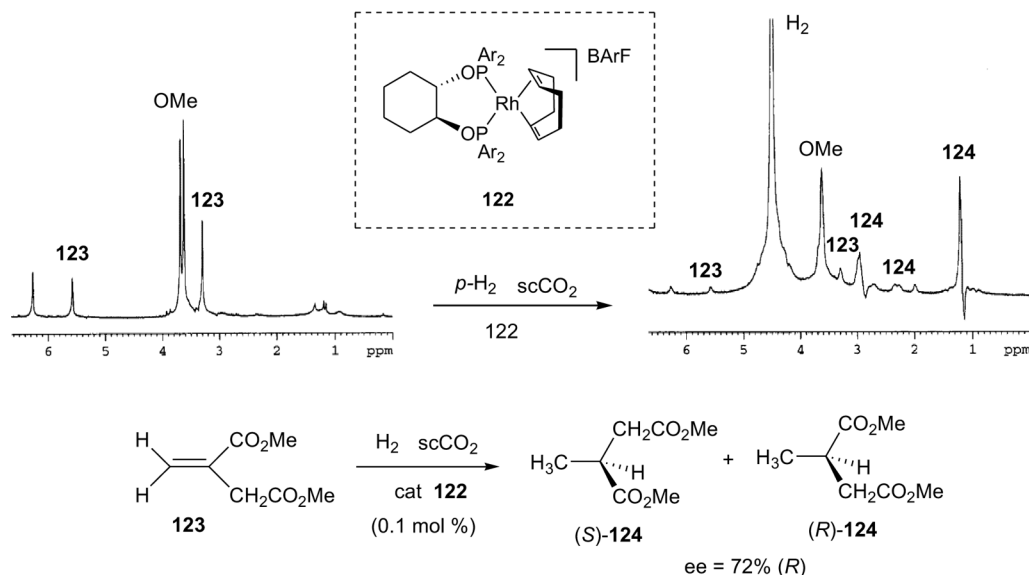
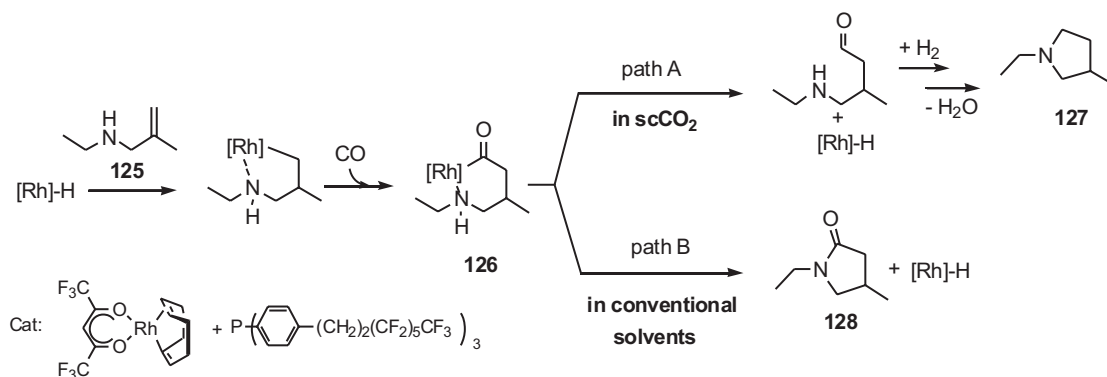


Figure 1.48 Left: standard ^1H spectrum of a reaction mixture containing **122** and **123** (1:100) in scCO_2 at 318 K and 150 bar. Right: PHIP spectrum of the same mixture after increasing the pressure to 180 bar with para H_2 . Chemical interactions between CO_2 and reactive intermediates of the catalytic pathway can be excluded as the source of the different catalytic behavior in the supercritical medium with respect to usual solvents.

of **123** to yield **124**, catalyzed by the rhodium complex **122** (Figure 1.48), it is concluded that the major catalytic pathway in scCO_2 is very similar, if not identical, to that found in a nonprotic organic solvent of low polarity [270].

The Rh-catalyzed cyclization of the amine **125** in scCO_2 affords the cyclic amine **127** as the major product (path A in Scheme 1.15), whereas in conventional sol-



Scheme 1.15 Different result of the Rh-catalyzed cyclization of **125** in scCO_2 (path A) and in conventional solvents (path B).

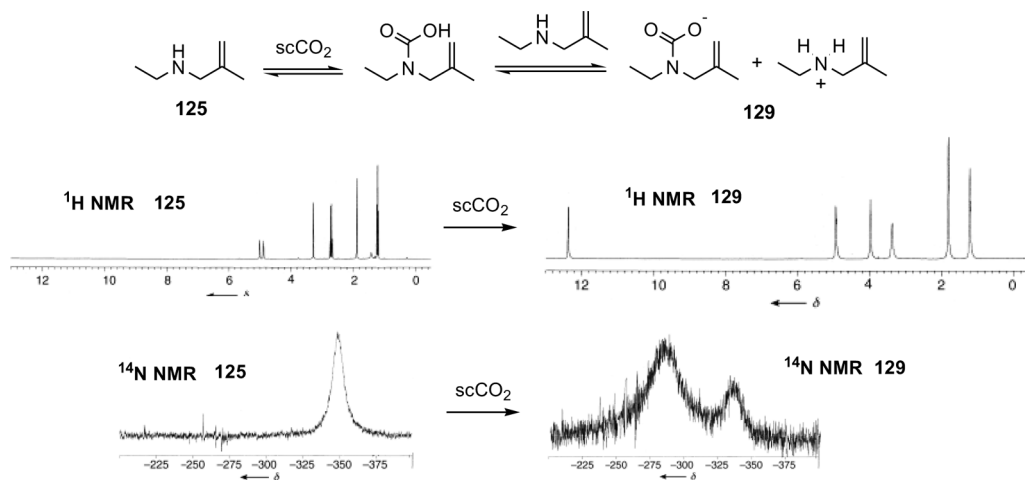


Figure 1.49 Left: ¹H NMR spectra of **125** in d⁸-THF (298 K, left) and in scCO₂/d⁸-THF (180 bar, 323 K, right). Right: ¹⁴N NMR spectra of **129** in d⁶-acetone (298 K, left) and scCO₂/d⁶-acetone (110 bar, 313 K, right; a smaller signal of a second species is visible under these conditions).

vents the cyclic amide **128** is formed preferentially (path B) [271]. HP ¹H and ¹⁴N NMR measurements in scCO₂ (Figure 1.49) have allowed the detection of an intermediate carbamic acid, **129**, in this solvent. In the ¹H NMR spectra, the broad signal of the NH proton of **125** at δ 1.4 is replaced by a new signal at δ 12.4, corresponding to **129**, and the resonances of both CH₂ protons directly adjacent to the N center of **125** exhibit a significant high frequency shift of 0.6 ppm in **129**. In the ¹⁴N NMR spectra, an induced shift of 64 ppm in the major resonance indicates the formation of the carbamic acid as the major species. This reversible formation of a carbamic acid in scCO₂ would reduce the tendency for intramolecular ring closure at the Rh-acyl intermediate **126**, and thus suppress path B in Scheme 1.15, explaining the low formation of cyclic amides in the supercritical solvent. Supercritical CO₂ would act simultaneously as solvent and temporary protecting group in this reaction [271].

1.6.4

Diffusion and Pulsed Gradient Spin Echo Measurements

PGSE (Pulsed Gradient Spin Echo) NMR diffusion methods were introduced in 1965 by Stejskal and Tanner [272]. The basic pulse sequence is based on a spin-echo with two incorporated pulsed field gradients (Figure 1.50). The effect of the two gradients is first, to defocus and, then, refocus the magnetization. However, if during the time Δ , the molecules diffuse from their positions after the first gradient, the effective magnetic field experienced will be different during both gradients. This results in incomplete refocusing of the spins and a decrease in the intensity of the detected NMR signals. Repetition of the experiment with increasing

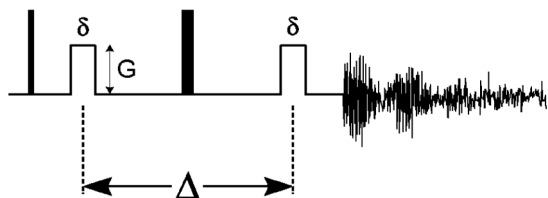


Figure 1.50 Basic pulse sequence for PGSE diffusion measurements. G = gradient strength, Δ = delay between the midpoints of the gradients, D = diffusion coefficient, δ = gradient length

gradient strengths, G , affords a set of signals from which the diffusion coefficient, D , can be obtained, according to Eq. (18). A typical plot is shown in Figure 1.51, for measurements on several different anions of a Ru(II) Binap complex [273]. Larger molecules will diffuse more slowly than smaller molecules, and thus afford smaller slopes, as in Figure 1.51. More elaborate pulse sequences have been proposed [274–279]. From the diffusion coefficients a hydrodynamic radius, r_h , and thus the molecular volume can be estimated, via the Stokes–Einstein equation (Eq. (19)).

$$\ln\left(\frac{I}{I_0}\right) = -(\gamma\delta)^2 G^2 \left(\Delta - \frac{\delta}{3}\right) D$$

$$D = \frac{kT}{6\pi\eta r_h}$$

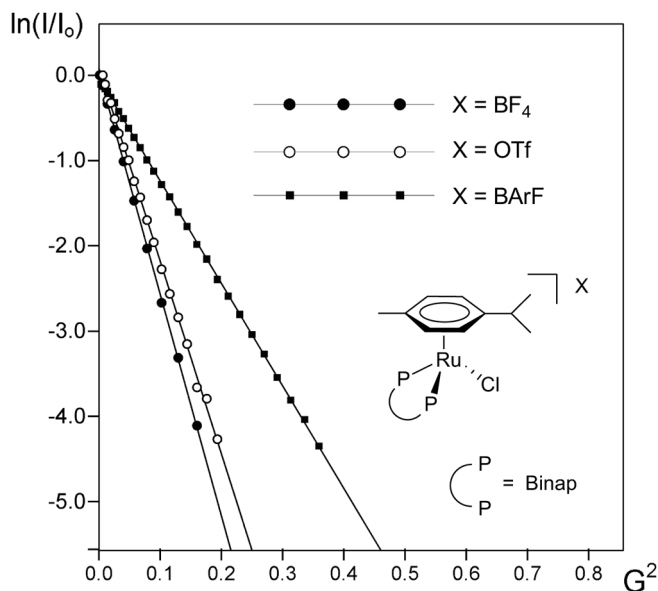


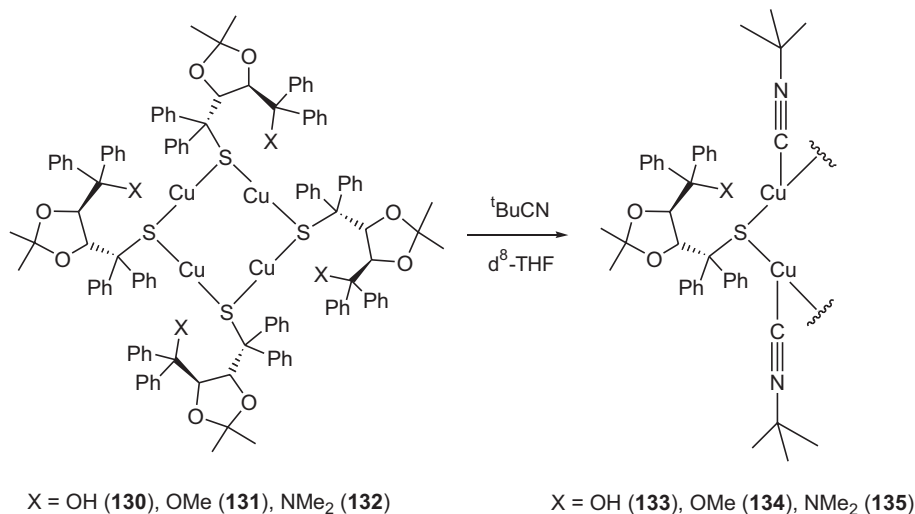
Figure 1.51 Plots of ^{19}F PGSE diffusion measurements on several salts of a Ru(II) *p*-cymene Binap complex. The larger the anion, the smaller the absolute value of the slope.

The PGSE methodology presents several advantages with respect to other methods for estimating molecular size and diffusion coefficients [280]. PGSE measurements are fast, noninvasive and require only small samples. They allow a reasonably accurate determination of D values over several orders of magnitude, without the need to set up and maintain a concentration gradient. Several components of a mixture can be measured simultaneously (as long as they afford resolvable signals), which makes the technique especially valuable for materials which are not readily isolable, or mixtures of special interest.

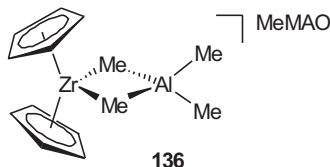
PGSE measurements have been widely applied in the investigation of small organic molecules [281], polymers [282, 283], surfactants [284], “container molecules” [285–288], supramolecular reagents [289], dendrimers [290, 291] and biomolecules [292–294]. There are also some few examples concerned with molecules in heterogeneous environments (e.g. in porous silica [295] and zeolites [296]). Recently, PGSE studies have been extended to the field coordination and/or organometallic chemistry, to address problems such as the formation of polynuclear complexes [76], ion pairing [4, 297, 298], hydrogen-bonding ligands [299], and otherwise aggregated species [115, 300, 301]. This subject has been reviewed [302–304]. Apart from nuclei with high receptivity (^1H and ^{19}F), PGSE measurements on inorganic and organometallic compounds can be successfully carried out with nuclei such as ^{31}P [298], ^{35}Cl [298] or ^7Li [305].

The first application of NMR diffusion measurements to determine the aggregation state of a transition metal catalyst concerned the chiral, tetranuclear $\text{Cu}(\text{I})$ catalysts **130–132**, used in the conjugate addition reactions of anions to α,β -unsaturated cyclic ketones. Compounds **130–132** react with isocyanides to form **133–135**, and do not degrade to lower molecular weight species (see Eq. (20)) [109].

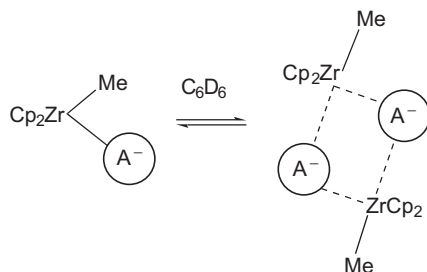
Britzinger and coworkers [306] have studied the polymerization catalyst $\text{MAO}/\text{ZrCp}_2\text{Me}_2$ in C_6D_6 . The calculated effective hydrodynamic radius of 12.2–12.5 Å



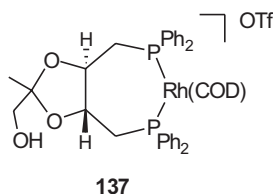
at different zirconocene and MAO concentrations indicates that the ion pair **136** remains associated even at the lowest concentrations studied. At elevated concentrations, aggregation to ion quadrupoles or higher aggregates is indicated by an apparent size increase [306].



Interestingly, for the series of zirconocene catalysts $[\text{Zr}]^+[\text{MeB}(\text{C}_6\text{F}_5)_3]^-$ Marks and coworkers [307] have found no evidence of significant aggregation to ion quadrupoles, as in Eq. (21). These authors have found that the tendency to form aggregates of higher nuclearity than simple ion-pairs is dependent on whether the anion is in the inner or outer coordination sphere of the metallocenium cation [308].



The PGSE methodology has also been applied to study the dependence of enantioselectivity on the distribution of the chiral Rh-hydrogenation catalyst **137** between an aqueous and micellar phase. The observed increase in enantioselectivity when amphiphiles are added to the water is associated with an aggregation of the catalyst to the micelles [309].



PGSE diffusion measurements have proved very valuable in studying ion-pairs. A relatively large number of cationic compounds are currently in use in homogeneous catalysis and/or organic synthesis. It has been shown that the counterion

may influence the rate and/or product distribution of some of these reactions [147, 310–315], as well as the stability of the compounds [316]. In principle, one can determine the diffusion coefficients for the cation and anion separately, and thus gain insight into whether they move together as a single unit (tight ion-pair) or separately. For anions such as PF_6^- , BF_4^- , OTf^- or BArF^- , ^{19}F represents both an alternative and a complement to ^1H PGSE methods. HOESY (Heteronuclear Overhauser Spectroscopy), and especially ^1H , ^{19}F HOESY measurements, also help to localize the position of anions such as PF_6^- or BArF^- , relative to a catalytically active transition metal cation [116, 147, 304, 317–319].

The Ir(I) catalyst precursors **138a** ($\text{X} = \text{BArF}^-$) and **138b** ($\text{X} = \text{B}(\text{C}_6\text{F}_5)_4^-$) have been shown to hydrogenate tri-substituted olefins in CH_2Cl_2 with excellent enantioselectivity. With the smaller anions $\text{X} = \text{PF}_6^-$, BF_4^- and OTf^- (**138c–d**) the rate of reaction is much lower [320]. PGSE diffusion measurements on **138a–d** in CDCl_3 afford very similar D -values for cation and anion in each compound, pointing to a complete ion-pairing in this solvent (e.g., for **138c** in CDCl_3 , $D(\text{cation}) = 7.13 \times 10^{-10} \text{ m}^2 \text{ s}^{-1}$ and $D(\text{PF}_6^-) = 7.21 \times 10^{-10} \text{ m}^2 \text{ s}^{-1}$) [321]. In CD_3OD , the cation and anion move separately, and in CD_2Cl_2 , there seems to be a partial, but not complete, ion-pairing [321]. Figure 1.52 shows the results from PGSE measurements on the cations of **138a–d** in CD_2Cl_2 . For **138a** and **138b** (white circles) the cations move significantly more slowly (lower slope) than for **138c–d** (black circles).

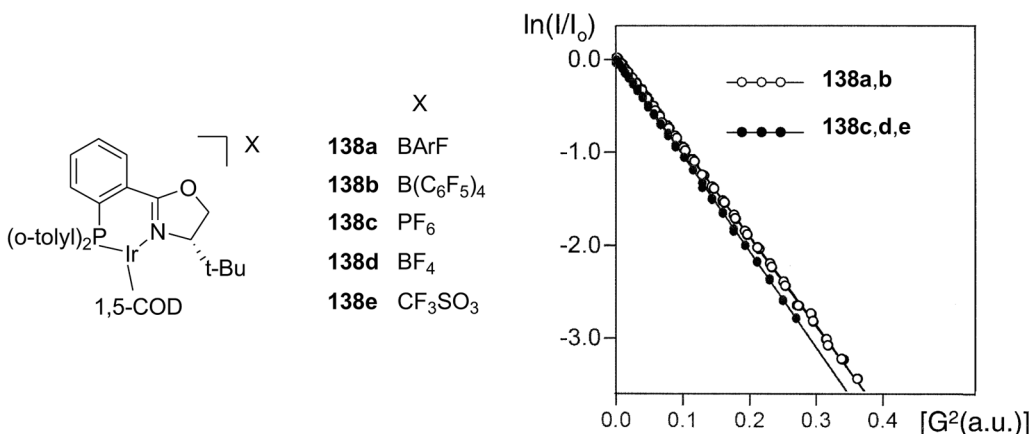
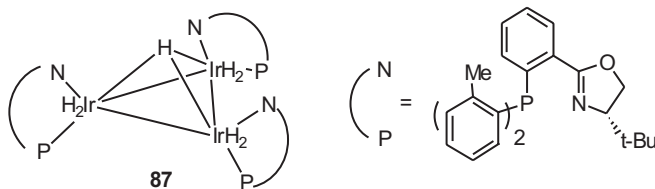


Figure 1.52 Plot of $\ln(I/I_0)$ vs. arbitrary units proportional to the square of the gradient amplitude for ^1H PGSE diffusion measurements on the cation of the five Ir(I) catalyst precursors **138a–d**, in CD_2Cl_2 .



Clearly, the (partial) ion-pairing with the larger boron anions, BArF^- and $\text{B}(\text{C}_6\text{F}_5)_4^-$, decreases the mobility of the cation in **138a,b** with respect to **138c–e**, where the anions are smaller. It is known that mononuclear Ir complexes such as **138** react under hydrogen in solution to afford trinuclear hydrido cluster complexes such as **87**, which have been shown not to be catalytically active in hydrogenation chemistry [110]. If the mechanism of the formation of these inactive Ir_3 clusters requires that two fairly large species associate, and subsequently add yet another large moiety, then, in CH_2Cl_2 , the lower mobility of **138a,b** compared to **138c–e** might explain the faster deactivation of the latter.

PGSE diffusion measurements can also be presented as a “2D spectrum” where the chemical shift is displayed in the first dimension and the diffusion coefficient in the second one. Such an experiment is called DOSY (Diffusion Ordered Spectroscopy) [274, 322, 323] and has also been referred to as “NMR chromatography”, for its ability to facilitate and visualize the resolution and assignment of complex mixtures. Although used in several areas of chemistry, such as micelles [324], polymers [325–328], resins [329], biochemistry [330–332] and organic chemistry [333–336],

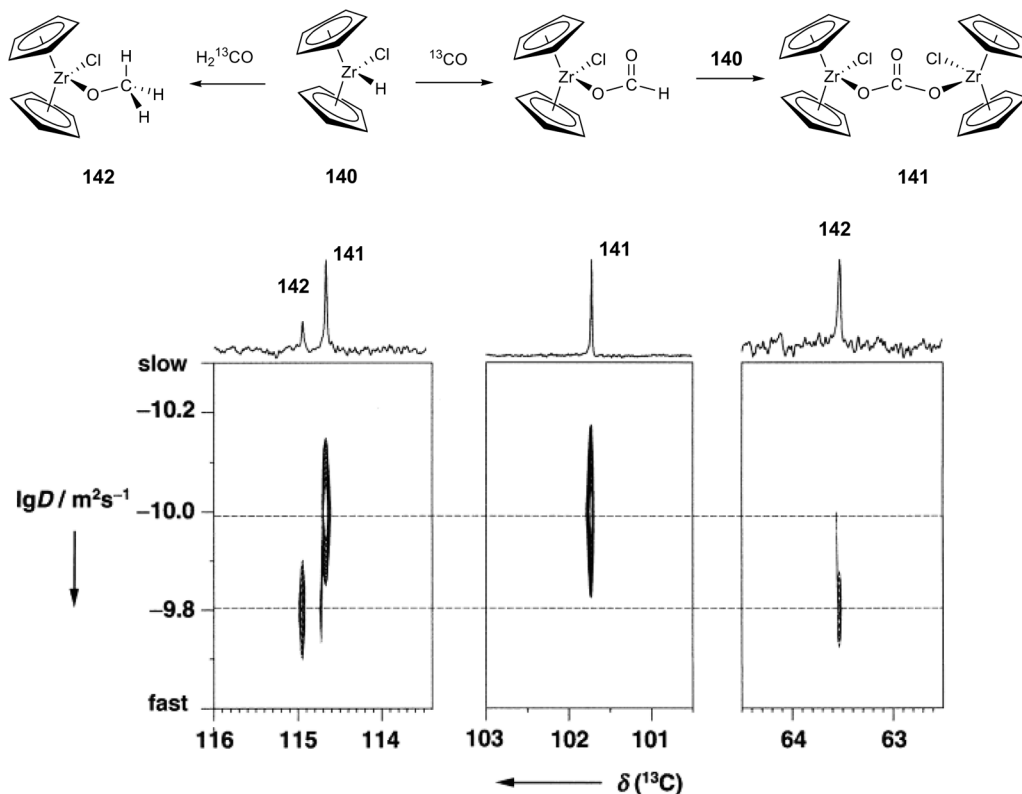


Figure 1.53 ^{13}C INEPT DOSY spectrum obtained during the reaction of **140** with $^{13}\text{CO}_2$ at 195 K in $\text{d}^8\text{-THF}$. The sections show the signals of **141** (δ 114.6 (Cp) and δ 101.7 (CH_2)) and **142** (δ 114.9 (Cp) and δ 63.5 (OMe)).

DOSY measurements have attracted very little attention in organometallic chemistry [337]. 3D versions of DOSY, where the diffusion dimension is added to a 2D experiment [338, 339], as well as heteronuclear detection, e.g. with ^{13}C [340–342], ^{31}P [335], ^{29}Si [343], and ^7Li [337] have been reported recently.

In a very recent example (Figure 1.53), ^{13}C INEPT DOSY has been applied to confirm the dinuclear nature of the unstable Zirconium intermediate **141** in the reaction of ^{13}CO with $[\text{ZrHCl}(\text{Cp})]$, **140** [344], a model reaction for the heterogeneously catalyzed hydrogenation of CO_2 to methanol [345]. As was expected for a binuclear compound, the diffusion coefficient of intermediate **141** is smaller than for the mononuclear **142**.

Comment: Whether it is used for simple monitoring, or to prove the existence of traces of a key intermediate (EXSY or PHIP), NMR spectroscopy has clearly developed into one of the catalytic community's most valuable analytical tools. NOE data will never afford a molecular picture which is quite as structurally exact as that from X-ray crystallography; however, this latter method cannot determine kinetic parameters, recognize equilibria, mimic catalytic conditions (HP) or recognize when ion-pairing is important (PGSE). NMR is not a very sensitive method; indeed, most methods are far more amenable to quantitative results. Nevertheless, its proven flexibility makes it indispensable.

References

- [1] N. Feiken, P. S. Pregosin, G. Trabe-singer, *Organometallics* **1997**, *16*, 3735.
- [2] D. Drago, P. S. Pregosin, A. Razavi, *Organometallics* **2000**, *19*, 1802.
- [3] D. Drago, P. S. Pregosin, *J. Chem. Soc., Dalton Trans.* **2000**, 3191.
- [4] P. G. Anil Kumar, P. S. Pregosin, T. Schmid, G. Consiglio, *Magn. Reson. Chem.* **2004**, *42*, in press.
- [5] J. Pawlas, Y. Nakao, M. Kawatsura, J. F. Hartwig, *J. Am. Chem. Soc.* **2002**, *124*, 3669.
- [6] R. A. M. Robertson, A. D. Poole, M. J. Payne, D. J. Cole-Hamilton, *J. Chem. Soc., Dalton Trans.* **2000**, 1817.
- [7] G. C. Lloyd-Jones, S. W. Krska, D. L. Hughes, L. Gouriou, V. D. Bonnet, K. Jack, Y. Sun, R. A. Reamer, *J. Am. Chem. Soc.* **2004**, *126*, 702.
- [8] T. Agapie, S. J. Schofer, J. A. Labinger, J. E. Bercaw, *J. Am. Chem. Soc.* **2004**, *126*, 1304.
- [9] S. C. van der Slot, P. C. J. Kamer, P. W. N. M. van Leeuwen, *Organometallics* **2001**, *20*, 1079.
- [10] T. Hayashi, K. Inoue, N. Taniguchi, M. Ogasawara, *J. Am. Chem. Soc.* **2001**, *123*, 9918.
- [11] G. C. Lloyd-Jones, *Org. Biomol. Chem.* **2003**, *1*, 215.
- [12] G. R. Eastham, R. P. Tooze, M. Kilner, D. F. Foster, D. J. Cole-Hamilton, *J. Chem. Soc., Dalton Trans.* **2002**, 1613.
- [13] R. Whyman, A. P. Wright, J. A. Iggo, B. T. Heaton, *J. Chem. Soc., Dalton Trans.* **2002**, 771.
- [14] H. Steinhagen, M. Reggelen, G. Helmchen, *Angew. Chem.* **1997**, *109*, 2199.
- [15] J. M. Brown, P. A. Chaloner, *J. Chem. Soc. Chem. Commun.* **1980**, 344.
- [16] A. S. C. Chan, J. J. Pluth, J. Halpern, *Inorg. Chim. Acta* **1979**, *37*, L477.
- [17] A. S. C. Chan, J. Halpern, *J. Am. Chem. Soc.* **1980**, *102*, 838.

- [18] J. M. Brown, P. A. Chaloner, *J. Am. Chem. Soc.* **1980**, *102*, 3040.
- [19] T. Hayashi, M. Takahashi, Y. Takaya, M. Ogasawara, *J. Am. Chem. Soc.* **2002**, *124*, 5052.
- [20] C. R. Landis, K. A. Rosaaen, D. R. Sillars, *J. Am. Chem. Soc.* **2003**, *125*, 1710.
- [21] A. L. Casado, P. Espinet, A. M. Gallego, J. M. Martínez-Harduya, *Chem. Commun.* **2001**, 339.
- [22] J. M. Brown, K. K. Hii, *Angew. Chem.* **1996**, *108*, 679.
- [23] K. K. Hii, T. D. W. Claridge, J. M. Brown, *Angew. Chem. Int. Ed. Engl.* **1997**, *36*, 984.
- [24] K. K. Hii, T. D. W. Claridge, J. M. Brown, A. Smith, R. J. Deeth, *Helv. Chim. Acta* **2001**, *84*, 3043.
- [25] G. R. Eastham, B. T. Heaton, J. A. Iggo, R. P. Tooze, R. Whyman, S. Zacchini, *Chem. Commun.* **2000**, 609; see J. Liu, B. T. Heaton, J. A. Iggo, R. Whyman, *Angew. Chem. Int. Ed. Engl.* **2004**, *43*, 90 for a comment on the carbomethoxy cycle.
- [26] W. Clegg, G. R. Eastham, M. R. J. Elsegood, B. T. Heaton, J. A. Iggo, R. P. Tooze, R. Whyman, S. Zacchini, *Organometallics* **2002**, *21*, 1832.
- [27] J. Wolowska, G. R. Eastham, B. T. Heaton, J. A. Iggo, C. Jacob, R. Whyman, *Chem. Commun.* **2002**, 2784.
- [28] K. L. Bray, J. P. H. Charmant, I. J. S. Fairlamb, G. C. Lloyd-Jones, *Chem.-Eur. J.* **2001**, *7*, 4205.
- [29] A. L. Casado, P. Espinet, *Organometallics* **1998**, *17*, 954.
- [30] A. L. Casado, P. Espinet, *Organometallics* **2002**, *2003*, 1305.
- [31] L. M. Alcazar-Roman, J. F. Hartwig, A. L. Rheingold, L. M. Liable-Sands, I. A. Guzei, *J. Am. Chem. Soc.* **2000**, *122*, 4618.
- [32] D. R. Sillars, C. R. Landis, *J. Am. Chem. Soc.* **2003**, *125*, 9894.
- [33] C. R. Landis, J. Halpern, *J. Am. Chem. Soc.* **1987**, *109*, 1746.
- [34] J. F. Hartwig, C. N. Muhoro, *Organometallics* **2000**, *19*, 30.
- [35] D. J. Tempel, L. K. Johnson, R. L. Huff, P. S. White, M. Brookhart, *J. Am. Chem. Soc.* **2000**, *122*, 6686.
- [36] C. S. Shultz, J. Ledford, J. M. DeSimone, M. Brookhart, *J. Am. Chem. Soc.* **2000**, *122*, 6351.
- [37] M. S. Sanford, J. A. Love, R. H. Grubbs, *J. Am. Chem. Soc.* **2001**, *123*, 6543.
- [38] Z. J. A. Komon, J. S. Rogers, G. C. Bazan, *Organometallics* **2002**, *21*, 3189.
- [39] B. T. Heaton, S. P. A. Hebert, J. A. Iggo, F. Metz, R. Whyman, *J. Chem. Soc., Dalton Trans.* **1993**, 3081.
- [40] J. W. Faller, D. G. D'Alliessi, *Organometallics* **2002**, *21*, 1743.
- [41] J. A. Wiles, S. H. Bergens, *Organometallics* **1998**, *17*, 2228.
- [42] J. A. Wiles, S. H. Bergens, K. P. M. Vanhessche, D. A. Dobbs, V. Rautenstrauch, *Angew. Chem. Int. Ed. Engl.* **2001**, *40*, 914.
- [43] T. J. Geldbach, P. S. Pregosin, *Helv. Chim. Acta* **2002**, *85*, 3937.
- [44] M. D. Leatherman, S. A. Svejda, L. K. Johnson, M. Brookhart, *J. Am. Chem. Soc.* **2003**, *125*, 3068.
- [45] L. H. Shultz, D. J. Tempel, M. Brookhart, *J. Am. Chem. Soc.* **2001**, *123*, 11539.
- [46] L. H. Shultz, M. Brookhart, *Organometallics* **2001**, *20*, 3975.
- [47] D. J. Tempel, M. Brookhart, *Organometallics* **1998**, *17*, 2290.
- [48] R. J. Deeth, A. Smith, K. K. Hii, J. M. Brown, *Tetrahedron Lett.* **1998**, *39*, 3229.
- [49] M. Rubina, V. Gevorgyan, *J. Am. Chem. Soc.* **2001**, *123*, 11107.
- [50] J. C. Conrad, G. P. A. Yap, D. E. Fogg, *Organometallics* **2003**, *22*, 1986.
- [51] S. Aeilts, D. R. Cefalo, P. J. Bonitatebus, J. H. Houser, A. H. Hoveyda, R. R. Schrock, *Angew. Chem. Int. Ed. Engl.* **2001**, *40*, 1452.
- [52] A. Albinati, P. S. Pregosin, F. Wombacher, *Inorg. Chem.* **1990**, *29*, 1812.
- [53] P. S. Pregosin, F. Wombacher, *Magn. Reson. Chem.* **1991**, *29*, S106.
- [54] P. S. Pregosin, in *Encyclopedia of Nuclear Magnetic Resonance*, Ed. B. Lever, Vol. 4, John Wiley & Sons Ltd., New York, **1996**, p. 2549.
- [55] P. S. Pregosin, "Phosphorus-31 NMR Spectroscopic Properties in Compound

- Characterization and Structural Analysis", Vol. 8, Eds. J. G. Verkade, L. D. Quin, VCH, Deerfield Beach, FL, 1987, p. 465.
- [56] P. S. Pregosin, R. W. Kunz, ³¹P and ¹³C NMR of Transition Metal Phosphine Complexes, Vol. 16, Springer Verlag, Berlin, 1979.
- [57] D. Touchard, P. Haquette, S. Guesmi, L. LePichon, A. Daridor, L. Toupet, P. H. Dixneuf, *Organometallics* **1997**, *16*, 3640.
- [58] M. Albrecht, J. R. Miecznikowski, A. Samuel, J. W. Faller, R. H. Crabtree, *Organometallics* **2002**, *21*, 3596.
- [59] A. Haynes, B. E. Mann, G. E. Morris, P. Maitlis, *J. Am. Chem. Soc.* **1993**, *115*, 4093.
- [60] D. C. Roe, R. E. Sheridan, E. E. Bunel, *J. Am. Chem. Soc.* **1994**, *116*, 1163.
- [61] M. Kollmar, G. Helmchen, *Organometallics* **2002**, *21*, 4771.
- [62] P. Dotta, P. G. A. Kumar, P. S. Pregosin, A. Albinati, S. Rizzato, *Organometallics* **2003**, *22*, 5345.
- [63] E. Martinez-Viviente, P. S. Pregosin, M. Tschoerner, *Magn. Reson. Chem.* **2000**, *38*, 23.
- [64] M. Tschoerner, R. W. Kunz, P. S. Pregosin, *Magn. Reson. Chem.* **1999**, *37*, 91.
- [65] M. Tschoerner, P. S. Pregosin, *Inorg. Chim. Acta* **1999**, *290*, 95.
- [66] D. Drago, P. S. Pregosin, *Organometallics* **2002**, *21*, 1208.
- [67] N. Feiken, P. S. Pregosin, G. Trabe-singer, A. Albinati, G. L. Evoli, *Organometallics* **1997**, *16*, 5756.
- [68] P. Dotta, A. Magistrato, U. Rothlis-berger, P. S. Pregosin, A. Albinati, *Organometallics* **2002**, *21*, 3033.
- [69] M. A. Bennett, I. J. McMahon, S. Pelling, M. Brookhart, D. M. Lin-coln, *Organometallics* **1992**, *11*, 127.
- [70] M. Bennett, A. K. Smith, *J. Chem. Soc., Dalton Trans.* **1974**, 233.
- [71] J. W. Faller, D. G. D'Alliessi, *Organometallics* **2003**, *22*, 2749.
- [72] J. W. Faller, J. Parr, *Organometallics* **2000**, *19*, 1829.
- [73] B. Therrien, T. R. Ward, M. Pilington, C. Hofmann, f. Gilardoni, J. Weber, *Organometallics* **1998**, *17*, 330.
- [74] P. J. Fagan, M. D. Ward, J. C. Ca-labrese, *J. Am. Chem. Soc.* **1989**, *111*, 1698.
- [75] C. W. Cyr, S. J. Rettig, B. O. Patrick, B. R. James, *Organometallics* **2002**, *21*, 4672.
- [76] T. J. Geldbach, P. S. Pregosin, A. Albinati, F. Rominger, *Organometallics* **2001**, *20*, 1932.
- [77] Y. Chen, M. Valentini, P. S. Pregosin, A. Albinati, *Inorg. Chim. Acta* **2002**, *327*, 4.
- [78] M. Kuriyama, K. Nagai, K. Yamada, Y. Miwa, T. Taga, K. Tomioka, *J. Am. Chem. Soc.* **2002**, *124*, 8932.
- [79] C. J. den Reijer, P. Dotta, P. S. Pregosin, A. Albinati, *Can. J. Chem.* **2001**, *79*, 693.
- [80] Q. Jaing, H. Rüegger, L. M. Venanzi, *Inorg. Chim. Acta* **1999**, *290*, 64.
- [81] J. G. Verkade, J. A. Mosbo, in *Phosphorus-31 NMR Spectroscopy in Stereo-Chemical Analysis*, Vol. 8, Eds. J. G. Verkade, L. D. Quin, VCH, Deefield Beach, FL, 1987, p. 425.
- [82] A. K. Roy, R. B. Taylor, *J. Am. Chem. Soc.* **2002**, *124*, 9510.
- [83] W. von Philipsborn, *Pure Appl. Chem.* **1986**, *58*, 513.
- [84] W. von Philipsborn, *Chem. Soc. Rev.* **1999**, *28*, 95.
- [85] J. S. Z. Sabounchei, B. T. Heaton, J. A. Iggo, C. Jacob, I. S. Podkorytov, *J. Cluster Sci.* **2001**, *12*, 339.
- [86] T. Eguchi, B. T. Heaton, *J. Chem. Soc., Dalton Trans.* **1999**, 3523.
- [87] B. T. Heaton, J. A. Iggo, I. S. Pod-korytov, D. J. Smawfield, S. P. Tunik, R. Whyman, *J. Chem. Soc., Dalton Trans.* **1999**, 1917.
- [88] S. P. Tunik, I. S. Podkorytov, B. T. Heaton, J. A. Iggo, J. Sam-panthar, *J. Organomet. Chem.*, **1998**, *550*, 221.
- [89] B. E. Mann, C. Spencer, *Inorg. Chim. Acta* **1982**, *65*, L57.
- [90] B. E. Mann, C. Spencer, *Inorg. Chim. Acta* **1983**, *76*, L65.
- [91] J. Ruiz, P. O. Bentz, B. E. Mann, C. Spencer, B. F. Taylor, P. Maitlis, *J. Chem. Soc., Dalton Trans.* **1987**, 2709.
- [92] K. Zamaraev, *J. Mol. Catal.* **1993**, *82*, 275.

- [93] For a useful study relating allyl ^{13}C chemical shifts in Pd(II) complexes to trans influence, see B. Åkermark, B. S. H. Krakenberger, A. Vitagliano, *Organometallics* **1987**, *6*, 620.
- [94] C. A. Tolman, P. Z. Meakin, D. L. Lindner, J. P. Jesson, *J. Am. Chem. Soc.* **1974**, *96*, 2762.
- [95] P. Dani, M. A. M. Toorneman, G. P. M. van Klink, G. van Koten, *Organometallics* **2000**, *19*, 5287.
- [96] L. Johansson, M. Tilset, J. A. Labinger, J. E. Bercaw, *J. Am. Chem. Soc.* **2000**, *122*, 10846.
- [97] A. Albinati, C. Ammann, P. S. Pregosin, H. Ruegger, *Organometallics* **1990**, *9*, 1826.
- [98] A. Albinati, R. W. Kunz, C. J. Ammann, P. S. Pregosin, *Organometallics* **1991**, *10*, 1800.
- [99] H. Ruegger, R. W. Kunz, C. J. Ammann, P. S. Pregosin, *Magn. Reson. Chem.* **1991**, *29*, 197.
- [100] R. E. Blumer, F. Lianza, P. S. Pregosin, H. Ruegger, A. Togni, *Inorg. Chem.* **1993**, *32*, 2663.
- [101] P. S. Pregosin, H. Ruegger, R. Salzmann, A. Albinati, F. Lianza, R. W. Kunz, *Organometallics* **1994**, *13*, 5040.
- [102] P. von Matt, G. C. Lloyd-Jones, A. B. E. Minidis, A. Pfaltz, L. Macko, M. Neuburger, M. Zehnder, H. Ruegger, P. S. Pregosin, *Helv. Chim. Acta* **1995**, *78*, 265.
- [103] P. Barbaro, P. S. Pregosin, R. Salzmann, A. Albinati, R. W. Kunz, *Organometallics* **1995**, *14*, 5160.
- [104] P. S. Pregosin, R. Salzmann, A. Togni, *Organometallics* **1995**, *14*, 842.
- [105] P. S. Pregosin, R. Salzmann, *Coord. Chem. Rev.* **1996**, *155*, 35.
- [106] G. Trabesinger, A. Albinati, N. Feiken, R. W. Kunz, P. S. Pregosin, M. Tschoerner, *J. Am. Chem. Soc.* **1997**, *119*, 6315.
- [107] P. S. Pregosin, G. Trabesinger, *J. Chem. Soc., Dalton Trans.* **1998**, 727.
- [108] P. S. Pregosin, in *Advances in Bio-Chirality*, Eds. G. Palyi, C. Zucchi, L. Caglioti, Elsevier, Amsterdam, **1999**, pp. 335-345.
- [109] A. Pichota, P. S. Pregosin, M. Valentini, M. Würle, D. Seebach, *Angew. Chem. Int. Ed. Engl.* **2000**, *112*, 153.
- [110] S. P. Smidt, A. Pfaltz, E. Martinez-Viviente, P. S. Pregosin, A. Albinati, *Organometallics* **2003**, *22*, 1000.
- [111] T. J. Geldbach, H. Ruegger, P. S. Pregosin, *Magn. Reson. Chem.* **2003**, *41*, 703.
- [112] J. S. Giovannetti, C. M. Kelly, C. R. Landis, *J. Am. Chem. Soc.* **1993**, *115*, 4040.
- [113] M. Kollmar, B. Goldfuss, M. Reggelin, F. Rominger, G. Helmchen, *Chem. Eur. J.* **2001**, *7*, 4913.
- [114] H. Steinhagen, M. Reggelin, G. Helmchen, *Angew. Chem. Int. Ed. Engl.* **1997**, *36*, 2108.
- [115] D. Zuccaccia, S. Sabatini, G. Bellachioma, G. Cardaci, E. Clot, A. Macchioni, *Inorg. Chem.* **2003**, *42*, 5465.
- [116] A. Macchioni, *Eur. J. Inorg. Chem.* **2003**, 195.
- [117] C. Zuccaccia, G. Bellachioma, G. Cardaci, A. Macchioni, *J. Am. Chem. Soc.* **2001**, *123*, 11020.
- [118] A. Macchioni, G. Bellachioma, G. Cardaci, G. Cruciani, E. Foresti, S. P., C. Zuccaccia, *Organometallics* **1998**, *17*, 5549.
- [119] A. Macchioni, G. Bellachioma, G. Cardaci, V. Gramlich, H. Ruegger, S. Terenzi, L. M. Venanzi, *Organometallics* **1997**, *16*, 2139.
- [120] J. M. Brown, *Chem. Soc. Rev.* **1993**, 25.
- [121] J. M. Brown, D. I. Hulmes, P. J. Guiry, *Tetrahedron* **1994**, *50*, 4493.
- [122] J. M. Brown, J. Perez-Torrente, N. Alcock, H. J. Clase, *Organometallics* **1995**, *14*, 207.
- [123] J. M. Brown, J. J. Perez-Torrente, N. W. Alcock, *Organometallics* **1995**, *14*, 1195.
- [124] C. J. A. Daley, S. H. Bergens, *J. Am. Chem. Soc.* **2002**, *124*, 3680.
- [125] J. A. Wiles, S. H. Bergens, *Organometallics* **1999**, *18*, 3709.
- [126] J. M. Canal, M. Gomez, F. Jimenez, M. Rocomora, G. Muller, E. Dunach, D. Franco, A. Jimenez, F. H. Canos, *Organometallics* **2000**, *19*, 966.
- [127] S. K. Mandal, G. A. N. Gowda, S. S. Krishnamurthy, C. Zheng,

- S. J. Li, N. S. Hosmane, *Eur. J. Inorg. Chem.* **2002**, 2047.
- [128] J. M. Brown, P. A. Chaloner, G. A. Morris, *J. Chem. Soc., Perkin Trans. 2* **1987**, 1583.
- [129] P. S. Pregosin, H. Ruegger, R. Salzmann, A. Albinati, F. Lianza, R. W. Kunz, *Organometallics* **1994**, *13*, 83.
- [130] R. M. Bullock, B. K. Bender, in *Encyclopedia of Catalysis*, Ed. I. T. Horvath, Wiley, New York, **2002**.
- [131] D. A. Singleton, A. A. Thomas, *J. Am. Chem. Soc.* **1995**, *117*, 9357.
- [132] R. H. Grubbs, G. W. Coates, *Acc. Chem. Res.* **1996**, *29*, 85.
- [133] C. R. Landis, K. A. Rosaaen, J. Uddin, *J. Am. Chem. Soc.* **2002**, *124*, 12062.
- [134] M. J. Tanner, M. Brookhart, J. M. DeSimone, *J. Am. Chem. Soc.* **1997**, *119*, 7617.
- [135] C. P. Casey, S. W. Singer, D. R. Powell, R. K. Hayashi, M. Kavana, *J. Am. Chem. Soc.* **2001**, *123*, 1090.
- [136] W. Leitner, J. M. Brown, H. Brunner, *J. Am. Chem. Soc.* **1993**, *115*, 152.
- [137] P.-E. Hansen, *Annu. Rep. NMR Spectrosc.* **1984**, *15*, 105.
- [138] D. D. Wick, K. A. Reynolds, W. D. Jones, *J. Am. Chem. Soc.* **1999**, *121*, 3974.
- [139] P. Burger, R. G. Bergman, *J. Am. Chem. Soc.* **1993**, *115*, 10462.
- [140] Z. X. Liu, E. Somsook, C. R. Landis, *J. Am. Chem. Soc.* **2001**, *123*, 2915.
- [141] Z. X. Liu, E. Somsook, C. B. White, K. A. Rosaaen, C. R. Landis, *J. Am. Chem. Soc.* **2001**, *123*, 11193.
- [142] J. Sandström, *Dynamic NMR Spectroscopy*, Academic Press, London, **1982**.
- [143] N. Chandrakumar, S. Subramanian, *Modern Techniques in High Resolution FT-NMR*, Springer-Verlag, New York, **1987**.
- [144] H. Kessler, M. Gehrke, C. Griesinger, *Angew. Chem. Int. Ed. Engl.* **1988**, *27*, 490.
- [145] C. L. Perrin, T. J. Dwyer, *Chem. Rev.* **1990**, *90*, 935.
- [146] H. Günther, *NMR Spectroscopy: Basic Principles, Concepts, & Applications in Chemistry*, 2nd edn., John Wiley & Sons, New York **1995**.
- [147] A. Macchioni, G. Bellachioma, G. Cardaci, M. Travaglia, C. Zuccaccia, B. Milani, G. Corso, E. Zangrando, G. Mestroni, C. Carfagna, M. Formica, *Organometallics* **1999**, *18*, 3061.
- [148] J. Ledford, C. S. Shultz, D. P. Gates, P. S. White, J. M. DeSimone, M. Brookhart, *Organometallics* **2001**, *20*, 5266.
- [149] P. A. Deck, C. L. Beswick, T. J. Marks, *J. Am. Chem. Soc.* **1998**, *120*, 1772.
- [150] S. J. Skoog, C. Mateo, G. G. Lavoie, F. J. Hollander, R. G. Bergman, *Organometallics* **2000**, *19*, 1406.
- [151] F. Teixidor, M. A. Flores, C. Vinas, R. Sillanpää, R. Kivekaes, *J. Am. Chem. Soc.* **2000**, *122*, 1963.
- [152] H. Valentini, K. Selvakumar, M. Worle, P. S. Pregosin, *J. Organomet. Chem.* **1999**, *587*, 244.
- [153] Z. Zhou, G. Facey, B. R. James, H. Alper, *Organometallics* **1996**, *15*, 2496.
- [154] V. K. Dioumaev, B. R. Yoo, L. J. Procopio, P. J. Carroll, D. H. Berry, *J. Am. Chem. Soc.* **2003**, *125*, 8936.
- [155] M. L. H. Green, L. L. Wong, A. Sella, *Organometallics* **1992**, *11*, 2660.
- [156] S. A. Baker, W. E. Hill, C. A. McAuliffe, *J. Chem. Soc., Dalton Trans.* **1986**, *129*, 7.
- [157] D. Seebach, J. F. M. Oth, J. Heinzer, *Helv. Chim. Acta* **1985**, *8*, 1848.
- [158] A. D. Bain, G. J. Duns, *J. Magn. Reson. Ser. A* **1995**, *112*, 258.
- [159] L. M. Jackman, F. A. Cotton, *Dynamic Nuclear Magnetic Resonance Spectroscopy*, Academic Press, New York, **1975**.
- [160] J. A. Iggo, *NMR Spectroscopy in Inorganic Chemistry*, Oxford University Press, Oxford, **2000**.
- [161] D. S. Stephenson, G. Binsh, *DNMR5, Quantum Chemistry Program Exchange; QCPE 365*. Modified by: Le Master, C. B.; Le Master, C. L.; True, N. S., *Quantum Chemistry Program Exchange; QCPE 059*.
- [162] Ivory-Soft, *g-NMR v. 5. 0. NMR simulation package* **2001**.
- [163] M. Q. Slaght, R. J. M. Klein Gebbink, M. Lutz, A. L. Spek, G. van Koten,

- J. Chem. Soc., Dalton Trans.* **2002**, 2591.
- [164] J. A. M. Brandts, E. Kruiswijk, J. Boersma, A. L. Spek, G. van Koten, *J. Organomet. Chem.* **1999**, 585, 93.
- [165] I. G. Jung, S. U. Son, K. H. Park, K.-C. Chung, J. W. Lee, Y. K. Chung, *Organometallics* **2003**, 22, 4715.
- [166] C. P. Casey, D. W. Carpenetti, H. Sakurai, *Organometallics* **2001**, 20, 4262.
- [167] D. Heller, R. Kadyrov, M. Michalik, T. Freier, U. Schmidt, H. W. Krause, *Tetrahedron: Asymmetry* **1996**, 7, 3025.
- [168] J. M. Brown, P. A. Chaloner, G. A. Morris, *J. Chem. Soc., Chem. Commun.* **1983**, 664.
- [169] R. Kadyrov, A. Borner, R. Selke, *Eur. J. Inorg. Chem.* **1999**, 705.
- [170] O. N. Bruker-Franzen Analytik GmbH and K. Il'yasov, WIN-DYNAMICS 1.0 Release 951220, *NMR Dynamic Spectra Simulation and Iteration*.
- [171] J. G. Knight, S. Doherty, A. Harri-man, E. G. Robins, M. Betham, G. R. Eastham, R. P. Tooze, M. R. J. Elsegood, P. Champkin, W. Clegg, *Organometallics* **2000**, 19, 4957.
- [172] J. K. M. Sanders, B. K. Hunter, *Modern NMR Spectroscopy*, Oxford University Press, Oxford, **1987**.
- [173] J. W. Faller, in *The Determination of Organic Structures by Physical Methods*, Vol. 5, Chap. 2, Academic Press, New York, **1973**.
- [174] K. G. Orrell, in *Annual Reports on NMR Spectroscopy*, Vol. 37, **1999**, pp. 1.
- [175] S. Schaeublin, A. Wokaun, R. R. Ernst, *J. Magn. Reson.* **1977**, 27, 273.
- [176] S. Schaeublin, A. Hoehener, R. R. Ernst, *J. Magn. Reson.* **1974**, 13, 196.
- [177] J. Halpern, *Science* **1982**, 217, 401.
- [178] H. B. Kagan, G. Wilkinson, F. G. A. Stone, in *Comprehensive Organometallic Chemistry*, Vol. 8, Pergamon Press, Oxford, **1982**, p. 463.
- [179] H. Bircher, B. R. Bender, W. v. Phillipsborn, *Magn. Reson. Chem.* **1993**, 31, 293.
- [180] L. Cronin, C. L. Higgitt, R. N. Perutz, *Organometallics* **2000**, 19, 672.
- [181] A. Togni, *Angew. Chem. Int. Ed. Engl.* **1996**, 108, 1581.
- [182] G. Pioda, A. Togni, *Tetrahedron Asymmetry* **1998**, 9, 3903.
- [183] T. K. Woo, G. Pioda, U. Rothlisberger, A. Togni, *Organometallics* **2000**, 19, 2144.
- [184] J. Herrmann, P. S. Pregosin, R. Salzmann, A. Albinati, *Organometallics* **1995**, 14, 3311.
- [185] P. Dotta, P. G. A. Kumar, P. S. Pregosin, *Magn. Reson. Chem.* **2002**, 40, 653.
- [186] J. L. Farrugia, *J. Chem. Soc., Dalton Trans.* **1997**, 1783.
- [187] W. Hieber, *Adv. Organomet. Chem.* **1970**, 8, 1.
- [188] N. Chatani, Y. Ishii, Y. Ie, F. Kakituchi, S. Murai, *J. Org. Chem.* **1998**, 63, 5129.
- [189] G. Gervasio, R. Giordano, D. Maraballo, E. Sappa, *J. Organomet. Chem.* **1999**, 588, 83.
- [190] U. Frey, L. Helm, A. E. Merbach, R. Roulet, *Advanced Applications of NMR to Organometallic Chemistry*, J. Wiley & Sons Ltd, Chichester, **1996**.
- [191] E. Abel, K. G. Orrell, S. P. Scanlan, D. Stephenson, T. Kemmit, W. J. Levason, *J. Chem. Soc., Dalton Trans.* **1991**, 591.
- [192] D. Shaw, *Fourier transform NMR spectroscopy*, Elsevier, Amsterdam, **1976**.
- [193] R. H. Crabtree, *Acc. Chem. Res.* **1990**, 23, 95.
- [194] G. J. Kubas, R. R. Ryan, B. I. Swanson, P. J. Vergamini, H. J. Wasserman, *J. Am. Chem. Soc.* **1984**, 106, 451.
- [195] P. J. Desrosiers, L. Cai, Z. Lin, R. Richards, J. Halpern, *J. Am. Chem. Soc.* **1991**, 113, 4173.
- [196] R. H. Morris, R. J. Wittebort, *Magn. Reson. Chem.* **1997**, 35, 243.
- [197] V. I. Bakhmutov, *Magn. Reson. Chem.* **2004**, 42, 66.
- [198] V. I. Bakhmutov, C. Bianchini, F. Maseras, A. Lledos, M. Peruzzini, E. V. Vorontsov, *Chem.-Eur. J.* **1999**, 5, 3318.
- [199] J. A. Ayllon, S. Gervaux, S. Sabo-Etienne, B. Chaudret, *Organometallics* **1997**, 16, 2000.

- [200] K. A. Earl, G. Jia, P. A. Maltby, R. H. Morris, *J. Am. Chem. Soc.* **1991**, *113*, 3027.
- [201] S. B. Duckett, C. L. Newell, R. Eisenberg, *J. Am. Chem. Soc.* **1994**, *116*, 10548.
- [202] S. B. Duckett, C. J. Sleigh, *Prog. Nucl. Magn. Reson. Spectrosc.* **1999**, *34*, 71.
- [203] S. B. Duckett, D. Blazina, *Eur. J. Inorg. Chem.* **2003**, 2901.
- [204] C. R. Bowers, D. P. Weitekamp, *J. Am. Chem. Soc.* **1987**, *109*, 5541.
- [205] K. F. Bonhoeffer, P. Harteck, *Z. Phys. Chem-Leipzig* **1929**, *B4*, 113.
- [206] J. Natterer, J. Bargon, *Prog. Nucl. Magn. Reson. Spectrosc.* **1997**, *31*, 293.
- [207] P. Hubler, R. Giernoth, G. Kummerle, J. Bargon, *J. Am. Chem. Soc.* **1999**, *121*, 5311.
- [208] L. Vaska, M. F. Werneke, *Trans. N. Y. Acad. Sci.* **1971**, *33*, 70.
- [209] R. Ugo, S. Cenini, A. Fusi, A. Pasini, *J. Am. Chem. Soc.* **1972**, *94*, 7364.
- [210] A. L. Sargent, M. B. Hall, *Inorg. Chem.* **1992**, *31*, 317.
- [211] S. K. Hasnip, S. B. Duckett, C. J. Sleigh, D. R. Taylor, G. K. Barlow, M. J. Taylor, *Chem. Commun.* **1999**, 1717.
- [212] S. K. Hasnip, S. A. Colebrooke, C. J. Sleigh, S. B. Duckett, D. R. Taylor, G. K. Barlow, M. J. Taylor, *J. Chem. Soc., Dalton Trans.* **2002**, 743.
- [213] D. Schleyer, H. G. Niessen, J. Bargon, *New J. Chem.* **2001**, *25*, 423.
- [214] M. Haake, J. Natterer, J. Bargon, *J. Am. Chem. Soc.* **1996**, *118*, 8688.
- [215] S. Aime, D. Canet, W. Dastru, R. Gobetto, F. Reineri, A. Viale, *J. Phys. Chem. A* **2001**, *105*, 6305.
- [216] D. Schott, C. J. Sleigh, J. P. Lowe, S. B. Duckett, R. J. Mawby, M. G. Partridge, *Inorg. Chem.* **2002**, *41*, 2960.
- [217] R. Whyman, in *Laboratory Methods in Vibrational Spectroscopy*, Eds. H. A. Willis, J. H. Van der Mass, R. G. J. Miller, Wiley, New York, **1987**.
- [218] J. E. Jonas, in "High Pressure NMR in NMR Basic Principles and Progress", Vol. 24, p. 85, Eds. P. Diehl, E. Fluck, H. Günther, R. Kosfeld, J. Selig Vol. 24, Springer, Berlin, **1991**.
- [219] I. T. Horvath, J. M. Millar, *Chem. Rev.* **1991**, *91*, 1339.
- [220] C. J. Elsevier, *J. Mol. Catal.* **1994**, *92*, 285.
- [221] D. C. Roe, P. M. Kating, P. J. Krusic, B. E. Smart, *Top. Catal.* **1998**, *5*, 133.
- [222] D. C. Roe, in *Homogeneous Transition Metal Catalyzed Reactions*, Eds. W. R. Moser, D. W. Slocum, American Chemical Society, Washington, **1992**.
- [223] T. B. Marder, D. C. Roe, D. Milstein, *Organometallics* **1988**, *7*, 1451.
- [224] M. Brookhart, A. F. J. Volpe, D. M. Lincoln, I. T. Horvath, J. M. Millar, *J. Am. Chem. Soc.* **1990**, *112*, 5634.
- [225] K. T. Moore, I. T. Horvath, M. J. Therien, *J. Am. Chem. Soc.* **1997**, *119*, 1791.
- [226] B. T. Heaton, L. Strona, J. Jonas, T. Eguchi, G. A. Hoffmann, *J. Chem. Soc., Dalton Trans.* **1982**, 1159.
- [227] B. T. Heaton, J. Jonas, T. Eguchi, G. A. Hoffmann, *J. Chem. Soc., Chem. Commun.* **1981**, 331.
- [228] D. T. Brown, T. Eguchi, B. T. Heaton, J. A. Iggo, R. Whyman, *J. Chem. Soc., Dalton Trans.* **1991**, 677.
- [229] R. C. Matthews, D. K. Howell, P. W., S. G. Train, W. D. Treleaven, G. G. Stanley, *Angew. Chem. Int. Ed. Engl.* **1996**, *35*, 2253.
- [230] D. C. Roe, *Organometallics* **1987**, *6*, 942.
- [231] I. T. Horvath, R. V. Kastrup, A. A. Oswald, E. J. Mozeleski, *Catal. Lett.* **1989**, *2*, 85.
- [232] I. Toth, T. Kegel, C. J. Elsevier, L. Kollar, *Inorg. Chem.* **1994**, *33*, 5708.
- [233] I. Toth, C. J. Elsevier, *J. Am. Chem. Soc.* **1993**, *115*, 10388.
- [234] G. Dekker, C. J. Elsevier, K. Vrieze, P. Vanleeuwen, *Organometallics* **1992**, *11*, 1598.
- [235] J. M. Millar, R. V. Kastrup, S. Harris, I. T. Horvath, *Angew. Chem. Int. Ed. Engl.* **1990**, 194.
- [236] M. Poyatos, P. Uriz, J. A. Mata, C. Claver, E. Fernandez, E. Peris, *Organometallics* **2003**, *22*, 440.
- [237] C. Bianchini, H. M. Lee, A. Meli, F. Vizza, *Organometallics* **2000**, *19*, 849.

- [238] K. Nozaki, T. Hiyama, S. Kacker, I. T. Horvath, *Organometallics* **2000**, *19*, 2031.
- [239] D. J. Darensbourg, H. P. Wiegreffe, P. W. Wiegreffe, *J. Am. Chem. Soc.* **1990**, *112*, 9252.
- [240] D. J. Darensbourg, P. Wiegreffe, C. G. Riordan, *J. Am. Chem. Soc.* **1990**, *112*, 5759.
- [241] D. J. Darensbourg, B. L. Mueller, C. J. Bischoff, S. S. Chojnacki, J. H. Reibenspies, *Inorg. Chem.* **1991**, *30*, 2418.
- [242] F. R. Bregman, J. M. Ernstring, F. Muller, M. D. K. Boele, L. A. van der Veen, C. J. Elsevier, *J. Organomet. Chem.* **1999**, *592*, 306.
- [243] G. Laurenczy, A. Merbach, *J. Chem. Soc., Chem. Commun.* **1993**, 187.
- [244] J. M. Millar, R. V. Kastrup, M. T. Melchior, I. T. Horvath, C. D. Hoff, R. H. Crabtree, *J. Am. Chem. Soc.* **1990**, *112*, 9643.
- [245] J. A. Iggo, Y. Kawashima, J. Liu, T. Hiyama, K. Nozaki, *Organometallics* **2003**, *22*, 5418.
- [246] S. C. van der Slot, P. C. J. Kamer, P. van Leeuwen, J. A. Iggo, B. T. Heaton, *Organometallics* **2001**, *20*, 430.
- [247] J. A. Iggo, D. Shirley, N. C. Tong, *New J. Chem.* **1998**, *22*, 1043.
- [248] P. S. Bearman, A. K. Smith, N. C. Tong, R. Whyman, *Chem. Commun.* **1996**, 2061.
- [249] J. W. Rathke, R. J. Klingler, R. E. Gerald, K. W. Kramarz, K. Woelk, *Prog. Nucl. Magn. Reson. Spectrosc.* **1997**, *30*, 209.
- [250] J. W. Rathke, *J. Magn. Reson.* **1989**, *85*, 150.
- [251] K. Woelk, J. W. Rathke, R. J. Klingler, *J. Magn. Reson. Ser. A* **1994**, *109*, 137.
- [252] H. G. Niessen, P. Trautner, S. Wiemann, J. Bargon, K. Woelk, *Rev. Sci. Instrum.* **2002**, *73*, 1259.
- [253] J. Bargon, J. Kandels, K. Woelk, *Z. Phys. Chem.* **1993**, *180*, 65.
- [254] J. W. Rathke, R. J. Klingler, R. E. Gerald, D. E. Fremgen, K. Woelk, S. Gaemers, C. J. Elsevier, in *Chemical Synthesis Using Supercritical Fluids*, Eds. P. G. Jessop, W. Leitner, Wiley-VCH, Weinheim, **1999**, p. 165.
- [255] P. G. Jessop, T. Ikariya, R. Noyori, *Chem. Rev.* **1999**, *99*, 475.
- [256] S. L. Wells, J. M. DeSimone, *Angew. Chem. Int. Ed. Engl.* **2001**, *40*, 518.
- [257] *Chemical Synthesis Using Supercritical Fluids*, Eds. P. G. Jessop, W. Leitner, Wiley-VCH, Weinheim, **1999**.
- [258] P. G. Jessop, T. Ikariya, R. Noyori, *Science* **1995**, *269*, 1065.
- [259] P. G. Jessop, T. Ikariya, R. Noyori, *Nature* **1994**, *368*, 231.
- [260] W. Leitner, in *Modern Solvents in Organic Synthesis*, in *Topics in Current Chemistry*, Ed. P. Knochel, Springer-Verlag, Berlin, Vol. 206, **1999**, p. 107.
- [261] J. M. Robert, R. F. Evilia, *J. Am. Chem. Soc.* **1985**, *107*, 3733.
- [262] D. M. Lamb, S. T. Adamy, K. W. Woo, J. Jonas, *J. Phys. Chem.* **1989**, *93*, 5002.
- [263] S. Gaemers, J. Groenevelt, C. J. Elsevier, *Eur. J. Inorg. Chem.* **2001**, 829.
- [264] S. Gaemers, C. J. Elsevier, *Chem. Soc. Rev.* **1999**, *28*, 135.
- [265] J. W. Rathke, R. J. Klingler, T. R. Krause, *Organometallics* **1991**, *10*, 1350.
- [266] H. G. Niessen, A. Eichhorn, K. Woelk, J. Bargon, *J. Mol. Catal. A* **2002**, *182–183*, 463.
- [267] R. J. Klingler, J. W. Rathke, *J. Am. Chem. Soc.* **1994**, *116*, 4772.
- [268] J. W. Rathke, R. J. Klingler, T. R. Krause, *Organometallics* **1992**, *11*, 585.
- [269] K. W. Kramarz, R. J. Klingler, D. E. Fremgen, J. W. Rathke, *Catal. Today* **1999**, *49*, 339.
- [270] S. Lange, A. Brinkmann, P. Trautner, K. Woelk, J. Bargon, W. Leitner, *Chirality* **2000**, *12*, 450.
- [271] K. Wittmann, W. Wisniewski, R. Mylott, W. Leitner, C. L. Kranemann, T. Rische, P. Eilbracht, S. Kluwer, J. M. Ernstring, C. L. Elsevier, *Chem.-Eur. J.* **2001**, *7*, 4584.
- [272] E. O. Stejskal, J. E. Tanner, *J. Chem. Phys.* **1965**, *42*, 288.
- [273] P. G. Anil Kumar, P. S. Pregosin, J. M. Goicoechea, M. K. Whittlesey, *Organometallics* **2003**, *22*, 2956.

- [274] C. S. J. Johnson, *Prog. NMR Spectrosc.* **1999**, *34*, 203.
- [275] P. Stilbs, *Prog. NMR Spectrosc.* **1987**, *19*, 1.
- [276] C. S. J. Johnson, in *Encyclopedia of Nuclear Magnetic Resonance*, Eds. D. M. Grant, R. K. Harris, Wiley, Chichester, **1996**, pp. 1626.
- [277] W. S. Price, *Concepts Magn. Reson.* **1998**, *10*, 197.
- [278] W. S. Price, *Concepts Magn. Reson.* **1997**, *9*, 299.
- [279] J. Kärger, H. Pfeifer, W. Heink, *Adv. Magn. Reson.* **1988**, *12*, 1.
- [280] H. J. V. Tyrrell, K. R. Harris, *Diffusion in Liquids* Butterworths, London, **1984**.
- [281] P. Stilbs, *Anal. Chem.* **1981**, *53*, 2135.
- [282] E. E. van Meerwal, *Adv. Polym. Sci.* **1984**, *54*, 1.
- [283] W. Brown, P. Stilbs, *Polymer* **1982**, *24*, 188.
- [284] P. Griffiths, P. Stilbs, *Curr. Opin. Colloid Interface Sci.* **2002**, *7*, 249.
- [285] L. Frish, S. E. Matthews, V. Böhmer, Y. Cohen, *J. Chem. Soc., Perkin Trans. 2* **1999**, 669.
- [286] K. S. Cameron, L. Fielding, *J. Org. Chem.*, **2001**, *66*, 6891.
- [287] L. Avram, Y. Cohen, *J. Am. Chem. Soc.* **2003**, *125*, 16180.
- [288] L. Frish, F. Sansone, A. Casnati, R. Ungaro, Y. Cohen, *J. Org. Chem.* **2000**, *65*, 5026.
- [289] B. Olenyuk, M. D. Lovin, J. A. Whiteford, P. J. J. Stang, *J. Am. Chem. Soc.* **1999**, *121*, 10434.
- [290] J. K. Young, G. R. Baker, G. R. Newkome, K. F. Morris, C. S. Johnson, *Macromolecules* **1994**, *27*, 3464.
- [291] R. C. van Duijvenbode, I. B. Rietvelt, G. J. M. Koper, *Langmuir* **2000**, *16*, 7720.
- [292] S. G. Yao, G. J. Howlett, R. S. Norton, *J. Biomol. NMR* **2000**, *16*, 109.
- [293] K. R. Deaton, E. A. Feyen, H. J. Nkulabi, K. F. Morris, *Magn. Reson. Chem.* **2001**, *39*, 276.
- [294] Y. Wan, J. K. Angleson, A. G. Kutateladze, *J. Am. Chem. Soc.* **2002**, *124*, 5610.
- [295] C. Förste, W. Heink, J. Kärger, H. Pfeifer, N. N. Feokistova, S. P. Zhdanov, *Zeolites* **1989**, *9*, 299.
- [296] G. H. Sorland, D. Aksnes, L. Gjerda-ker, *J. Magn. Reson.* **1999**, *137*, 397.
- [297] T. J. Geldbach, F. Breher, V. Gramlich, P. G. Anil Kumar, P. S. Pregosin, **2004**, *43*, 1920.
- [298] E. Martinez-Viviente, H. Ruegger, P. S. Pregosin, J. Lopez-Serrano, *Organometallics* **2002**, *21*, 5841.
- [299] E. Martinez-Viviente, P. Pregosin, *Helv. Chim. Acta* **2003**, *86*, 2364.
- [300] A. Burini, J. P. Fackler, R. Galassi, A. Macchioni, M. A. Omary, M. A. Rawashdeh-Omary, B. R. Pietroni, S. Sabatini, C. Zuccaccia, *J. Am. Chem. Soc.* **2002**, *124*, 4570.
- [301] A. Macchioni, A. Romani, C. Zuccaccia, G. Guglielmetti, C. Querci, *Organometallics* **2003**, *22*, 1526.
- [302] M. Valentini, H. Ruegger, P. S. Pregosin, *Helv. Chim. Acta* **2001**, *84*, 2833.
- [303] P. S. Pregosin, E. Martinez-Viviente, P. G. A. Kumar, *Dalton Trans.* **2003**, 4007.
- [304] B. Binotti, A. Macchioni, C. Zuccaccia, D. Zuccaccia, *Comments Inorg. Chem.* **2002**, *23*, 417.
- [305] R. E. Hoffman, E. Shabtai, M. Rabinovitz, V. S. Iyer, K. Müllen, A. K. Rai, E. Bayrd, L. T. Scott, *J. Chem. Soc., Perkin Trans. 2* **1998**, 1659.
- [306] D. E. Babushkin, H. Brintzinger, *J. Am. Chem. Soc.* **2002**, *124*, 12869.
- [307] N. G. Stahl, C. Zuccaccia, T. R. Jensen, T. J. Marks, *J. Am. Chem. Soc.* **2003**, *125*, 5256.
- [308] C. Zuccaccia, N. G. Stahl, A. Macchioni, M.-C. Chen, R. J. A., T. J. Marks, *J. Am. Chem. Soc.* **2004**, *126*, 1448.
- [309] M. Ludwig, R. Kadyrov, H. Fiedler, K. Haage, R. Selke, *Chem.-Eur. J.* **2001**, *7*, 3298.
- [310] K. Fagnou, M. Lautens, *Angew. Chem. Int. Ed. Engl.* **2002**, *41*, 27.
- [311] Y.-X. Chen, M. V. Metz, L. Li, C. L. Stern, T. J. Marks, *J. Am. Chem. Soc.* **1998**, *120*, 6287.
- [312] E. P. Kündig, C. M. Saudan, G. Bernardinelli, *Angew. Chem.* **1999**, *111*, 1298.
- [313] E. P. Kündig, C. M. Saudan, F. Viton, *Adv. Synth. Catal.* **2001**, *343*, 51.

- [314] D. A. Evans, J. A. Murray, P. von Matt, R. D. Norcross, S. J. Miller, *Angew. Chem.* **1995**, *107*, 864.
- [315] U. Burckhardt, M. Baumann, A. Togni, *Tetrahedron Asymmetry* **1997**, *8*, 155.
- [316] C. Bianchini, C. Mealli, M. Peruzzini, F. Zanobini, *J. Am. Chem. Soc.* **1992**, *114*, 5905.
- [317] K. Gruet, E. Clot, O. Eisenstein, D. H. Lee, B. Patel, A. Macchioni, R. H. Crabtree, *New J. Chem.* **2003**, *27*, 80.
- [318] A. Macchioni, A. Magistrato, I. Orabona, F. Ruffo, U. Rothlisberger, C. Zuccaccia, *New J. Chem.* **2003**, *27*, 455.
- [319] B. Binotti, C. Carfagna, E. Foresti, A. Macchioni, P. Sabatino, C. Zuccaccia, D. Zuccaccia, *J. Organomet. Chem.*, **2004**, 689, 647.
- [320] A. Pfaltz, J. Blankenstein, R. Hilgraf, E. Hormann, S. McIntyre, F. Menges, M. Schonleber, S. P. Smidt, B. Wustenberg, N. Zimmermann, *Adv. Syn. Catal.* **2003**, *345*, 33.
- [321] E. Martinez-Viviente, P. S. Pregosin, *Inorg. Chem.* **2003**, *42*, 2209.
- [322] K. F. Morris, C. S. J. Johnson, *J. Am. Chem. Soc.* **1992**, *114*, 3139.
- [323] M. D. Pelta, H. Barjat, G. A. Morris, A. L. Davis, S. J. Hammond, *Magn. Reson. Chem.* **1998**, *36*, 706.
- [324] K. F. Morris, P. Stilbs, C. S. J. Johnson, *Anal. Chem.* **1994**, *66*, 211.
- [325] A. Jerschow, N. Müller, *Macromolecules* **1998**, *31*, 6573.
- [326] D. A. Jayawickrama, C. K. Larive, E. F. McCord, D. C. Roe, *Magn. Reson. Chem.* **1998**, *36*, 755.
- [327] T. Zhao, H. W. Beckham, *Macromolecules* **2003**, *36*, 9859.
- [328] T. Zhao, H. W. Beckham, H. W. Gibson, *Macromolecules* **2003**, *36*, 4833.
- [329] C. Gambs, T. J. Dickerson, S. Mahajan, L. B. Pasternack, K. D. Janda, *J. Org. Chem.* **2003**, *68*, 3673.
- [330] S. Viel, D. Capitani, L. Mannina, A. Segre, *Biomacromolecules* **2003**, *4*, 1843.
- [331] M. D. Diaz, S. Berger, *Carbohydr. Res.* **2000**, *329*, 1.
- [332] D. P. Hinton, C. S. Johnson, Jr., *J. Phys. Chem.* **1993**, *97*, 9064.
- [333] E. J. Cabrita, S. Berger, *Magn. Reson. Chem.* **2001**, *39*, S142.
- [334] S. Viel, L. Mannina, A. Segre, *Tetrahedron Lett.* **2002**, *43*, 2515.
- [335] G. S. Kapur, E. J. Cabrita, S. Berger, *Tetrahedron Lett.* **2000**, *41*, 7181.
- [336] A. Hori, K. Kumazawa, T. Kusukawa, D. K. Chand, M. Fujita, S. Sakamoto, K. Yamaguchi, *Chem. Eur. J.* **2001**, *7*, 4142.
- [337] I. Keresztes, P. G. Williard, *J. Am. Chem. Soc.* **2000**, *122*, 10228.
- [338] H. Barjat, G. A. Morris, A. G. Swanson, *J. Magn. Reson.* **1998**, *131*, 131.
- [339] E. Gozansky, D. G. Gorenstein, *J. Magn. Reson. Ser. B* **1996**, *111*, 94.
- [340] G. S. Kapur, M. Findeisen, S. Berger, *Fuel* **2000**, *79*, 1347.
- [341] D. Wu, A. Chen, C. S. Johnson, Jr., *J. Magn. Reson. Ser. A* **1996**, *123*, 215.
- [342] D. Wu, A. Chen, C. S. Johnson, Jr., *J. Magn. Reson. Ser. A* **1996**, *121*, 88.
- [343] R. K. Harris, K. A. Kinneer, G. A. Morris, M. J. Stchedroff, A. Samadi-Maybadi, *Chem. Commun.* **2001**, 2422.
- [344] N. E. Schlörer, E. J. Cabrita, S. Berger, *Angew. Chem. Int. Ed. Engl.* **2002**, *41*, 107.
- [345] N. E. Schlörer, S. Berger, *Organometallics* **2001**, *20*, 1703.